Dissertation

Hadron-Nucleus Interactions in the Nucleon Resonance Region

Stefanie Geßler
geb. Lourenço

Juni 2017

Justus-Liebig-Universität Gießen
Fachbereich 07
Institut für Theoretische Physik

1. Gutachter: Prof. Dr. Horst Lenske (Justus-Liebig-Universität Gießen)
2. Gutachter: Prof. Dr. Christian S. Fischer (Justus-Liebig-Universität Gießen)

Abstract

Experiments with high-energy hadron beams have found renewed attention. In the near future nuclear studies with hadron beams are planned at least at two facilities, namely J-PARC in Japan and GSI/FAIR. The aim of this work is an exploratory investigation of interactions of mesons and baryons with nuclei at energies of interest for future research with antiprotons at FAIR.

The theoretical discussion is started with an introductory presentation of the optical model and Eikonal theory as appropriate tools for the description of scattering processes at high energies. In antiproton interactions with nucleons and nuclei, annihilation processes into pions are playing the major role for the reaction dynamics. Therefore, we consider first the interactions of pions with nuclei by deriving an extended self-energy scheme for a large range of incident pion energies. In order to have a uniform description over a broad energy interval, the existing approaches had to be reconsidered and in essential parts reformulated and extended. A central result is the treatment of pion-nucleus self-energies from high lying N* resonances. Only by including those channels in a proper manner into the extended pion optical potential, pion-nucleus scattering could be described over the required large energy range. At low energies the well known Kisslinger potential is recapped.

Next, the same type of reaction theory is used to analyze antiproton-nucleon and nucleus scattering from low to highly relativistic energies. The reaction dynamics of antiproton interactions with nuclear targets is discussed. We start with a new approach to antiproton-nucleon scattering. A free-space antiproton-nucleon T-matrix is derived, covering an energy range as wide as from 100 MeV up to 15 GeV. Eikonal theory is used to describe the antiproton scattering amplitudes in momentum and in coordinate space. We consider, in particular, interactions with nuclei at energies around and well above 1 GeV. The antiproton-nucleus self-energies are obtained microscopically in a folding model using the previously derived T-matrix interactions and nuclear ground state densities form HFB calculations. For a quantitative description, an extended eikonal reaction theory is used.

Finally, an outlook is given to applications of the results as ISI and FSI in pion production in antiproton annihilation on nuclei. Two reaction scenarios are identified and studied in exploratory calculations.

Zusammenfassung

Experimente mit hochenergetischen Hadronenstrahlen sind erneut von großem Interesse. In naher Zukunft sind mindestens zwei neue Experimente mit hochenergetischen Hadronenstrahlen geplant: J-PARC in Japan und FAIR in der GSI an Darmstadt. Ziel dieser Arbeit ist es die Wechselwirkung von Mesonen und Baryonen mit Atomkernen exemplarisch zu untersuchen in Energiebereichen, die relevant für zukünftige Forschung mit Antiprotonen an der FAIR Beschleunigeranlage sind.

Die Arbeit beginnt mit einer einführenden Diskussion der zugrundeliegenden Theorien, wie die des optisches Potentials und der Eikonaltheorie, als passende Werkzeuge zur Behandlung von hochenergetischen Streuproblemen. Hauptteil der zugrundeliegenden Reaktionsdynamik von Antiprotonen Wechselwirkungen mit Nukleonen und Atomkernen sind Annihilationsprozesse, die in der Erzeugung von Pionen resultieren. Aus diesem Grund betrachten wir zunächst die Wechselwirkung von Pionen mit Kernen und erweitern die zugrundeliegenden Selbstenergien zur Beschreibung eines großen Spektrums von eingehenden Pionenenergien. Um eine einheitliche Beschreibung über große Energiebreiche zu erhalten, wurden bereits existierende Ansätze zusammenfassend betrachtet und schließlich essentielle Teile neu formuliert und erweitert. Ein zentrales Ergebnis ist die Behandlung der höheren Resonanzen in Pion-Kern Selbstenergien. Nur durch Einbinden dieser Resonanzen in ein erweitertes optisches Potential konnte die Streuung von Pionen mit Kernen korrekt über weite Energiebereiche beschrieben werden. Für niedrige Energien wird das bekannte Kisslinger-Potential vorgestellt.

Als nächstes wurde innerhalb derselben Reaktionstheorie Antiproton-Nukleon und Antiproton-Kern Streuung von niedrigen bis zu relativistischen Energien analysiert. Ein neuer Ansatz zur Beschreibung von Antiproton-Nukleon-Streuung wird präsentiert. Die Antiproton-Kern T-Matrix wird mit einem Ansatz gerechnet, der eine Beschreibung von einem Energiebereich von wenigen MeV bis zu 15 GeV ermöglicht. Die Eikonaltheorie wird dazu genutzt, die Streuamplitude sowohl im Orts- als auch im Impulsraum zu berechnen. Die Antiproton-Kern Selbstenergien werden durch Faltung der Grundzustandskerndichte, Ergebnis von HFB Berechnungen, und der zuvor erwähnten T-Matrix berechnet. Im Ausblick werden schließlich die Anwendungen dieser Rechnungen als Input für Eingans- und Ausgangskanalwechselwirkungen komplexer Reaktionen diskutiert: der Pionproduktion bei Antiproton-Annihilation im Kern. Zwei Reaktionsszenarien werden vorgestellt und exemplarische Berechnungen präsentiert.

Contents

1 Introduction

Within the last decades, many questions concerning fundamental physics have risen and later been answered by scattering experiments. This is especially true for the understanding of how the matter surrounding us is built. One of the most important breakthroughs was made by Rutherford, who observed that the atomic nucleus is concentrated at a small core, while the electrons surround it at some distance with nothing in between. But what keeps the nucleus, especially the protons so close together? From the Coulomb-force one would expect the protons to repel each other due to the electric charge. So there must be an additional force acting. This force is called "strong force" and counts as one of the four fundamental forces, along with the already mentioned electromagnetic force (Coulomb), the weak interaction and gravity. These forces are transferred by the exchange of bosons. The exchange boson investigated best is the massless photon, which transmits the electromagnetic interaction but has no electric charge itself. This is different for the gluons, which are mediators of the strong force, but carry colour charge themselves. Therefore, the gluons interact with each other as well as with quarks.

The reason why protons and neutrons are bound within a nucleus is only indirectly caused by the strong force. As mentioned before, the strong interaction acts between quarks and gluons, due to their colour charge. The nucleons, however, are colour-neutral, but a residual force acts between them. This is comparable to the binding of neutral atoms that form a molecule. The so-called Van-der-Waals force is induced by the polarization of the atoms. Two atoms, which are electrically neutral, can not feel the strength of the Coulomb force as long as they keep a distance larger than a typical electron cloud surrounding the nucleus. When the atoms come closer, their electron cloud gets polarized, which induces a dipole moment, finally leading to the Van-der-Waals force and binding. When colour-neutral nucleons come as close as a typical quark distribution, their inside also gets polarized, and a residual interaction leads to the binding.

Because the colourless nucleons do not couple to the strong force directly, the interaction can be described on the basis of the exchange of colour-neutral bosons. The idea of the model goes back to Hideki Yukawa, who predicted the existence of such an exchange particle, which was found later and called pion. The pion is an isospin triplet particle and formed by an antiquark-quark pair from the first generation. The pion with its small mass of about 140 MeV is the lightest meson and therefore well suited to describe the long-range behaviour of the NN-interaction. Because the one-pion-

exchange (OPE) model was so successful, also other, heavier particles, were considered to describe the NN-interaction. The models, which have been developed and discussed most actively are the Paris-, Jülich- and Nijmegen-models.

The pion is interesting due to at least two reasons. First, because it is a mediator of the strong force, and second, because it is the lightest meson and therefore it appears in many reactions. The pion is of central interest for strong-interaction physics, due to its Goldstone-boson character and because it is the lowest member of the pseudo scalar octet. The work of [EE66] was a breakthrough in the description of pion interactions with the nuclear medium and nuclei and inspired many models [OTW82, Klu91, LR02]. At very low energies the pion can be captured by the nucleus and becoming deeply bound, building a pionic atom. The derived spectra from the pion cascading down to its bound state revealed a lot of information about nuclei. Nowadays, this very low energy region can be well described within Chiral Perturbation Theory, due to the dominance of s-waves in this energy region [OGRN95, KW01, KFW02, DO08]. Approaching the threshold of the Δ-resonance at 1232 MeV, p-wave contributions become more and more important and lead to a more complicated description. An approved model of [JS96] succeeded with an extension of the work of [EE66] to a the higher energy region. This was done by the use of a phenomenological optical potential applied within an effective Klein-Gordon wave-equation.

In this work, however, an approach capable of describing pion-nucleon and pion-nucleus interactions over wide energy-ranges is presented. Good descriptions of pion interactions can be used for investigation where the pion appears in the final state. Upcoming experiments studying matter-antimatter interactions, where final state interactions are known to be of importance, are for example PANDA and AIC. To describe such complex reaction mechanisms, the consistent description starting with the initial state $N\overline{N}$ interactions, including the production mechanism and finally describing the final state πN interactions, is mandatory. It is known from former LEAR experiments that there is a broad distribution of pion multiplicities in antinucleon-nucleon interactions in nuclei, peaking at five pions. The produced pions may be absorbed by the nucleus and make it difficult to distinguishexperimentally between two types of events: Both involve initial production and the same number of pions in the final state, but in one case, all pions escape the nucleus, and in the other, some are absorbed. This situation calls for a consistent theoretical description which is sensitive to such details. In this work, steps towards such a description are presented.

First steps towards the pion production in antiproton nuclear reactions are presented within this work. Motivated by the upcoming experiments in the near future, we aim for a description in a wide energy range from 100 MeV up to 1 GeV for both, pions and antiprotons. This work is organized as follows:

Starting in chapter two with the introduction of hadron-nucleus interactions, the treatment of many-body scattering problems within an optical approach is presented.

The formulation of the Klein-Gordon wave equation reveals the special character of the pions being the lightest mesons and is used to describe the long-range part of the nucleon-nucleon interaction. After the success of the one-pion exchange models, many other models have been developed treating more and more particles as exchange particles. The Eikonal theory is briefly introduced and the derivation of the Eikonal is presented, serving as a basis the for later calculation for interaction cross sections.

In the third chapter the basics of pion-nucleus inetarction are presented. Starting with rather low energies, the suitable Kisslinger-potential is recovered and extended to higher energies.

The extension does not only include higher resonances of the pion-nucleon interaction, but also contains a more involved density dependence, contributing especially to the "true absorption" term. The description of the density is improved for interactions located at the nuclear center, leading to the regularized Fermi-function.

An improvement of higher-order corrections to the Eikonal approach failed due to divergence of the procedure. The calculations are presented but neglected in our final calculations. The description of the pion-nucleus interaction is compared to the pion-nucleus cross section at the energy range of interest. The same parameter set is used for all our calculations, and comparisons to light nuclei such as Lithium up to heavy nuclei like Bismuth are presented.

In chapter four the antinucleon-nucleon interaction is tackled in the same manner as the pion-nucleon inetarction. A folding approach is presented and microscopic models are briefly introduced, namley the Jülich/Bonn, the Paris and the Nijmegen model. These models derive their description from G-parity transformed nucleon-nucleon potentials and additional antinucleon-nucleon terms. Due to limitations to rather low energies a simple phenomenological approach is presented, agreeing well with antiproton-proton cross section data. The findings of pion-nucleus and antinucleon-nucleus interactions are combined in chapter five to the description of pion production in antinucleon-annihilation by nuclei. Two different reaction mechanisms are presented.

2 Theory of Hadron-Nucleus Interactions

This chapter covers the bases which underly the models used within this work. First, the solution of the Klein-Gordon equation is derived by studying pion interactions as am exemple. Starting with an effective interaction Lagranian, the well-known Yukawa potential is derived. Extending the static *ansatz* by a time-dependency, the interaction is described by particle exchange. The one-meson-exchange theory builds a theory using mesons as exchange particles leading to a description of the nucleon-nucleon (NN) interaction. The nucleon-nucleon interaction is relevant for the understanding of effects of the nuclear medium, and it also builds the basis of the microscopic models of Paris and Bonn. These models use the G-parity transformation of NN models to derive Anti-nucleon-nucleon potentials as introduced in section 4.1.2. The aim of this work is to develop a model describing both, the scattering of pions as an interesting reaction itself and the pion production in antiproton-nucleus annihilations within one framework.

2.1 The Optical Model

The optical model is inspired by the scattering of light on an obstacle. The refractive index changes due to the properties of the obstacle, making studies of the obstacles possible by detecting the light. We face a similar situation when particles scatter by a nucleus and the scattered particles are detected for nuclear structure studies. To analyze the nucleus, however, the interactions along the reaction must be well understood and reasonably described. The nucleus is composed of interacting nucleons, which are moving inside. With an increasing number of nucleons involved, the description of the scattering process gets more complicated. An exact solution of pion-nucleus scattering can not be calculated. Therefore, in this section some techniques and approximations will be introduced, which will help to approach the solution of the pion nucleus scattering problem. The major properties of this scattering problem are assumed to be based on free pion-nucleon interactions and on nuclear structure effects. Therefore, closely following [SS74, Klu91], the pion-nucleon scattering problem is briefly discussed and applied to a nuclear environment afterwards.

Starting point is the non-relativistic Schrödinger equation for free pion-nucleon scat-

tering:

$$H\psi(\boldsymbol{r}) = [H_0 + v_j(\boldsymbol{r})]\,\psi(\boldsymbol{r}) = E\psi \tag{2.1}$$

where the Hamiltonian H_0 is composed of the kinetic energy operators of the pion and of the nucleon $H_0 = K_\pi + K_N$. The potential v_j of eq. 2.1 describes a two-body interaction between the pion and the jth nucleon. At a large distance from the reaction centre, this potential will vanish, and the solution of eq. 2.1 becomes a plane wave $|\varphi\rangle$. The general solution of the full scattering problem $|\psi\rangle$, however, is a sum of the homogeneous solution (the plane wave) and the particular solution to the inhomogeneous equation. This general structure of the solution is typical for scattering processes, which can not easily been seen from eq. 2.1. It is convenient to transform the Schrödinger equation into an integral equation, namely the Lippmann-Schwinger equation using ket-vectors:

$$|\psi\rangle = |\varphi\rangle + G_0 v_j |\psi\rangle \tag{2.2}$$

where the Green's function $G_0 = 1/(E - H_0 + i\epsilon)$ carries the information about the boundary conditions. A very powerful tool is to use the free scattering operators t_j instead of the potential, leading to a more symmetric description in the sense that on the right hand side of eq. 2.2 the same ket-vectors occur:

$$|\psi\rangle = |\varphi\rangle + G_0 t_j |\varphi\rangle \tag{2.3}$$

In t_j, all possible processes are included, and it is connected to the potential in the following way:

$$t_j = v_j + v_j G_0 t_j. \tag{2.4}$$

Before the inner structure or possible solutions of t_j are discussed, this *ansatz* is embedded into the nuclear medium. The nucleons of the nucleus differ from the free nucleons mainly by the fact that they are bound and their location is spatially restricted. The discussion of surface effects we shift to 3.2.4 and assume infinite nuclear matter for now. The Hamiltonian is modified such, that it contains the target Hamiltonian H_A, where the subscript A indicates the mass number of the target nucleus. It enters into the Green's function $G = 1/(E - K_\pi - H_A + i\epsilon)$, which is modified by the nuclear medium. The interaction potential, however, is still assumed to be of two-body character, which leads us to the effective pion nucleon scattering operator

$$\tau_j = v_j + v_j G \tau_j = v_j + v_j \frac{1}{E - K_\pi - H_A + i\epsilon} \tau_j. \tag{2.5}$$

To derive the pion nucleus scattering operator T_A we need to collect all nucleons

$$T_A = \sum_{j=1}^{A} v_j + \sum_{j=1}^{A} v_j \frac{1}{E - K_\pi - H_A + i\epsilon} \tau_j \tag{2.6}$$

After replacing the potential by the τ_j operator and performing an iteration of eq. 2.6 [Klu91], we derive:

$$T_A = \sum_j \tau_j + \sum_{j,k}{}' \tau_j G \tau_k + \sum_{j,k,l}{}' \tau_j G \tau_k G \tau_l + \dots \tag{2.7}$$

Here, the notation of a primed sum is introduced, which stands for the exclusion of equal indices e.g. $j \neq k$. Eq. 2.7 is called multiple-scattering series and carries still the full complexity of the pion-nucleus many-body problem. Nevertheless, eq. 2.7 helps with the interpretation from the physics point of view: The pion-nucleus interaction is a sequence of medium affected pion-nucleon scattering events. The first term corresponds to scattering with one nucleon, the next term describes scattering on two nucleons and so forth. To reduce the complexity, we introduce briefly the concept of the optical potential. Within the framework of an optical potential, the many-body scattering problem is truncated to an effective one-body interaction described in a corresponding Schrödinger or Lippmann-Schwinger equation. The aim is to find a scattering amplitude which is an exact solution of the multiple-scattering series of πN scattering. To perform those calculations, it is necessary to introduce and discuss approximation schemes in the following.

Coherent Approximation In the following, excitations of the nucleus in the final state are neglected. Accordingly, the expectation value of the ground state $|0\rangle$ gives:

$$\left\langle 0 \left| T_A^0 \right| 0 \right\rangle = \left\langle 0 \left| \sum_{j=1}^{A} \tau_j \right| 0 \right\rangle + \sum_{k,j}{}' \left\langle 0 \left| \tau_k \frac{1}{E - K_\pi - H_A + i\epsilon} \tau_j \right| 0 \right\rangle + \dots \tag{2.8}$$

The equation above contains the full nuclear Hamiltonian, which fulfils the equation:

$$H_A |n\rangle = \epsilon_n |n\rangle \tag{2.9}$$

Now, intermediate nuclear excitations can be explicitly expressed in a multiple-scattering series:

$$\left\langle 0 \left| T_A^0 \right| 0 \right\rangle = \left\langle 0 \left| \sum_{j=1}^{A} T_A^j \right| 0 \right\rangle + \sum_{k,j}{}' \sum_n \langle 0|\tau_k|n\rangle \frac{1}{E - K_\pi - \epsilon_n + i\epsilon} \langle n|\tau_j|0\rangle + \dots \tag{2.10}$$

The probability to scatter the incident pion with the same nucleon twice is small, because very large momentum transfer is needed to get such large angles involved. However, the pion might scatter on two nucleons, which has a non-neglicible effect as discussed in 3.2.4. If there are no shell-model correlations [Klu91], only the ground state $n = 0$ contributes, and the nucleus remains in the ground state throughout the scattering event. Therefore, the expectation value of T_A gives:

$$\left\langle 0 \left| T_A^0 \right| 0 \right\rangle = A \left\langle 0 \left| \tau_j \right| 0 \right\rangle + (A-1) \langle 0|\tau_j|0\rangle \frac{1}{E - K_\pi - \epsilon_0 + i\epsilon} \left(\frac{A}{A-1} \langle 0|T_A^0|0\rangle \right), \tag{2.11}$$

where the optical potential is defined by:

$$U_{\text{opt}} = \left\langle 0 \left| \sum_{j=1}^{A} \tau_j \right| 0 \right\rangle = A\langle 0|\tau_j|0\rangle \tag{2.12}$$

To calculate the expectation value, the ground state wave function must be known. The antisymmetrisation of the wave function within a many-body system is challenging [Hü75]. In our approach, an eikonal *ansatz* is used for the wave function. In section 2.4 the derivation of such an Eikonal wave funktion is briefly introduced. Extensions to the standard Eikonal are discussed in section 3.3.3 along with effects of momentum dependent potentials. Consequences of complex potentials are presented in section 4.1.3.

Impulse Approximation The exact solution of 2.3 takes into account both, the scattering itself, but also the binding energy of the target nucleons. Finding a solution without approximations is too challenging, but within this work, the dynamics of the system and the nuclear structure and its spatial form are of interest. The impulse approximation disantagles the bounding effects from the two-body interaction and treats the nucleons as quasi-free. This is a plausible approximation because the incident energy of the pion is high compared to the nucleon binding energies. This argument is supported by the πN collision time, which is much shorter than the time associated with the nucleon motion. Therefore, the reaction mechanism is expected to be dominated by one-step processes, where the pion interacts only with one nucleon of the target nucleus. This will finally lead to a linear dependence on the nuclear density. Interactions with two nucleons lead to a quadratic dependence accordingly, as shown in section 3.2.4. Neglect of the binding energy of the nucleons is reflected in the truncation of the scattering operator to the free one:

$$\tau_j = t_j \tag{2.13}$$

Even within the impulse approximation, it is possible to consider binding effects after derivation of the transition matrix, as it is discussed in [Sch72].

No-Recoil Approximation If the incident energy of the pion is high, the nucleons are assumed to be frozen, which means that their positions are unchanged during the scattering process. As an illustration we calculate the expectation value for nucleon 1 with associated coordinates $\mathbf{R}_1$, $\mathbf{R}'_1$ and coordinates $\mathbf{r}$, $\mathbf{r}'$ referring to the projectile:

$$\langle \mathbf{r}', \mathbf{R}'_1|t_1|\mathbf{r}, \mathbf{R}_1\rangle \approx \langle \mathbf{r}', \mathbf{R}_1|t_1|\mathbf{r}, \mathbf{R}_1\rangle \delta^3(\mathbf{R}'_1 - \mathbf{R}_1) \tag{2.14}$$

$$= \delta^3(\mathbf{R}'_1 - \mathbf{R}_1) \int \mathrm{d}^3k \mathrm{d}^3k' e^{-i\mathbf{k}'\cdot(\mathbf{r}'-\mathbf{R}_1)} \langle \mathbf{k}'|t|\mathbf{k}\rangle e^{-i\mathbf{k}\cdot(\mathbf{r}'-\mathbf{R}_1)} \tag{2.15}$$

Lowest Order Optical Potential Putting all findings so far together, one gets

$$\langle \mathbf{r}'|t_{1C}|\mathbf{r}\rangle = \iint \mathrm{d}^3R_1\mathrm{d}^3R_1'\psi_1^*(\mathbf{R}_1')\langle \mathbf{r}', \mathbf{R}_1'|t_1|\mathbf{r}, \mathbf{R}_1\rangle\psi_1(\mathbf{R}_1) \tag{2.16}$$

$$= \iint \mathrm{d}^3k\mathrm{d}^3k' e^{-i\mathbf{k}'\cdot\mathbf{r}'}\langle \mathbf{k}'|t|\mathbf{k}\rangle \int \mathrm{d}^3R_1|\psi_1(\mathbf{R}_1)|^2 e^{-i(\mathbf{k}-\mathbf{k}')\cdot\mathbf{R}_1)}. \tag{2.17}$$

Referring to nucleon 1, summation over all nucleons leads to

$$\sum_{\alpha=1}^{A}\int |\psi_\alpha(\mathbf{R}_\alpha)|^2 e^{-i(\mathbf{k}-\mathbf{k}')\cdot\mathbf{R}_\alpha)}\mathrm{d}^3R_\alpha = A\int \rho(\mathbf{R})e^{-i(\mathbf{k}-\mathbf{k}')\cdot\mathbf{R})}\mathrm{d}^3R = A\rho(\mathbf{k}-\mathbf{k}') \tag{2.18}$$

which depends on the nuclear density ρ, which has the Fourier-transform $\rho(\mathbf{k}-\mathbf{k}')$. For a nucleus with arbitrary isospin and spin configuration and the pion isospin operator $\mathbf{t}_\pi$, the final optical potential in momentum space is [SS74]

$$\langle \mathbf{k}'|V|\mathbf{k}\rangle A\rho(\mathbf{k}-\mathbf{k}')\left[\langle \mathbf{k}'|t_0|\mathbf{k}\rangle + \frac{1}{A}\langle \mathbf{k}'|t_s|\mathbf{k}\rangle \mathbf{I}\cdot\mathbf{k}\times\mathbf{k}' + \langle \mathbf{k}'|t_T|\mathbf{k}\rangle \mathbf{T}\cdot\mathbf{t}_\pi\right] \tag{2.19}$$

This is a very important result, in the sense that it will build the basis of the potential to describe the pion-nucleus interaction 3.56. As a first order potential, eq. 2.19 depends on the nuclear density linearly. For more involved considerations, higher orders in the nuclear density will become of importance, as will be seen later in section 3.2.4. In addition to the nuclear density, the optical potential depends on the two-body pion-nucleon t-matrix and on the spin and isospin configuration of the pion-nucleus system. The properties of the pion and the pion-nucleon system are summarized in section 3.1.

In this section we have discussed the scattering of a pion with a nucleus within the scope of a complex many-body approach resulting in a comparatively simple phenomenological optical potential. The derived optical potential separates the nuclear properties from the reaction mechanism. The nuclear density takes into account nuclear properties, and the reactions are described by an effective pion-nucleon interaction. Several approximations have been introduced to make calculations manageable more easily. Those simplifications have been used frequently and are approved in the low-density region and for pions with high kinetic energy. When the pion is scattered by the nucleus the absorption domiantes the interaction and the pion can not penetrate deeply into the nucleus, as shown in our results, in section 3.4. This work, however, is also directed towards the pion creation within antinucleon-nucleus interactions. The annihilation causes also a surface dominance of the interaction, but the trajectories of the produced pions might also point in the direction of the center of the nucleus, rather than escaping trough the low-density region. Therefore, an advanced treatment of the density-dependence is discussed in section 3.2.4.

While in this section we discussed a general structure of the potential derived in a many-body approach, we will examine general aspects of the Klein-Gordon equation and its solution for exploratory studies within a field-theoretical framework in the following section.

2.2 The Klein-Gordon Wave Equation

Pions and (anti-)nucleons are composed of quarks, and their interaction is based on the strong force. The corresponding fundamental theory to describe strong interactions is quantum chromo dynamics (QCD), where quarks and gluons build the basis of the description. In this work, however, hadronic degrees of freedom are used, mainly due to two facts: First, in a low and intermediate energy range the inner structure of pions and (anti-)nucleons can not be resolved. And second, a description of hadron dynamics on a quark level is nowadays possible on the lattice [EM12], but complex reactions involving several hadrons are both time- and computing-power-consuming, which makes it effective to work with microscopic models using hadronic degrees of freedom.

Microscopic models work with effective degrees of freedom, treating hadrons as elementary, structureless particles. There has been a lot of success describing NN and $\pi\, N$ reactions in this so called One Boson Exchange (OBE) models. As the name already suggests the strong force (or rather the whole interaction) is described in terms of boson exchange. This theory is built on the theoretical investigations of Hideki Yukawa. In this approach, the lightest bosons, namely the pions, are the mediator of the strong force. Later, one found that pions, due to their low mass, are well suited to describe the long-range part of the NN interaction, while the exchange of heavier mesons made the breakthrough in the description of the short-range area. These theoretical investigations are usually built in a field theoretical framework. In quantum mechanics, Dirac could succeed with introducing Dirac-spinors, where particles and also antiparticles could be treated in one theory, with all their spin and isospin properties. In quantum theory, the second quantisation is a powerful tool to express potentials and their connected Hamiltonians with creation and destruction-operators, defining the characteristics of specific states. In field theory, one takes one step further, and all particles are treated as fields. The guideline, how to implement such fields to a reaction and how interactions in general are treated is shown in the following.

The pion field: mediator of the strong force Field theory is a very powerful theory which can describe many phenomena in physics. There are mainly two types of field theories: the classical field theories and the quantum field theories. The classical field theories are often applied to electromagnetic problems, while the quantum field theory is heavily discussed in quantum chromo-dynamical frameworks nowadays. In both classical and quantum field theory one usually aims for the Lagrangian density or Hamilton operator which then lead to the equation of motion. In this work, we will use an effective field theory, where the underlying quark and gluon effects enter into effective couplings and form factors. Therefore the pion, the nucleon and so forth are treated as elementary particles.

This section is organized as follows: first, we would like to discuss basic aspects of a

field in case of a free pion field, and second, we will study the response of the pion field to an external disturbance, closely following [dWS86]. In the following the pion field will be introduced and general aspects of interactions with it. Before mathematical aspects and Feynman diagrams will be discussed, it is necessary to clarify what a field is. A field describes physical particles, but in addition it also acts as a mediator of a force. The pion field is denoted by ϕ and enters into the Lagrangian, which in the case of a free pion looks like this:

$$\mathcal{L} = -\frac{1}{2}\left(\partial_\mu \phi\right)^2 - \frac{1}{2}m^2\phi^2. \tag{2.20}$$

The Lagrangian is Lorentz-invariant and a scalar. To derive the equation of motion, the Lagrangian is then implemented into the Euler-Lagrange equation

$$\partial_\mu \frac{\partial \mathcal{L}}{\partial(\partial_\mu \phi)} - \frac{\partial \mathcal{L}}{\partial \phi} = 0. \tag{2.21}$$

Because the pion is a spin 0 particle and it is treated relativistically the expected Klein-Gordon equation

$$\Box\phi - m^2\phi = 0 \tag{2.22}$$

is derived, where $\Box = \partial_\mu^2 = \nabla^2 - \partial_t^2$.

Solution of the Klein-Gordon equation with source term The purpose of our studies, however, is to get a better understanding of the interaction of the pion with a medium. Therefore, an external disturbance to the free pion field is applied and its response is examined. For the Lagrangian, it is assumed

$$\mathcal{L} = -\frac{1}{2}\left(\partial_\mu \phi\right)^2 - \frac{1}{2}m^2\phi^2 + J\phi \tag{2.23}$$

which leads to the following equation of motion

$$(\Box - m^2)\phi = -J \tag{2.24}$$

with an external source term J. The solution of the Klein-Gordon equation with source term is composed of the homogeneous solution (with $J = 0$) and the particular solution of the disturbed differential equation. In a physical picture this means that the field of a free pion denoted by ϕ_0 is modified by the interaction $\delta\phi$

$$\phi = \phi_0 + \delta\phi. \tag{2.25}$$

The field of a free pion is known, but in the following $\delta\phi$ will be in focus. Because J in 2.24 has the same structure as a charge current in electromagnetics the solution is

constructed accordingly by using the Green's function $G(x)$. The Green's function is a solution of

$$(\Box - m^2)G(x) = \mathrm{i}\delta^4(\mathrm{x}) \tag{2.26}$$

with the four dimensional δ-distribution, which is given in the Dirac representation

$$\delta^4(x) = \frac{1}{(2\pi)^4}\int \mathrm{d}^4k\mathrm{e}^{\mathrm{i}k\cdot x}. \tag{2.27}$$

By comparison it is straightforward to construct the Green's function in such a way that it solves 2.26

$$G(x) = \frac{1}{\mathrm{i}(2\pi)^4}\int \mathrm{d}^4k\frac{\mathrm{e}^{\mathrm{i}k\cdot x}}{k^2+m^2} \tag{2.28}$$

Finally a general solution of the Klein-Gordon equation with a source term of 2.24 is derived:

$$\phi(x) = \phi_0(x) + \int \mathrm{d}y\mathrm{i}G(x-y)J(y). \tag{2.29}$$

To be able to interpret the solution on a physics level, a concrete source term of a static piont-like source will be discussed as an explicit example in the following. The point-like source term is located at $\boldsymbol{r}_0$

$$J(\boldsymbol{x},t) = g\delta^3(\boldsymbol{x}-\boldsymbol{r}_0) \tag{2.30}$$

The deviation caused by the point-like source is:

$$\delta\phi = \mathrm{i}g\int \mathrm{d}^4yG(x-y)\delta^3(\boldsymbol{x}-\boldsymbol{r}_0) \tag{2.31}$$

$$= \frac{g}{(2\pi)^3}\int \mathrm{d}^3k\frac{\mathrm{e}^{\mathrm{i}\boldsymbol{k}\cdot(\boldsymbol{x}-\boldsymbol{r}_0)}}{\boldsymbol{k}^2+m^2} \tag{2.32}$$

$$= \frac{g}{8\pi^2 r}\int_{-\infty}^{+\infty}\mathrm{d}k\left(\frac{1}{k+\mathrm{i}m}+\frac{1}{k-\mathrm{i}m}\right)\mathrm{e}^{\mathrm{i}k\cdot r} \tag{2.33}$$

After performing contour integration in the upper half of the complex k plane, the final result gives

$$\delta\phi(x) = \frac{g}{4\pi r}\mathrm{e}^{-mr}. \tag{2.34}$$

If one considers two point-like sources, the calculation results in the Yukawa potential, named after Hideki Yukawa, who predicted a particle acting as a mediator of the strong force with a mass about 100 MeV. This particle was later discovered as the pion with a mass of about 140 MeV. This was a breakthrough in understanding the long-range characteristics of the strong interaction, and Hideki Yukawa was honered with the Nobel Prize. In addition, this potential inspired and built the basis of all boson exchange models, where the bosons act as mediator of a force between two sources. As has already been mentioned, fields also have a particle interpretation, which we would like to discuss in the following

The pion field: particle interpretation, its mathematical implementation and the Feynman rules To deepen the understanding of the pion field, the external source will no longer be restricted to be static, but be time dependent. Writing the time dependence explicitly

$$\delta\phi(x) = \int \mathrm{d}^3k \mathrm{e}^{\mathrm{i}\boldsymbol{k}\cdot\boldsymbol{x}} \int \mathrm{d}k_0 \mathrm{e}^{-\mathrm{i}k_0 t} \frac{J(\boldsymbol{k}, k_0)}{\boldsymbol{k}^2 + m^2 - k_0^2}. \tag{2.35}$$

The factor $\mathrm{e}^{-\mathrm{i}k_0 t}$ characterises the intrinsic time scale in which the source variations take place. If the rest of the integrand is regular, $\delta\phi$ will be zero due to the Riemann-Lebesgue theorem. Therefore, only the poles of 2.35 will survive the quick oscillations at large values of $|t|$. These contributions are plane waves whose energies and momenta obey the dispersion relation

$$k_0^2 - \boldsymbol{k}^2 - m^2 = 0. \tag{2.36}$$

The poles introduced by 2.36 correspond to real particles. All contributions to the propagator which do not obey 2.36 are called virtual. This will become more clear when the actual integration is performed and details about the mathematical calculation are revealed. The integral occurring in 2.35 has the form

$$I(t) = \int_{-\infty}^{+\infty} \mathrm{d}k_0 \mathrm{e}^{-\mathrm{i}k_0 t} f(k_0) \tag{2.37}$$

and can be solved by contour integration. The contour integration is calculated by shifting the integration contour from the real axis to a, into the lower half of the complex k_0-plane, displayed in fig. 2.1. The integrand of 2.37 is not changed as long as the contribution vertical to the real axis vanishes, then

$$I(t) = \mathrm{e}^{-at} \int_{-\infty}^{+\infty} \mathrm{d}k_0 \mathrm{e}^{-\mathrm{i}k_0 t} f(k_0 - \mathrm{i}a) + \oint_C \mathrm{d}k_0 \mathrm{e}^{-\mathrm{i}k_0 t} f(k_0). \tag{2.38}$$

The contour integral will mainly give the poles due to Cauchy's residue theorem:

$$\oint_C \mathrm{d}k_0 \mathrm{e}^{-\mathrm{i}k_0 t} f(k_0) = 2\pi\mathrm{i} \sum_n \mathrm{e}^{-\mathrm{i}\omega_n t} f(\omega_n) \tag{2.39}$$

where ω_n give the location of the poles of $f(k_0)$. If there is more than one pole, the one closest to the real axis will dominate the asymptotic behaviour. Mathematically, negative times are also allowed and can be handled in the same way by shifting the integral contour into the upper k_0-plane, accordingly. The poles appear at $k_0 = \pm\omega(\boldsymbol{k}) = \sqrt{\boldsymbol{k}^2 + m^2}$. The poles shifted into the upper k_0-plane will dominate

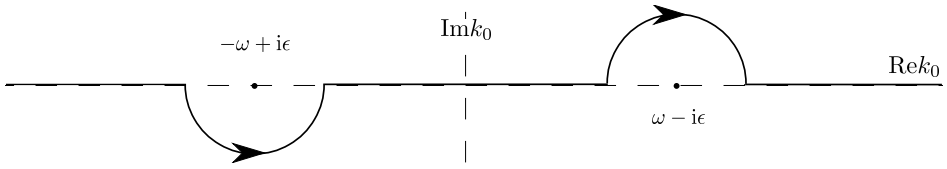

Figure 2.1: Schematic demonstration of contour integral

the asymptotic behaviour at large negative time, while shifting the poles into the lower k_0-plane will give the dominance of asymptotic behaviour at large positive time. Because poles belong to real quantum mechanical particles, the system is asymptotically dominated by a quantum mechanical wave moving with momentum $\boldsymbol{k}$ and energy $\omega(\boldsymbol{k})$ at large positive time. In addition, the contributions from $k_0 = -\omega(\boldsymbol{k})$ should be suppressed. This is achieved by shifting the $k_0 = \omega(\boldsymbol{k})$ slightly below the real axis and move the $k_0 = -\omega(\boldsymbol{k})$ contribution above the real axis. The integrand of eq. 2.35 gives:

$$\mathrm{e}^{\mathrm{i}\boldsymbol{k}\cdot\boldsymbol{x}} \int \mathrm{d}k_0 \frac{\mathrm{e}^{-\mathrm{i}k_0 t} J(\boldsymbol{k}, k_0)}{\boldsymbol{k}^2 + m^2 - k_0^2} = \begin{cases} 2\pi\mathrm{i} J\left(\boldsymbol{k}, \omega(\boldsymbol{k})\right) \exp[\mathrm{i}(\boldsymbol{k}\cdot\boldsymbol{x} - \omega(\boldsymbol{k})t)]/(2\omega(\boldsymbol{k})) & k_0 = +\omega(\boldsymbol{k}) \\ 2\pi\mathrm{i} J\left(\boldsymbol{k}, -\omega(\boldsymbol{k})\right) \exp[\mathrm{i}(\boldsymbol{k}\cdot\boldsymbol{x} + \omega(\boldsymbol{k})t)]/(2\omega(\boldsymbol{k})) & k_0 = -\omega(\boldsymbol{k}) \end{cases} \tag{2.40}$$

Solution 2.40 introduces two kind of scenarios. Either the particle is emitted with momentum $\boldsymbol{k}$ by a source $J(\boldsymbol{k})$ or the particle with momentum $-\boldsymbol{k}$ is absorbed by the source. If two sources are considered, the Greens function becomes the mediator of the force between those two sources. With this *ansatz*, the full emission and absorption scenario can be described. The emitted wave of the first source carries its intrinsic properties to the second source, where it is absorbed. The Greens function is therefore called propagator.

$$G(x) = \frac{\mathrm{i}}{(2\pi)^4} \int \mathrm{d}^3k \mathrm{e}^{\mathrm{i}\boldsymbol{k}\cdot\boldsymbol{x}} \int\limits_{C_-} \mathrm{d}k_0 \frac{\mathrm{e}^{-\mathrm{i}k_0 t}}{k_0^2 - \omega(\boldsymbol{k})^2 + \mathrm{i}\epsilon}, \qquad t > 0, \tag{2.41}$$

$$G(x) = \frac{\mathrm{i}}{(2\pi)^4} \int \mathrm{d}^3k \mathrm{e}^{\mathrm{i}\boldsymbol{k}\cdot\boldsymbol{x}} \int\limits_{C_+} \mathrm{d}k_0 \frac{\mathrm{e}^{-\mathrm{i}k_0 t}}{k_0^2 - \omega(\boldsymbol{k})^2 + \mathrm{i}\epsilon}, \qquad t < 0. \tag{2.42}$$

Pictographically this is expressed in a Feynman graph. The solution valid for negative time is identified with an antiparticle, while the solutions for positive time describes a particle. The great advantage of using Feynman diagrams is that they are understandable intuitively, even though the underlying mathematical structure can be very complex.

In this section, we discussed the pion in a field-theoretical approach. In vacuum, the pion is described by a field which satisfies the free Klein-Gordon equation. In addition to the description of physical particles, the pion field can also be the mediator of the strong force. This is already clear from its response to two static, point-like

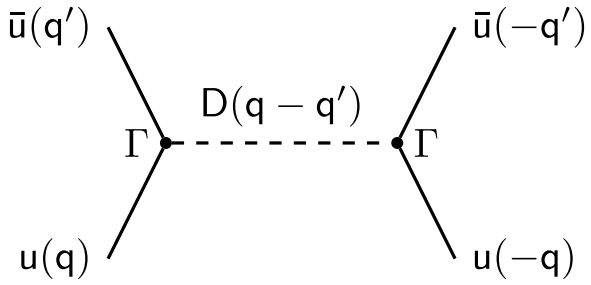

Figure 2.2: Schematic demonstration of lowest order Feynman-diagrams for one-meson exchange potentials

external sources leading to the Yukawa-Potential. The study of the time dependence of an external source leads to the definition of virtual and real particles. Those findings are then summarized in Feynman diagrams, which take care of the full physical interpretation and the mathematical structure. It also expresses the propagation of antiparticles which travel backwards in time. The Feynman rules are therefore a very powerful tool to study possible contributions to the interaction from the exchange of virtual particles.

2.3 Meson Exchange Theory

Our interest is directed towards the understanding of the pion-nucleon and the (anti-)nucleon-nucleon interaction. (Anti-)nucleon-nucleon and pion-nucleon interactions are described by different potentials, but they are connected via rotation in Mandelstam-space as discussed in [RHKS96]. To understand in-medium effects, like those which are visible in our results in section 3.4, a basic knowledge of NN interaction is helpful. The NN interaction also enters indirectly to the nuclear densties, which accompany all our potentials. Using the G-parity transformation of the NN potentials leads to a contribution to microscopic antinucleon-nucleon potentials developed by the groups from Paris and Jülich/Bonn briefly introduced in section 4.1.2. In this section, the NN interaction is, therefore, in the focus of the discussion, but the general form and the way to construct the Lagrangians from particle exchange are very similar.

The meson exchange potential $V_\alpha(\mathbf{q}, \mathbf{q}\,')$, where α stands for any possible mesons exchanged, $\alpha = \pi, \rho, \sigma, \ldots$, has the general structure

$$V_\alpha = g_1 \bar{u}_1(\mathbf{q}\,')\Gamma_1 u_1(\mathbf{q}) D_\alpha(q - q') g_2 \bar{u}_2(-\mathbf{q}\,')\Gamma_2 u_2(-\mathbf{q}), \tag{2.43}$$

as is shown schematically in fig. 2.2. In this notation, u_i ($\bar{u}_i$) are the incoming (outgoing) particle-fields, while Γ_i denotes the vertex-function and D_α the meson propagator:

$$D_\alpha = \frac{d_\alpha}{(q - q')^2 - m_\alpha^2}, \tag{2.44}$$

where d_α depends on the type of the exchanged meson. To construct an interaction Lagrangian there are symmetries which need to be fulfilled and are therefore crucial for the structure of e.g. the vertex-functions. The constructed Lagrangians need to fulfil the Lorentz invariance and be scalar. To build a Lagrangian, bilinear forms of $\bar{\psi}(x)\Gamma\psi(x)$ with definite Lorentz-transformation properties are required. The possible bilinear covariants [NV86] are:

$\bar{\psi}'(x)\psi'(x)$	scalar
$\bar{\psi}'(x)\gamma_5\psi'(x)$	pseudo-scalar
$\bar{\psi}'(x)\gamma^\mu\psi'(x)$	vector
$\bar{\psi}'(x)\gamma_5\gamma^\mu\psi'(x)$	axial vector
$\bar{\psi}'(x)\sigma^{\mu\nu}\psi'(x)$	second rank tensor

Depending on the particle coupling to the nucleon, the Lagrangian is composed of one or several bilinear covariants above. The Lagrangians are derived in a field-theoretical approach by symmetry considerations. The Lagrangian densities are scalar functions and Lorentz invariant. According to the basic tree Feynman diagrams, the interactions are constructed from the particle fields themselves, the coupling and the propagator of the exchanged particle.

This interaction can be described effectively by an exchange of a meson, just like the photon is the mediator of the electromagnetic interaction. The crucial point is that the meson carries a mass, and as a consequence, the range, calculated from the Compton wavelength, is finite, even short-ranged. The pion (as the lightest boson) expresses in this picture the long-range part of the interaction. Accordingly, the exchange of heavier mesons (σ) can be used for the description of the intermediate-range part of the NN interaction. Depending on the quantum numbers of the mesons and the way they couple to the nucleon, they give different contributions to the interaction, like in fig. 2.3.

The ordering of the diagrams is difficult and the complexity increases with energy, because more and more particles can be produced. Because there are infinite diagrams to consider in an effective theory, one treats specific channels explicitly and use a

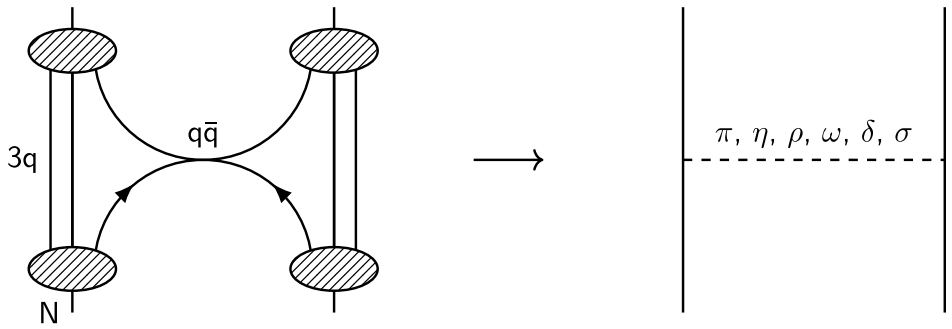

Figure 2.3: Pictographic display of the one meson exchange theory, like [MP00]

phenomenological *ansatz* for all other contributions. Even though this procedure is very powerful also in the NN interaction as has been shown by Jülich, Paris and Nijmegen groups, these models are limited to an incident kinetic energy of the pion of about 300 MeV. The reason is that, in case of NN and πN interactions, the Δ and many more channel thresholds are reached and it is impossible to include all reactions.

For completeness, an example of an one-pion exchange (OPE) potential is shown [EW88]:

$$V_{OPE} = \frac{1}{3} m_\pi c^2 \frac{f^2}{4\pi c} \frac{\mathrm{e}^{-\mu r}}{\mu r} \left(\vec{\boldsymbol{\sigma}}_1 \cdot \vec{\boldsymbol{\sigma}}_2 + \left[1 + \frac{3}{\mu r} + \frac{3}{(\mu r)^2} \right] \boldsymbol{S}_{12} \right) \vec{\boldsymbol{\tau}}_1 \cdot \vec{\boldsymbol{\tau}}_2 \tag{2.45}$$

$$\mu = m_\pi c = \frac{1}{\lambda_{C,\pi}} \tag{2.46}$$

where the Yukawa function $\exp(-\mu r)/\mu r$ is characteristic for the exchange of massive mesons and gives the typical finite range behaviour of the NN interaction. f is the coupling constant which gives the strength of the interaction between the nucleon and the corresponding exchanged meson. $\vec{\boldsymbol{\sigma}}_{1,2}$ ($\vec{\boldsymbol{\tau}}_{1,2}$) are the spin (isospin) pauli matrices and $\boldsymbol{S}_{12}$ the tensor component. This effective description of the NN interaction comes to its limits at very short ranges, when the relevant degrees of freedom change. When the distance between the two nucleons becomes smaller than 1 fm, their density distributions have a large overlap, and the underlying quark- and gluon-dynamics come into play. To take care of this phenomenologically, extra terms like cut-off functions are introduced. The newly introduced parameters are fixed with experimental data.

One basic rule in QCD is that any formed object must be colourless, or so-called white. The necessity of the colour quantum number can be understood by analysing the Ω^{--}. Quarks are fermions, and therefore obey the Pauli-principle: Two fermions of the same kind cannot occupy the same state. In addition, the wave function of a fermion must be antisymmetric. All quarks of the Ω^{--} have the same flavour and charge, but different colour.

Similar to the interaction between neutral atoms via the Van-der-Waals interaction the white nucleons interact via an effective interaction, induced by the strong force. Therefore, in understanding the nucleon-nucleon interaction lies the link between the fundamental QCD and corresponding effective theories. In the case of atoms nowadays it is possible to derive the atom-atom interaction from numerical solutions of the quantum mechanical many-electron-problem, but the extraction of nucleon-nucleon interaction from solving QCD relies usually on either truncations or on specific assumptions. The impressive success gained within Lattice-QCD frameworks [EM12] is still quite time- and computational-power-consuming. Therefore, it is worthwhile to look into the properties of the NN interaction, which are already known from experiments, to build a basis of a phenomenological model.

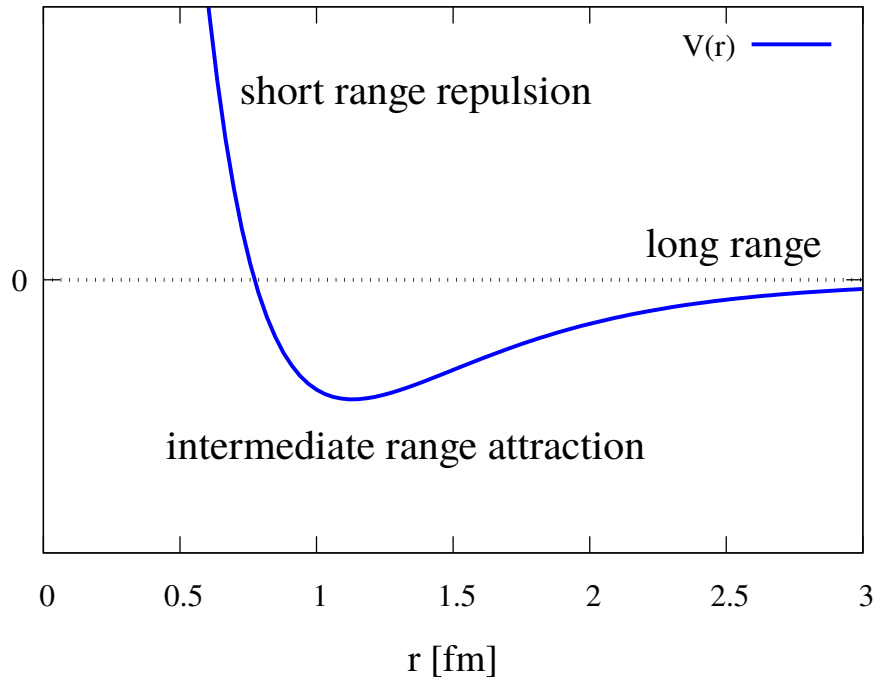

Figure 2.4: The exchange of pions dominates the long-range part of the central potential and is also responsible for a strong tensor contribution in the long-range part. The σ meson is used to describe the intermediate-range attraction and can be understood as effectively describing correlated two-pion exchange. The vector mesons (such as δ) contribute to the repulsive core. Identifying the contributing exchange-particles, the pion-nucleon potential is derived in a similar way [SHS+95].

In the following some facts about the NN interaction are collected to build an *ansatz* for a nucleon-nucleon potential. The NN-interaction potential can be divided into three characteristic sections: the short range part ($|r| < 1$ fm), the intermediate range ($|r| = 1 - 2$ fm) and the long range part ($|r| > 1$ fm).

short-range Figure 2.4 indicates a repulsion at small distances. The analyses of the phase show a change of sign from positive to negative. Therefore, at small momenta with corresponding large distances between the nucleons, the interaction is attractive, while for large momenta with corresponding small distances, the interaction is repulsive. A repulsion at small distances also means that increasing force is required to bring nucleons closer together. This is also seen in the saturation of the nuclear density. However, the saturation is mainly caused by the Pauli-blocking.

intermediate range The intermediate range of the NN-potential shows a minimum at about 1 fm seen in fig.2.4. This is due to the fact that bound nuclei exist. The average distance between neighbouring nucleons is of the order of $1-2$ fm, which can be extracted from the nuclear matter density of about $\rho_0 = 0.17$ fm^{-3}, and therefore gives the scale in which the NN interaction is attractive.

long range The interaction between two nucleons dies out quite quickly, which can be seen in fig.2.4. This is because the NN interaction is of short-range character. This is also seen in the scaling-behavior of the binding energy. The binding energy is mostly proportional to the mass number, rather than scaling with the number of interaction partners (A(A-1)/2). This indicates that the nucleon interacts with a constant number of neighbours and therefore the long-range part of the potential reaches zero already at small distances of less than 3 fm. Despite the properties discussed above which are characteristic for their individual intervals, there are additional properties, which are of general character. First, the tensor part of the nucleon-nucleon interaction, and second, the spin-orbit effects. The non-vanishing quadrupole moment and the magnetic moment of the deuteron indicate, that the ground state has not only s-wave contributions, but also a component of d-wave character. This mixture can only appear in a non-central interaction, where matrix elements with different angular momenta are not equal to zero. The so called Tensor interaction is the simplest form to cause these effects.

Alltogether, these arguments have consequences for the mathematical structure of the involved Hamiltonian, which will only be briefly mentioned. The Hamilton operator must be: hermitian, invariant against particle exchange, translational invariant, Galilei invariant, rotational invariant, time translation invariant, invariant against time reversal, parity invariant and independent of electric charge. After taking these constraints into account, an *ansatz* for the NN potential can be composed by three potentials

$$V_{NN} = V_Z + V_T + V_{LS} \tag{2.47}$$

where V_Z is the central part of the interaction, V_T the tensor part and V_{LS} the contribution from spin-orbit effects. The central potential V_Z is expressed in terms of spin and isospin potentials

$$V_Z = \sum_{S,T=0,1} V_{ST} \left[\vec{\boldsymbol{\sigma}}_1 \cdot \vec{\boldsymbol{\sigma}}_2\right]^S \left[\vec{\boldsymbol{\tau}}_1 \cdot \vec{\boldsymbol{\tau}}_2\right]^T \tag{2.48}$$

$$= V_{00} + V_{01}\vec{\boldsymbol{\tau}}_1 \cdot \vec{\boldsymbol{\tau}}_2 + V_{10}\vec{\boldsymbol{\sigma}}_1 \cdot \vec{\boldsymbol{\sigma}}_2 + V_{11}\vec{\boldsymbol{\sigma}}_1 \cdot \vec{\boldsymbol{\sigma}}_2\vec{\boldsymbol{\tau}}_1 \cdot \vec{\boldsymbol{\tau}}_2 \tag{2.49}$$

which can also be represented by spin and isospin projectors

$$V_Z = V_W + V_B \mathrm{P}_{\boldsymbol{\sigma}} + V_H \mathrm{P}_{\boldsymbol{\tau}} + V_M \mathrm{P}_{\boldsymbol{r}} \tag{2.50}$$

where the notation comes from corresponding findings about the NN force: Wigner (W), Bartlett (B), Heisenberg (H), and Majorana (M). While V_W does not contain contributions from exchange of spin or isospin, V_B is connected to spin exchange, V_M to isospin exchange and V_H to the combination of both. The tensor part of the NN potential has the following structure

$$V_T = [V_1 + V_\tau \vec{\boldsymbol{\tau}}_1 \cdot \vec{\boldsymbol{\tau}}_2] \, \boldsymbol{S}_{12} \tag{2.51}$$

$$\boldsymbol{S}_{12} = \frac{3}{r^2} [\vec{\boldsymbol{r}} \cdot \vec{\boldsymbol{\sigma}}_1] [\vec{\boldsymbol{r}} \cdot \vec{\boldsymbol{\sigma}}_2] - \vec{\boldsymbol{\sigma}}_1 \cdot \vec{\boldsymbol{\sigma}}_2 \tag{2.52}$$

and the spin orbit contribution can be expressed as follows

$$V_{LS} = [V_1 + V_\tau \vec{\boldsymbol{\tau}}_1 \cdot \vec{\boldsymbol{\tau}}_2] \, \vec{\boldsymbol{L}} \cdot \vec{\boldsymbol{S}} \tag{2.53}$$

$$\vec{L} = \vec{r} \times \vec{p} \tag{2.54}$$

$$\vec{S} = \vec{s}_1 + \vec{s}_2 = \frac{1}{2} (\vec{\boldsymbol{\sigma}}_1 + \vec{\boldsymbol{\sigma}}_2) \tag{2.55}$$

At present there is a large variety of potentials, which are of almost equal quality. This is due to the fact that the potential must be extracted from phases, which makes it an inverse scattering problem. The solution is not unique, or in other words: there is an infinite number of potentials which lead to the same phase.

2.4 Eikonal Approach to the Wave Equation

The Eikonal approximation is used to describe a scattering process. The approximation works best for high-energy scattering, where the projectiles are mainly scattered in forward direction. Initially, the Eikonal theory was introduced by [Bru95], who worked on the scattering of light with atoms. This idea was taken over by [GBD67], who applied the techniques used in Eikonal theory to scattering of particles with the nucleus. In this work, the Eikonal approximation is used to describe the scattering of both pions and antinucleons with various nuclei. The main idea of the Eikonal approximation is to use an *ansatz* for the wave function

$$\psi = e^{\mathrm{i}\tilde{S}} = e^{\mathrm{i}S + \mathrm{i}kz} \tag{2.56}$$

Because the energy region of interest is high, small scattering angles are expected for the scattered wave. Therefore, cylindrical coordinates are used. The incident momentum k defines the z-direction, and the impact parameter b describes the distance to the nucleus, as can be seen in fig 2.5. The interaction is described within the optical model, which is taken into account by a potential U. The potential is then implemented into a wave equation. Within this work, both the pion-nucleus interaction and the antinucleon-nucleus interaction are calculated within the same framwork. Pions and antiprotons are usually described with different wave equations, namely the Klein-Gordon and the Dirac equation, but both are merged into a Schrödinger-like equation.

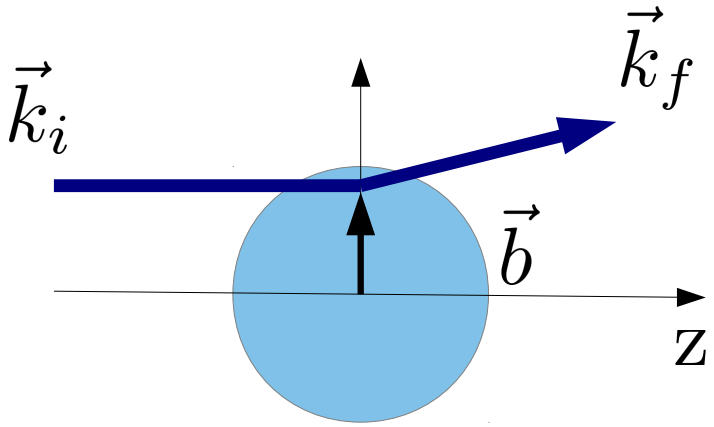

Figure 2.5: Schematic demonstration of scattering

Therefore, the introduction of the Eikonal theory and also the derivation of the Eikonal are presented with the Schrödinger equation.

The Eikonal- model got a lot of attention when [GM70] extended the original Eikonal method to use it within many-body interactions. Initially, the Eikonal-model was used to describe scattering of light. The Eikonal-method took advantage of the fact that the scattered light contains information about the target. In other words, when the scattered wave is understood, properties of the target can be studied. This was done successfully with the scattering of light on atoms, and many atoms were probed with this technique. Being so successful, the use of Eikonal models was extended to other research fields, for example nuclear scattering, where massive projectiles are used instead of massless photons. The Eikonal theory brings together two important ideas: on the one hand, the intuitive understanding, due to its origin in optics, where the behaviour of the wave can be described with geometrical help, and on the other hand, the quantum mechanical character, including the wave functions and phases.

In this work, the Eikonal model is used to find a description of scattering cross-sections. Before a brief summary of the mathematical background of the Eikonal theory is given and the derivation of the Eikonal is shown, a more intuitive way to approach the Eikonal theory is presented. Limitations of the Eikonal and the challenges to find higher-order corrections are discussed in section 3.3.3. The Eikonal approximation is especially well suited for scattering processes where the projectile has a high kinetic energy compared to its mass. In such scattering processes, small angles are expected in the final state. This goes well along with the picture of scattering of light, where the description is based on beams of light. Analogously, for an incoming wave in z-direction $\phi = \mathrm{e}^{\mathrm{i}kz}$, the outgoing wave is assumed to be a plane wave, but disturbed by the so-called Eikonal S in such a way that $\phi_f = \mathrm{e}^{\mathrm{i}(kz+S)}$. The disturbance depends on the influence of the target. The corresponding interaction is denoted by a potential U.

The Eikonal approximation may be implemented to any kind of wave equation, but in the following the Klein-Gordon equations is chosen:

$$[\nabla^2 + K^2]\phi = 0. \tag{2.57}$$

Using the Eikonal approximation, with corresponding derivatives:

$$\phi = \mathrm{e}^{\mathrm{i}\vec{k}\cdot\vec{r}+\mathrm{i}S(\vec{r})} \tag{2.58}$$

$$\vec{\nabla}\phi = \mathrm{i}\left(\vec{k} + \vec{\nabla}S\right)\phi \tag{2.59}$$

$$\nabla^2\phi = \left(-k^2 - \left(\vec{\nabla}S\right)^2 + \mathrm{i}\vec{\nabla}^2 S\right)\phi \tag{2.60}$$

leading to the Eikonal equation:

$$\mathrm{i}\vec{\nabla}^2 S - \left(\vec{\nabla}S\right)^2 + K^2 - k^2 = 0 \tag{2.61}$$

In order to solve the Klein-Gordon equation, a solution of S is needed, finally giving:

$$S = S_+ = \int_{-\infty}^{z} \mathrm{d}z' \sqrt{K^2 - k^2} \tag{2.62}$$

The solution is found under the assumption that $\nabla^2 S$ is small compared to S or even ∇S. This is reasonable, because a rather smooth behaviour of S is expected and the corresponding derivative of first and second order should be small. However, the discussion of consideration of higher order terms is in section 3.3.3.

Even though the structure of the solution is rather simple, it strongly depends on the included potential and its complexity. The constraints to the potential and the limits to the validity of the solution can be understood better by following the arguments of the derivation of the introduced solution, which is briefly discussed in the following.

To finally derive the cross section in Eikonal representation, the scattering amplitude is calculated from the wave function. The scattering amplitude is defined as:

$$f = -2\pi^2 \langle \phi_{k_f} | U | \phi_{k_i}^{(+)} \rangle \tag{2.63}$$

$$= -\frac{(2\pi)^{3/2}}{4\pi} \int \exp(-\mathrm{i}\vec{k}_f\vec{r}')U(\vec{r}')\phi_{k_i}^{(+)}. \tag{2.64}$$

Implementing the previously introduced wave function gives:

$$f_E = -\frac{1}{4\pi} \int \mathrm{d}\vec{r} \exp(-\mathrm{i}\vec{k}_f\vec{r})U(\vec{r}) \exp\left(-\mathrm{i}\vec{k}_i\vec{r} - \frac{1}{2k}\int_{-\infty}^{z} U(x,y,z')\mathrm{d}z'\right) \tag{2.65}$$

By substituting the wave vector transfer $\Delta = k_i - k_f$ into the equation above, we get [Joa75]

$$f_E = -\frac{1}{4\pi}\int \mathrm{d}\vec{r}\exp(-\mathrm{i}\vec{\Delta}\vec{r})U(\vec{r})\exp\left(-\frac{\mathrm{i}}{2k}\int_{-\infty}^{z} U(x,y,z')\mathrm{d}z'\right) \tag{2.66}$$

Using cylindrical coordinates, the decomposition of vector $\vec{r}$ reads

$$\vec{r} = \vec{b} + z\hat{k}_i \tag{2.67}$$

where b is an "impact parameter" and the z-component is chosen to be in the z-direction of the incident wave $\hat{k}_i$. The scalar product in 2.66 gives:

$$\vec{\Delta}\vec{r} = \vec{\Delta}(\vec{b} + z\hat{k}_i) = \vec{\Delta}\vec{b} + kz(1-\cos\theta) \approx \vec{\Delta}\vec{b} \tag{2.68}$$

As previously mentioned, from high-energy scattering, mainly forward scattering is expected, justifying the neglect of the term quadratic in θ. Nevertheless, it is still possible to achieve the relation of eq. 2.68 by choosing a more clever coordinate system. If the integration of z' is performed along the bisector of the scattering angle, accordingly

$$\vec{r} = \vec{b} + z\hat{n}. \tag{2.69}$$

The scalar product of $\vec{r}$ and $\vec{b}$ gives exactly $\vec{\Delta}\vec{b}$, because the vector $\hat{n}$ is perpendicular to $\vec{\Delta}$. Without approximation, the scattering amplitude gives [Joa75]:

$$f_E = \frac{k}{2\pi\mathrm{i}}\int \mathrm{d}^2\vec{b}\exp(\mathrm{i}\vec{\Delta}\vec{b})\left[\exp(\mathrm{i}\chi(k,\vec{b})) - 1\right] \tag{2.70}$$

where

$$\chi = -\frac{1}{2k}\int_{-\infty}^{+\infty} U(\vec{b},z)\mathrm{d}z \tag{2.71}$$

If the potential has cylindrical symmetry, the expression of the scattering amplitude can be simplified with the Bessel function

$$J_0(x) = (2\pi)^{-1}\int_0^{2\pi}\mathrm{d}\phi\exp(\mathrm{i}x\cos\phi) \tag{2.72}$$

which gives

$$f_E = \frac{k}{\mathrm{i}}\int_0^{\infty}\mathrm{d}b\; bJ_0(\vec{\Delta}\vec{b})\left[\exp(\mathrm{i}\chi(k,\vec{b})) - 1\right]. \tag{2.73}$$

Here the angular dependence was integrated out, leaving χ only depending on b and k. The meaning of χ (eq. 2.71) can be understood when the derived Eikonal scattering amplitude is compared to its expansion in partial waves

$$f(\theta) = \frac{1}{2\mathrm{i}k} \sum_{\ell=0}^{\infty} (2\ell+1)[\exp(2\mathrm{i}\delta_\ell(k)) - 1] P_\ell \cos\theta, \tag{2.74}$$

where $P_\ell \cos\theta$ are the Legendre-polynomials. Because high-energy scattering is considered, many partial waves of high order are expected to contribute significantly to the amplitude, so that the sum is replaced by an integral. Furthermore, the impact parameter is approximated by

$$b \simeq \sqrt{\ell(\ell+1)}/k \approx (\ell + 1/2) \tag{2.75}$$

giving

$$f(\theta) = k\mathrm{i} \int_0^\infty \mathrm{d}b \; bJ_0(2kb\sin(\theta/2)) \left[\exp(2\mathrm{i}\delta(k,b)) - 1\right] \tag{2.76}$$

With the help of the just found scattering amplitude, the scattering cross sections are calculated in the following. In order to give a more general formula, an (at this step unspecified) optical potential $U = V + \mathrm{i}W$ is considered. The total cross section is given by the optical theorem

$$\sigma_{tot} = \frac{4\pi}{k} \mathrm{Im} f(\theta = 0) = 2 \int \mathrm{d}^2 b [1 - \exp(-\mathrm{Im}\chi) \cos \mathrm{Re}\chi]. \tag{2.77}$$

With an azimuthal symmetric potential, the angular dependence can be integrated out, giving

$$\sigma_{tot} = 4\pi \int_0^\infty \mathrm{d}b \; b[1 - \exp(-\mathrm{Im}\chi) \cos \mathrm{Re}\chi]. \tag{2.78}$$

The total elastic cross section is given by

$$\sigma_{tot}^{el} = \int \mathrm{d}\Omega |f_E|^2. \tag{2.79}$$

After extension of the upper integration limit of the momentum transfer and the use of the completeness of the Bessel function [Joa75],

$$\sigma_{tot}^{el} = 4\pi \int_0^\infty \mathrm{d}b \; b[1 - \exp(-\mathrm{Im}\chi) \cos \mathrm{Re}\chi] - 2\pi \int_0^\infty \mathrm{d}b \; b[1 - \exp(-2\mathrm{Im}\chi)] \tag{2.80}$$

where azimuthal symmetry of U is again implied. While the first term in equation 2.80 gives exactly the result which was achieved beforehand for the total cross section, the second term has also an interpretation. Because the total cross section contains all processes, the subtraction of just the elastic scattering leaves only those contributions which are actual reactions.

$$\sigma_{tot}^{r} = 2\pi \int_0^\infty \mathrm{d}b \; b[1 - \exp(-2\mathrm{Im}\chi)] \tag{2.81}$$

Although, the description of these scattering cross sections is an approximation, covering mainly forward scattering, we are also interested in an angular distribution. The differential cross section is calculated in the following way:

$$\frac{\mathrm{d}\sigma}{\mathrm{d}\Omega} = |f_E|^2 \tag{2.82}$$

Finally, the scattering amplitude, the wave function and cross sections (both elastic and inelastic) are derived. To get these results, a smoothly varying potential was assumed i.e., the kinetic energy of the projectile is expected to be so high that possible fluctuations in the interacting potential are on a different scale. As can be seen later in this work, reasonable results can be achieved within the Eikonal model, but the limits of the model need to be understood as discussed in section 3.3.3.

3 Pion-Nucleus Interactions

3.1 Properties of the Pion

After introducing basic models and techniques of hadron-nucleus interactions, the focus in this chapter is to present more concrete approaches. To derive the pion-nucleus potential, we summarize some properties of the pion. First, we present the isospin structure and its consequences for the expected cross sections. Second, the partial wave decomposition is derived, leading us to the corresponding amplitudes. Finally, the self energy is briefly introduced. The following section covers the low-energy behavior, while the intermediate-energy range is described by the Kisslinger-potential presented afterwards. The consequences from the momentum dependent potentials are presented, and the potential is extended to higher resonance regions. Finally, the results are presented for several nuclei, covering a large energy range.

3.1.1 Isospin

The investigation of underlying symmetries of pion-nucleon interactions is helpful in two ways: First, the corresponding calculations may become easier to perform when the system's complexity is reduced, and second, the understanding of symmetries gives the possibility to make predictions beyond the existing data. In 1932 the fact that the proton and neutron have almost the same mass inspired Heisenberg to interpret them as different states of the same particle, the nucleon. This idea is only valid when the electromagnetic interaction is negligible, because the proton and neutron differ by their electric charge. However, when only the strong force is considered, they are indistinguishable particles. According to Noether's theorem, this underlying symmetry introduces an invariant, the isospin. The isospin is no observable, but a theoretical construct, where we need to chose the notation. Unfortunately, the choice of notation differs in the literature. Similar to the spin, only the magnitude I and one component of the isospin, I_3, can be specified simultaneously. Therefore, in this work the isospin is denoted by $|II_3\rangle$ and chosen for the nucleons in the following way:

$$p = \left|\frac{1}{2}\tau\ \frac{1}{2}\tau_3\right\rangle = \left|\frac{1}{2}\ \frac{1}{2}\right\rangle, \qquad n = \left|\frac{1}{2}\tau\ \frac{1}{2}\tau_3\right\rangle = \left|\frac{1}{2}\ -\frac{1}{2}\right\rangle \tag{3.1}$$

where we have chosen $\tau = 1$ and $\tau_3 = \pm 1$ to be an integer and write the factor $1/2$ explicitly. The isospin of the pion is defined accordingly, with total isospin $t = 1$ and

a third component which is equal to the pion charge.

$$\pi^- = |1\ -1\rangle\,, \pi^0 = |1\ 0\rangle\,, \pi^+ = |1\ 1\rangle \tag{3.2}$$

As has already been mentioned: Symmetries introduce invariances, and in fact, the isospin is an invariant in strong interactions. Vice versa, the knowledge of the isospin is also knowledge of underlying symmetries. The investigation of the isospin structure of the pion-nucleon interaction will therefore tell us something about the symmetries we can expect from the cross section. Therefore, we would like to exploit the derivation of the isospin-decomposition of each reaction in detail, to get a good understanding of the connection to the cross section. This is necessary, because we chose to work with isospin amplitudes, and by going beyond the Δ-resonance in energy we soon leave the (nowadays) experimentally accessible region. In this sense, the derived cross sections will be predictions. In our work, we are interested in elastic scattering, which will serve us as basis for the pion-nucleus interaction. In pion-nucleon interaction, however, there are six elastic processes:

$$\begin{array}{lrcl}
(a) & \pi^+ + p & \rightarrow & \pi^+ + p \\
(b) & \pi^0 + p & \rightarrow & \pi^0 + p \\
(c) & \pi^- + p & \rightarrow & \pi^- + p \\
(d) & \pi^+ + n & \rightarrow & \pi^+ + n \\
(e) & \pi^0 + n & \rightarrow & \pi^0 + n \\
(f) & \pi^- + n & \rightarrow & \pi^- + n
\end{array}$$

In addition to the elastic processes above, there are also four single charge exchange processes:

$$\begin{array}{lrcl}
(g) & \pi^0 + p & \rightarrow & \pi^+ + n \\
(h) & \pi^- + p & \rightarrow & \pi^0 + n \\
(i) & \pi^+ + n & \rightarrow & \pi^0 + p \\
(j) & \pi^0 + n & \rightarrow & \pi^- + p
\end{array}$$

These channels also carry isospin, which can be decomposed into the pion and nucleon isospin. To derive the total isospin of the reaction, we couple the isospin of nucleon and pion with the help of the Clebsch-Gordon coefficients. For our purposes, the coupling

of 1 and 1/2 is of importance. It is summarized in the following:

$$
\begin{aligned}
\pi^+ + p: &\quad \left|1 \quad 1\right\rangle \left|\frac{1}{2} \quad \frac{1}{2}\right\rangle &&= \left|\frac{3}{2} \quad \frac{3}{2}\right\rangle \\
\pi^0 + p: &\quad \left|1 \quad 0\right\rangle \left|\frac{1}{2} \quad \frac{1}{2}\right\rangle &&= \sqrt{\frac{2}{3}}\left|\frac{3}{2} \quad \frac{1}{2}\right\rangle - \sqrt{\frac{1}{3}}\left|\frac{1}{2} \quad \frac{1}{2}\right\rangle \\
\pi^- + p: &\quad \left|1 \quad -1\right\rangle \left|\frac{1}{2} \quad \frac{1}{2}\right\rangle &&= \sqrt{\frac{1}{3}}\left|\frac{3}{2} \quad -\frac{1}{2}\right\rangle - \sqrt{\frac{2}{3}}\left|\frac{1}{2} \quad -\frac{1}{2}\right\rangle \\
\pi^+ + n: &\quad \left|1 \quad 1\right\rangle \left|\frac{1}{2} \quad -\frac{1}{2}\right\rangle &&= \sqrt{\frac{1}{3}}\left|\frac{3}{2} \quad \frac{1}{2}\right\rangle + \sqrt{\frac{2}{3}}\left|\frac{1}{2} \quad \frac{1}{2}\right\rangle \\
\pi^0 + n: &\quad \left|1 \quad 0\right\rangle \left|\frac{1}{2} \quad -\frac{1}{2}\right\rangle &&= \sqrt{\frac{2}{3}}\left|\frac{3}{2} \quad -\frac{1}{2}\right\rangle + \sqrt{\frac{1}{3}}\left|\frac{1}{2} \quad -\frac{1}{2}\right\rangle \\
\pi^- + n: &\quad \left|1 \quad -1\right\rangle \left|\frac{1}{2} \quad -\frac{1}{2}\right\rangle &&= \left|\frac{3}{2} \quad -\frac{3}{2}\right\rangle
\end{aligned}
$$

With the knowledge of the isospin decomposition of each channel, we can now determine the matrix element, which will give us information about the cross section. As we have already discussed in the introduction of this section, the isospin is conserved in the strong interaction. Therefore, initial and final total isospin must be the same and are characteristic for each matrix element:

$$M_{fi} = \langle \psi_f | \, M \, | \psi_i \rangle \tag{3.3}$$

$$M_I = \langle \psi(I) | A_{if} | \psi(I) \rangle \tag{3.4}$$

which is finally connected to the cross section:

$$\sigma \propto |M_I|^2 \tag{3.5}$$

Each reaction channel is now described by a matrix element, which is composed of different isosspins with certain weights:

$$M_a = \quad M_{3/2} \tag{3.6}$$

$$M_b = \frac{2}{3} M_{3/2} + \frac{1}{3} M_{1/2} \tag{3.7}$$

$$M_c = \frac{1}{3} M_{3/2} + \frac{2}{3} M_{1/2} \tag{3.8}$$

$$M_d = \frac{1}{3} M_{3/2} + \frac{2}{3} M_{1/2} \tag{3.9}$$

$$M_b = \frac{2}{3} M_{3/2} + \frac{1}{3} M_{1/2} \tag{3.10}$$

$$M_f = \quad M_{3/2} \tag{3.11}$$

The charge-exchange processes all have the same weighting of isospin

$$M_g = M_h = M_i = M_j = \frac{\sqrt{2}}{3} M_{3/2} - \frac{\sqrt{2}}{3} M_{1/2}. \tag{3.12}$$

which gives the following ratios between the different reaction channels:

$$\sigma_a : \sigma_b : \sigma_c : \sigma_g = 9 \left|M_{3/2}\right|^2 : \left|M_{3/2} + 2M_{1/2}\right|^2 : \left|M_{3/2} + 2M_{1/2}\right|^2 : 2 \left|M_{3/2} - M_{1/2}\right|^2 . \tag{3.13}$$

In order to obtain extract information about the cross section, we simplify the *ansatz* by assuming a negligible contribution from the isospin 1/2 amplitudes. This is valid in the region of the Δ-resonance, which is seen prominently in the cross section. The ratios between the different reactions is then given by:

$$\sigma_a : \sigma_b : \sigma_c : \sigma_g = 9 \left|M_{3/2}\right|^2 : \left|M_{3/2}\right|^2 : \left|M_{3/2}\right|^2 : 2 \left|M_{3/2}\right|^2 , \tag{3.14}$$

so that finally we expect the ratio of π^+ to π^- cross section to be:

$$\frac{\pi^+ p \to \pi^+ p}{\pi^- p \to \pi^- p} = \frac{9}{2+1} = 3 \tag{3.15}$$

This, in fact, describes the ratio of the cross sections in the Δ-region. Due to the dominance of the Δ-resonance, we explicitly introduce a model for it.

3.1.2 Partial Wave Decomposition

The pion-nucleon or pion-nucleus interaction has been approached from two sides so far. First, in a field-theoretical description leading to an effective interaction mediated by exchange of particles. Second, a description within a many-body scattering problem leading to a truncation to a two-body interaction within a surrounding nuclear medium. In this section, these findings are joined into a phenomenological approach. To give a connection between the scattering problem and the particle-exchange picture, the K-matrix is introduced, and corresponding contributions are briefly presented, taken from [EW88].

The K-matrix is a convenient way to describe the interaction. If the K-matrix is chosen to be symmetric and purely real, it automatically guarantees unitarity of the S-matrix

$$S_\alpha = \frac{1 + \mathrm{i}|\boldsymbol{q}|K_\alpha}{1 - \mathrm{i}|\boldsymbol{q}|K_\alpha} \tag{3.16}$$

At threshold the K-matrix is related to the scattering length (in case of s-wave) or scattering volume (in case of p-wave)

$$a_\alpha = \lim_{|\boldsymbol{q}|\to 0} |\boldsymbol{q}|^{-2l} K_\alpha \tag{3.17}$$

In case of purely elastic reactions, it is also connected to the experimentally accessible phase shift

$$K_\alpha = \frac{1}{|\boldsymbol{q}|} \tan \delta_\alpha \tag{3.18}$$

which itself enters into the S-matrix

$$S_\alpha(\omega) = \mathrm{e}^{2\mathrm{i}\delta_\alpha(\omega)} \tag{3.19}$$

and finally connects to the scattering amplitude

$$f_\alpha(\omega) \frac{1}{2\mathrm{i}|\boldsymbol{q}|} [S_\alpha(\omega) - 1] \tag{3.20}$$

In the previous sections, we discussed how to handle the scattering process in a Lippmann-Schwinger approach. The central quantity is the free pion-nucleon transition operator, which can be adopted within a nuclear-matter problem. In this section, we will focus on the inner structure of the transition operator $t_{\pi N}$ and its isospin structure. The $t_{\pi N}$ is connected to the scattering amplitude:

$$f(\theta) = -\frac{\mu}{2\pi} \langle \varphi' | t_{\pi N} | \varphi \rangle \tag{3.21}$$

where μ is the reduced mass of the pion and the nucleon. The total differential cross section is then calculated by:

$$\mathrm{d}\sigma/\mathrm{d}\Omega = |\mathrm{f}(\theta)|^2 \tag{3.22}$$

Our aim is to describe pion-nucleus interactions over a wide energy range. As basis we use pion-nucleon interactions, which gives us the opportunity to study nuclear matter effects when the pion interacts inside a medium. Therefore it is useful to describe already the pion-nucleon interaction in such a way that it can also be used for bound nucleons. This is achieved in a phenomenological approach, where the main dynamics of the s- and p-wave are well reproduced. After giving a brief introduction to main quantities in scattering theory, a phenomenological *ansatz* for both s- and p-wave will be presented.

Partial Wave Expansion of the pion-nucleon scattering amplitude The scattering amplitude can be expressed in terms of Legendre polynomials $\mathrm{P_l(x)}$ and the corresponding derivatives $\mathrm{P_l'(x) = dP_l(x) = dP_l/dx}$

$$\begin{aligned} \mathcal{F}(\boldsymbol{q}', \boldsymbol{q}) = \sum_I \hat{P}_I \Bigg\{ & \sum_l \left[(l+1) f_{I,l^+} + l f_{I,l^-} \right] \mathrm{P_l}(\cos\theta) \\ & -i\boldsymbol{\sigma} \cdot \boldsymbol{n} \sum_l \left[f_{I,l^+} - f_{I,l^-} \right] \mathrm{P_l'}(\cos\theta) \Bigg\} \end{aligned} \tag{3.23}$$

using the isospin projectors $\hat{P}_I$ and the unit vector $\boldsymbol{n} = (\boldsymbol{q} \times \boldsymbol{q}')/|(\boldsymbol{q} \times \boldsymbol{q}')|$ perpendicular to the scattering plane. It is found that in the energy range of interest, the scattering amplitude is dominated by p- and s-waves.

s-wave interaction The interaction of a pion with a nucleon can be described in an effective field-theoretical framework by exchanging particles. A good starting point are the easiest possible Feynman diagrams, which contribute as so called Born terms. Especially for scattering of two particles it is convenient to introduce Lorentz-invariant variables. The so called Mandelstam-variables are characterized by the invariant mass of the propagator. When $q_\mu = (\omega, \boldsymbol{q})$ ($q'_\mu = (\omega, \boldsymbol{q'})$) denotes the initial (final) 4-momenta of the pion and $p_\mu = (\omega, \boldsymbol{p})$ ($p'_\mu = (\omega, \boldsymbol{p'})$) the 4-momenta of the nucleon the Mandelstam variables are defined

$$s = (p_\mu + q_\mu)^2 = (E + \omega)^2 = \left(\sqrt{M^2 + q^2} + \sqrt{m_\pi^2 + q^2}\right)^2 \tag{3.24}$$

$$t = (q_\mu - q'_\mu)^2 = -2q^2(1 - \cos\theta) \tag{3.25}$$

$$u = (p_\mu - q'_\mu)^2 = (E - \omega)^2 - 2q^2(1 + \cos\theta) \tag{3.26}$$

Possible candidates for the exchanged bosons B in the s-channel are restricted to the involved quantum numbers. A systematic procedure to identify forbidden quantum numbers is to look for Feynman rules. At each vertex, the quantum numbers have to be conserved. In the πN interaction, there are two vertices: one is the $\pi\pi B$ vertex, and the second the NNB vertex. The isospin of the boson must be 0 or 1, because the isospin transfer to the involved nucleon can only be smaller or equal 1. In addition to the isospin transfer, the momentum transfer is also restricted to smaller or equal to 1. In the static limit, where the nucleons are assumed to be infinitely heavy, the boson can at most flip the nucleon spin. The possible angular momentum of the boson will be 0 or 1. Due to the vertex of the exchanged boson with the pion line, the boson needs also to be able to transform into two pions. The wave function of a pion pair must be totally symmetric, therefore the only possible exchange mechanisms are scalar-isoscalar exchange and vector-isovector exchange. These can be identified with t-channel ρ-exchange (vector-isovector) and σ-exchange (scalar-isoscalar). In the approach of the Jülich group, they dynamically produce the mass of the σ by considering it as a two-pion correlated state [RHKS96, SHS$^+$95]. The s-wave contribution to the πN-interactions is especially of interest in the very low energy region. In a nuclear medium, a pion with very low kinetic energy might be captured by the nucleus and bound in a pionic atom [IYSNH, GROS88, OGRN95]. A typical phenomenological Hamiltonian is presented in terms of isospin-even (λ_1) and isospin-odd (λ_2) scattering length:

$$\mathcal{L}_{int} = \lambda_\sigma \boldsymbol{\Phi} \cdot \boldsymbol{\Phi} \overline{\Psi} \Psi + \lambda_\delta \boldsymbol{\Phi} \times \boldsymbol{\Phi} \overline{\Psi} \boldsymbol{\tau} \Psi + \lambda_\rho \boldsymbol{\Phi} \times \partial_\mu \boldsymbol{\Phi} \overline{\Psi} \gamma^\mu \boldsymbol{\tau} \Psi \tag{3.27}$$

$$H_s = \frac{4\pi}{m_\pi} \lambda_1 \boldsymbol{\Phi} \cdot \boldsymbol{\Phi} + \frac{4\pi}{m_\pi^2} \lambda_2 \boldsymbol{\tau} \cdot \boldsymbol{\Phi} \times \partial_t \boldsymbol{\Phi} \tag{3.28}$$

introduced by Koltun and Reitan [KR66]. In this approach, the λ_2 can be identified with the isovector ρ-exchange, while there are mainly two contribuitions to λ_1, the virtual pair creation and the exchange of the σ.

p-wave interaction The most prominent structure in pion-nucleon interaction in both $\pi^- p$ and $\pi^+ p$ is the Δ-resonance, which is a p-wave resonance. Hence, it is important

to describe the Δ-resonance well. This inspired some groups to treat the Δ isobar as an elementary particle and develop the so-called Δ-isobar model [EW88]. The inner degrees of freedom of the Δ are neglected. Together with the nucleon, the Δ builds the basis of the πN interaction in the Δ-isobar model. This phenomenological *ansatz* is constructed from an effective static Hamiltonian, which introduces the coupling of a one-pion state to the vacuum.

Nucleon

$$\langle \pi_b(q')|H_{\pi NN}(x)|0\rangle = \frac{\mathrm{i}f}{m_\pi}\boldsymbol{\sigma}\cdot\boldsymbol{q}'\tau_b \mathrm{e}^{\mathrm{i}q'\cdot x} \tag{3.29}$$

$$\langle 0|H_{\pi NN}(x)|\pi_a(q)\rangle = \frac{-\mathrm{i}f}{m_\pi}\boldsymbol{\sigma}\cdot\boldsymbol{q}\tau_b \mathrm{e}^{\mathrm{i}q\cdot x} \tag{3.30}$$

Using second order perturbation theory with $H_{\pi NN}$, the expectation value of the Born terms of the transition matrix T for the direct and crossed reaction is

$$\langle \pi_b(q')|T^{(d)}_{\mathrm{Born}}|\pi_a(q)\rangle = \frac{f^2}{m_\pi}\frac{(\boldsymbol{\sigma}\cdot\boldsymbol{q}')(\boldsymbol{\sigma}\cdot\boldsymbol{q})}{E_i-(\omega_q+E)}\tau_b\tau_a \approx \frac{f^2}{m_\pi}\frac{(\boldsymbol{\sigma}\cdot\boldsymbol{q}')(\boldsymbol{\sigma}\cdot\boldsymbol{q})}{-\omega_q}\tau_b\tau_a \tag{3.31}$$

$$\langle \pi_b(q')|T^{(c)}_{\mathrm{Born}}|\pi_a(q)\rangle = \frac{f^2}{m_\pi}\frac{(\boldsymbol{\sigma}\cdot\boldsymbol{q})(\boldsymbol{\sigma}\cdot\boldsymbol{q}')}{(E_i+\omega_q+\omega_{q'})-(E+\omega_q)}\tau_a\tau_b \approx \frac{f^2}{m_\pi}\frac{(\boldsymbol{\sigma}\cdot\boldsymbol{q})(\boldsymbol{\sigma}\cdot\boldsymbol{q}')}{\omega_{q'}}\tau_a\tau_b \tag{3.32}$$

where d denotes the direct Born terms and c the crossed Born terms.

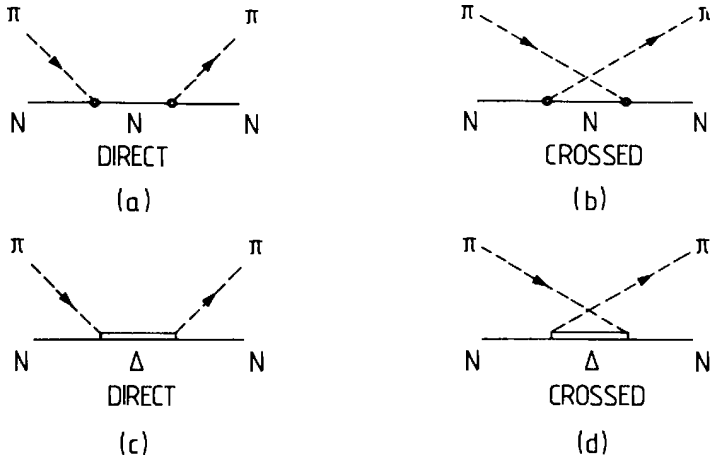

Figure 3.1: Nucleon and Δ direct and crossed Born terms, taken from [EW88]

Δ-isobar In analogy with the πNN coupling, the static effective Hamiltonian $H_{\pi N\Delta}$ is

$$H_{\pi N\Delta} = -\frac{f_\Delta}{m_\pi}\left(\boldsymbol{S}^+\cdot\boldsymbol{\nabla}\right)\left(\boldsymbol{T}^+\cdot\boldsymbol{\phi}\right) + h.c. \tag{3.33}$$

The correct coupling to the spin and isospin amplitudes is guaranteed by the spin and isospin transition matrices $\boldsymbol{S}^+$ and $\boldsymbol{T}^+$, respectively. These can be derived in the Rarita-Schwinger formalism, which introduces the implementation of (iso)-spin 3/2 fields, in analogy to (iso)-spin 1/2 field in the Dirac theory. The static effective Hamiltonian for pion-nucleon interaction is composed of both Hamiltonians introduced above:

$$H_{\text{int}} = H_{\pi NN} + H_{\pi N\Delta} \tag{3.34}$$

In the K-matrix approach, intermediate states appear as poles on the real axis at the value of the physical mass. Therefore, in the Δ-isobar model, the contributing poles are at the masses of the nucleon and the pion. In the static limit, the K-matrix is the sum of those two contributions

$$\langle \pi_b(q')K|\pi_a(q)\rangle = K_N + K_\Delta \tag{3.35}$$

$$\langle \boldsymbol{q}', N'|K(s,u)|\boldsymbol{q}, N\rangle \propto \sum_X \frac{\langle \boldsymbol{q}', N'|H_{\pi NX}|X\rangle\langle X|H^+_{\pi NX}|\boldsymbol{q}, N\rangle}{M_X - \sqrt{s}} \tag{3.36}$$

Phenomenological expression of the scattering amplitude It is useful to express the scattering amplitude in the following way:

$$\mathcal{F} = b_0 + b_1(\boldsymbol{t}\cdot\boldsymbol{\tau}) + [c_0 + c_1(\boldsymbol{t}\cdot\boldsymbol{\tau})]\,(\boldsymbol{q}\cdot\boldsymbol{q}') + i\,[d_0 + d_1(\boldsymbol{t}\cdot\boldsymbol{\tau})]\,\boldsymbol{\sigma}\cdot(\boldsymbol{q}\times\boldsymbol{q}') \tag{3.37}$$

where the introduced complex and energy dependent amplitudes are composed of scattering lengths and scattering volumes in the following way [EW88]:

$$\begin{aligned}
b_0 &= (a_1 + 2a_3)/3 & b_1 &= (a_3 - a_1)/3 \\
c_0 &= (4a_{33} + 2a_{31} + 2a_{13} + a_{11})/3 & c_1 &= (2a_{33} + a_{31} - 2a_{13} - a_{11})/3 \\
d_0 &= (-2a_{33} + 2a_{31} - a_{13} + a_{11})/3 & d_1 &= (-a_{33} + a_{31} + a_{13} - a_{11})/3
\end{aligned} \tag{3.38}$$

The d-amplitudes in eq. 3.37 are the so called spin-flip amplitudes and known to play a minor role in pion-nucleus interactions. Therefore, they are neglected in the following discussions. The structure of the partial wave expansion of the scattering amplitude in eq. 3.37 describes the s- and p-wave behaviour. The subscript 0 denotes spin and isospin averaged parameters, while the subscript 1 is carried by isospin dependent parameters. The b-amplitudes are dominated by s-waves, while parameters named c have p-wave character. Because the intermediate pion-nucleon scattering is dominated by p-waves, these c parameters are of importance. The introduced isospin-averaged amplitudes contain very complex information, covering energy-dependence of the whole reaction process. Until today, they cannot be derived from fundamental interactions, but especially in the s-wave part, connections could be given in the low energy regime, where chiral effective field theory is successful [DO08].

3.1.3 Self-Energy

In previous sections, the concept of virtual particles and its application to form an effective interaction description have been developed (see section 2.2). Virtual particles are used in an effective field-theoretical framework as mediator of the strong force. Like in the previous section, these interactions are commonly built from the exchange of virtual particles in so-called tree diagrams. Those diagrams are able to describe the main features of the interaction and dominate the model. Nevertheless, beyond those diagrams, closed loops can also be formed, and the corresponding consequences are briefly introduced in this section. These loop diagrams lead to quantum-mechanical corrections to the classical field theory introduced so far. In a picture where loop diagrams are taken into account, a real particle permanently emits and absorbs virtual particles, and a so called virtual cloud surrounds it. This picture changes the nature of the physical particle in such a way that the strength of the interaction depends on the momentum transfer. It becomes a composite object, which introduces non-trivial functions of external momenta which are usually truncated to a form factor. To study effects which are introduced by loop diagrams, all possible Feynman diagrams with two external legs need to be collected. As an example the contributing diagrams to the σ-π-π vertex (discussed in [dWS86]) are shown in figure 3.2. Intuitively, one might expect

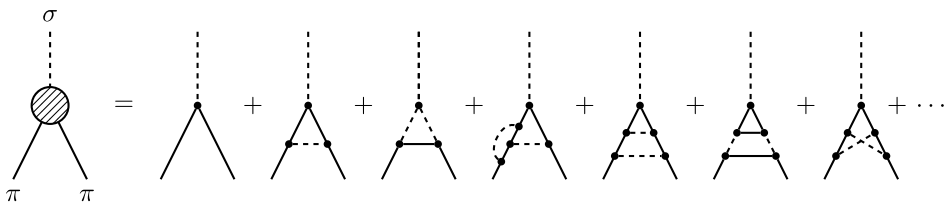

Figure 3.2: Quantum corrections to the σ-π-π vertex, like [dWS86]

from figure 3.2 that taken into account quantum corrections via loop diagrams comes along with more than one pole to consider. In fact, all those contributions are generated by only one propagator. In order to understand that, only irreducible diagrams are to be considered. Irreducible means that a diagram can not be divided into two stand-alone diagrams without cutting the external line. By denoting all reducible diagrams by $\Sigma(p)$, the sum of all irreducible diagrams read explicitly

$$G(p) = \frac{1}{\mathrm{i}(2\pi)^4}\frac{1}{p^2+m^2} + \frac{1}{\mathrm{i}(2\pi)^4}\frac{1}{p^2+m^2}\Sigma(p)\frac{1}{\mathrm{i}(2\pi)^4}\frac{1}{p^2+m^2} + \ldots \tag{3.39}$$

$$= G_0 + G_0\Sigma G_0 + \ldots \tag{3.40}$$

$$= \sum_{j=0}^{\infty}(G_0\Sigma)^j G_0 \tag{3.41}$$

with the geometric series giving finally

$$G = \frac{1}{1-G_0\Sigma}G_0 \tag{3.42}$$

which is called Dyson equation. From eq. 3.42 we see that the structures given in the Feynman-diagram were generated by only one propagator. The corresponding mass of a particle is given by the poles of its propagator, hence

$$G = \frac{1}{\mathrm{i}(2\pi)^4} \frac{1}{p^2 + m^2 - \Sigma(p)/(\mathrm{i}(2\pi)^4)} = \frac{1}{\mathrm{i}(2\pi)^4} \frac{1}{p^2 + M^2} \tag{3.43}$$

where

$$M^2 = m^2 - \frac{1}{\mathrm{i}(2\pi)^4} \Sigma(p)\Big|_{p^2=-M^2} \tag{3.44}$$

The permanent emission and absorption leads to a change of the mass of the physical particle and is called self energy. So far, the contributions to the pion self-energy from a surrounding virtual particle cloud was calculated in the vacuum, leading to a change of the mass of the pion by the amount of the self-energy. In other words: The mass of the pion depends on its interactions.

When the pion is applied to the nuclear medium, the Feynman-diagrams must be identified and calculated accordingly. The commonly used folding appoach assumes a form seperable of the pion-nucleus self-energy $\Pi_{\pi N}$ into pion nucleon scattering amplitude $f_{\pi N}$ and the nuclear density ρ:

$$\Pi_{\pi N} \propto f_{\pi N} \rho \tag{3.45}$$

In this work the pion interaction within a nuclear medium and especially pion-like low lying nucleon-hole excitations contribute strongly to the pionic field. The effect on the pion is therefore twofold: On one side, the pion affects the nuclear matter, and on the other side, the pion is affected by the nuclear matter. Both contributions can be taken into account by the self-energy.

3.2 Pion-Nucleus Interaction Potential

3.2.1 Low Energy Behaviour

For low-energy pions, the self-energy can also be determined within a perturbation theory framework, which demands a clear ordering of the included diagrams. This has been investigated for low-energy s-wave interaction [KW01]. The calculations of [KW01] are performed beyond the linear density approximation and are designed for asymmetric nuclear matter. Some of the diagrams used within the calculation are shown in figure 3.3. The nucleons are characterized with the solid line, the pion with the dashed lines accordingly. The first diagram in fig. 3.3 contributes to the linear approximation. The last three diagrams are coming from the scattering process of two nucleons from the Fermi-sea and represent two-nucleon correlations.

In the study of [KW01], pionic self-energies are obtained beyond the standard linear density approximation by including various 2-loop diagrams. The self-energy is, therefore, separated into the linear approximation term Π_f, the relativistic correction Π_{rel} (for second diagram) and the correlation term Π_{corr}

$$\Pi^-(k_{p,n}) = \Pi^-_{\mathrm{f}}(k_{p,n}) + \Pi^-_{\mathrm{rel}}(k_{p,n}) + \Pi^-_{\mathrm{corr}}(k_{p,n}) \tag{3.46}$$

$$\Pi^-_{\mathrm{f}}(k_p, k_n) = \frac{k_n^3}{3\pi^2}\left(T^{(-)}_{\pi N} - T^{(+)}_{\pi N}\right) - \frac{k_p^3}{3\pi^2}\left(T^{(-)}_{\pi N} + T^{(+)}_{\pi N}\right) \tag{3.47}$$

with the isospin-odd and isospin-even pion-nucleon threshold T-matrices $T^{(-)}_{\pi N}$, $T^{(+)}_{\pi N}$.

$$\Pi^-_{\mathrm{rel}}(k_p, k_n) = -\frac{g_A^2 m_\pi}{10(M\pi f_\pi)^2}(k_n^5 - k_p^5) \tag{3.48}$$

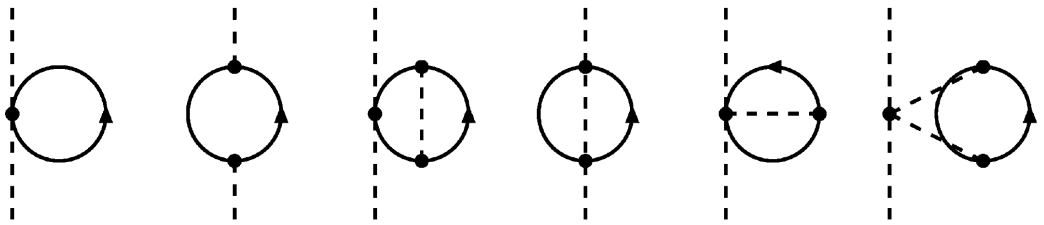

Figure 3.3: Pion-self energies diagram from [KW01], displaying linear density diagrams, calculated to 1-loop order in χPT and corrections accounting for relativistic and two-nucleon correlation effects.

$$\begin{aligned}\Pi^{-}_{\mathrm{corr}}(k_{p,n}) =& \frac{4m_\pi^2}{(4\pi f_\pi)^4}\left\{2(k_n^2+k_p^2)^2+2k_nk_p(k_n-k_p)^2+(k_n^2-k_p^2)^2\ln\frac{|k_n-k_p|}{k_n+k_p}\right\}\\ &+\frac{g_A^2m_\pi^2}{(4\pi f_\pi)^4}\left\{2k_n^2(m_\pi^2-2k_n^2)+2k_p^2(m_\pi^2-2k_p^2)\right.\\ &+8k_n^3m_\pi\arctan\frac{2k_n}{m_\pi}+8k_p^3m_\pi\arctan\frac{2k_p}{m_\pi}\\ &\left.-m_\pi^2\left(\frac{m_\pi^2}{2}+4k_n^2\right)\ln\left(1+\frac{4k_n^2}{m_\pi^2}\right)-m_\pi^2\left(\frac{m_\pi^2}{2}+4k_p^2\right)\ln\left(1+\frac{4k_p^2}{m_\pi^2}\right)\right\}.\end{aligned} \tag{3.49}$$

where f_π is the weak pion decay constant and g_A the nucleon axial vector coupling constant. The description in terms of proton- and neutron-number densities is derived by integrating over the according Fermi-spheres

$$\rho_{p,n} = tr_s\left(\int\frac{d^3k}{(2\pi)^3}n_s(k,\mu_{p,n})\right) \tag{3.50}$$

where n_s is the momentum distribution function, depending on the chemical potential μ. In our context, cold (T=0) and spin-saturated nuclear matter is considered, which simplifies eq. 3.50 to

$$n_s(k,\mu_{p,n}) = \Theta(k_{p,n}^2-k^2), \tag{3.51}$$

leading to the connection of proton- or neutron-number density with the Fermi-momentum k_F:

$$\rho_{p,n}(k_{p,n}) = \frac{k_{p,n}^3}{3\pi^2} \tag{3.52}$$

This leads to to a power series of the nuclear density, which makes the description of pion-nucleus scattering complicated and makes it necessary to care about terms of high order in ρ. The power series of the nuclear density can be interpreted in the following way: While the term linear in ρ is understood as the interaction with one nucleon, the quadratic term can be identified with the interaction with two nucleons. Therefore, the dependency of higher order terms of the nuclear density expresses contributions of interactions with more than one nucleon. This is seen in the low-energy region, but gets even more relevant at higher energies. To describe these effects, a phenomenological approach is developed. It is introduced in section 3.2.4. Independent of the choice of the describing model, the complete pionic self-energy would include all possible interaction scenarios and is therefore very sensitive to the surrounding matter. The self energy is composed of the well known folding approach and additional contributions which can be interpreted es polarization effects. As has been briefly mentioned, the mass of the pion depends on its interaction with its environment. The creation of virtual pairs in the vacuum already involved calculations of loop diagrams leading to quantum

corrections of the pion self-energies. The situation is even more complicated when the pion is applied to the nuclear medium, even if the Dirac sea is occupied up to the Fermi momentum, blocking those states also for virtual nucleons. On the one hand, the pion polarizes the nuclear medium, and on the other hand, the nuclear medium affects the pion-self energy.
The pion self-energy is connected to the corresponding interaction potential. For low energies the dependencies simplify to:

$$2\omega U_{\text{opt}} = \Pi_s(r) \tag{3.53}$$

where $\Pi_s(r)$ is the low-energy s-wave dominated self-energy [DO08]. In this section, the pion self-energy was studied in nuclear medium. In addition to the change of mass, the self-energy depends on the nuclear density in a non-trivial way. Even though investigations of low s-wave contributions lead to a power series of high order in the nuclear density, in this work only up to quadratic order is used. This is justified, due to the surface-dominance in the energy region of interest. Keeping the relation between the self-energy and the potential 3.53 in our mind, we will focus in the following section on the development of the concrete interaction potential. In this work, we study pions with an incident energy up to 1.5 GeV, which is (still) not high enough to penetrate into the nucleus deeply. Therefore, the corresponding description of the interaction is dominated by its surface character. This we take as a justification to neglect higher-than-quadratic order terms, due to the low density at the nuclear surface region.

3.2.2 Kisslinger Potential

Kisslinger [Kis55] invented the form of a velocity-dependent term, expressed by the scalar product of incoming and outgoing momentum, giving therefore also the off-shell behaviour. After a double Fourier transformation one then derives the so-called Kisslinger-type potential. The velocity-dependence leads to a potential, which is accompanied by derivatives. These derivatives act also on the nuclear density, which leads to a surface dominated interaction like we find in pion-nucleus scattering. The *ansatz* of Kisslinger was also used in the work [JS96] leading to quite a good description of pion-nucleus scattering data. The work of [JS96] can be understood as starting point for our model [LLW12a, LLW12b, LLW13]and will therefore be introduced in the following. Because our aim is an exploratory study of pion-nucleus interactions over a broad energy range, we were interested to have one unified working scheme with one parameter set. The corresponding extensions and also new introduced concepts are presented afterwards. When the Kisslinger-potential is entered into the Klein-Gordon equation, the wave equation, which needs to be solved reads:

$$\left\{-(\hbar c)^2\boldsymbol{\nabla}^2 + 2\omega(U_K + V_C^2)\right\}\varphi = (\hbar k c)^2\varphi \tag{3.54}$$

where ω denotes the total energy of the pion in the center of mass, k is the wave number, V_C the Coulomb potential and U_K the Kisslinger-potential. Solutions of eq.

3.54 are equivalent to those of a Schrödinger-like equation [Sat92] (see section 3.3.2):

$$\left[-\hbar^2/(2\mu)\boldsymbol{\nabla}^2 + U_L + V_C\right]\varphi = E_{\mathrm{cm}}\varphi \tag{3.55}$$

neglecting the quadratic contribution from the Coulomb potential $V_C^2 = 0$. Eq. 3.54 reduces to the Schrödinger equation 3.55 with reduced mass μ and the center of mass energy $E_{\mathrm{cm}} = (\hbar k)^2/2\mu$ with the reduced mass $\mu = \omega/c^2$ and a local potential U_L. This formalism is called Krell-Ericson transformation, and its derivation is shown in section 3.3.2 as well as an alternative procedure derived within the Eikonal approach. Because the Krell-Ericson transformation is well established, we chose it for our calculations. Starting with the Kisslinger-type potential

$$U_K = U_s + \boldsymbol{\nabla} U_p \boldsymbol{\nabla} \tag{3.56}$$

where U_s is the part of the potential dominated by s-waves, while U_p is dominated by p-waves accordingly. In our model, we use the basis of [JS96] with extensions to higher energies. In [JS96], the authors use isospin-averaged amplitudes separated into contributions from an isoscalar and isovector nucleon density.

$$\rho = \rho_n + \rho_p \tag{3.57}$$

$$\delta\rho = \rho_n - \rho_p \tag{3.58}$$

used in the formulation of the potentials:

$$U_s(r) = -4\pi\ \gamma_1[\ b_0\varrho(r) - q_\pi b_1 \delta\varrho(r)] - 4\pi\ \gamma_2[\ B_0 4\varrho(r)_n\varrho(r)_p - Q_\pi B_1\delta\varrho(r)] \tag{3.59}$$

The complex energy-dependent interaction paramters b_i and c_i $(i = 0, 1)$ have already been defined within the partial wave expansion (see eq. 3.38). The paramters B_i, C_i, however are defined in [GJ80, JS96, JS83b, JS83a]. These amplitudes are taken from Johnson and Satchler who discuss their findings in [JS96]. Equation 3.59 and the following equations of the pion-nucleus potential are valid for all three charge states of the pion, using the electric charge $q_\pi = 0, \pm 1$. $U_s(r)$ is the amplitude for s-wave interactions, which is composed of the isospin averaged amplitudes $b_{0,1}$ and $B_{0,1}$. These amplitudes are mostly important for low-energy scattering of the pion well under the range of th Δ-resonance and adjusted to pionic-atoms data. For our purposes, these amplitudes are of minor interest. Following Johnson and Satchler we do our studies with $B_{0,1} = 0$. The kinematic transformation factors γ_i depend on the nucleon mass M which enters into $\epsilon = \omega/Mc^2$, giving: $\gamma_1 = 1 + \epsilon$, $\gamma_2 = 1 + \epsilon/2$. The p-wave dominated potential is composed of two amplitude α_1 and α_2. Where the latter one describes two nucleon interactions:

$$U_p(r) = \frac{\alpha_1}{1 + \xi/3\alpha_1} + \alpha_2 \tag{3.60}$$

where the Ericson-Ericson-Lorentz-Lorenz factor ξ [EW88] is used in other calculations [KE69, MFJ$^+$89, JS96] is neglected in our calculations $\xi = 1$ due to weak effects in the calculations.

$$\alpha_1(r) = 4\pi\ [c_0\ \varrho_0(r) - q_\pi c_1 \varrho_1(r)]/\gamma_1 \tag{3.61}$$

$$\alpha_2(r) = 4\pi\ [C_0\ 4\varrho_n(r)\varrho_p(r) - q_\pi C_1\ \varrho_1(r)\varrho_0(r)]/\gamma_2. \tag{3.62}$$

In our approach, we use the parameters for highest energy available of Johnson and Satchler (at 297 MeV) and add higher resonances, which are occurring in the pion-proton cross section. In section 3.2.3 it is shown how the higher amplitudes are attached to the model. The amplitude α_2 is dominated by two-nucleon interactions, and a new description is found presented in section 3.2.4.

$$U_s(r) = U_s(r)\Big|_{B_{0,1}=0} + U_s(r)\Big|_{b_{0,1}(297\ \mathrm{MeV})} + \sum_I q_\pi^I f_I \rho_I \tag{3.63}$$

The sum in eq. 3.63 indicates the summation over several higher resonances. Section 3.2.3 shows, how the resonances are apllied to our potential. After defining the s-wave contribution to the potential, we focus on the p-wave contribution. The Kisslinger-potential is a function of the scattering amplitude and the nuclear density:

$$U_K = U_K(f;\varrho) \tag{3.64}$$

The amplitudes c_i and C_i are the p-wave dominated amplitudes containing also the Δ-resonance. The Δ-resonance is the strongest structure visible in the pion-nucleon total cross section, for both π^+- and π^--scattering. In the work of [JS96], parameters for three different energies were presented. For our purposes, however, the full energy-dependence is required. Therefore, in the following, the development of the amplitude describing the Δ-resonance is presented.
As a starting point we recap the partial wave decomposition of the scattering amplitude (eq. 3.37). The composition of the scattering amplitude f and also the density ϱ depends on the quantum numbers of the pion and the nucleus, which will be discussed later. Omitting the small contribution of the spin-flip amplitude, the partial wave decomposition can be written as:

$$f = \sum_I \hat{P}_I \left\{ \sum_l [(l+1)f_{l+} + l f_{l-}] P_l(cos\theta) \right\} \tag{3.65}$$

where the f_{l+} amplitude corresponds to spin $j = l + 1/2$ and the f_{l-} amplitude corresponds to spin $j = l - 1/2$. $P_l(cos\theta)$ are the Legendre-polynomials and $\hat{P}_I$ are the projection operators of the total isospin I with possible values $I = 1/2, 3/2$.

$$\hat{P}_{\frac{1}{2}} = \frac{1}{3}(1 - \boldsymbol{t}\cdot\boldsymbol{\tau}); \qquad \hat{P}_{\frac{3}{2}} = \frac{1}{3}(2 + \boldsymbol{t}\cdot\boldsymbol{\tau}) \tag{3.66}$$

Because the s- and p-waves dominate the interaction, we express them explicitly:

$$f = \sum_I \hat{P}_I \left\{ f_{0^+} + (2f_{1^+} + f_{1^-})\cos\theta + \sum_{l\geq 2} f \right\} \tag{3.67}$$

In the region of interest, there are several p-wave amplitudes listed in [B$^+$12]:

$$f_{1^+} = \Delta(1232) + \Delta(1600) + \Delta(1920) + N(1720) \tag{3.68}$$
$$f_{1^-} = \Delta(1750) + \Delta(1910) + N(1440) + N(1710) \tag{3.69}$$

Unfortunately, the situation is not clear, because many resonances are listed in the literature, while the evidence of the existence of some resonances is very poor. After deriving this general form of f in eq. 3.67, we will now focus on the isospin-structure. The scattering amplitude is often expressed in isoscalar and isovector amplitudes, which gives:

$$f = b_0 + b_1 \left(\boldsymbol{t} \cdot \boldsymbol{\tau}\right) + \left[c_0 + c_1 \left(\boldsymbol{t} \cdot \boldsymbol{\tau}\right)\right] |\boldsymbol{k}'| \cdot |\boldsymbol{k}| \cos\theta \tag{3.70}$$

$$f_{33} = \frac{1}{3}(2 + \boldsymbol{t} \cdot \boldsymbol{\tau}) 2 \cos\theta \Delta(1232) \tag{3.71}$$
$$= \frac{2}{\boldsymbol{k}' \cdot \boldsymbol{k}} \left(\Delta(1232)\right) \boldsymbol{k}' \cdot \boldsymbol{k} \tag{3.72}$$

where we assumed an off-shell amplitude, which was initially introduced by [Kis55]. In his work, the cosine term of the on-shell amplitude (in eq. 3.71) is interpreted as the scalar product of initial and final momentum (eq. 3.72), while taking the reciprocal quadratic momentum into the definition of the amplitude.

$$f_{33} = 2 f_\Delta \boldsymbol{k}' \cdot \boldsymbol{k} \tag{3.73}$$

Thus, on the energy shell

$$f_\Delta = -\frac{1}{2k^2}\, f^{3/2}_{(1232)}. \tag{3.74}$$

Because an extrapolation far above the maximum is required, we assume an off-shell separable form of Breit-Wigner type:

$$f_\Delta(k, k') = \frac{\gamma\ v(k) v(k')}{E_r - E - i\gamma k^3\ [v(k)]^2}, \tag{3.75}$$

with a form-factor $v(k)$ and position of the maximum E_r that determine the profile of $\Delta(1232)$. As a starting point, we used the form factor of the form

$$v(k) = \exp\left(-\frac{k^2}{\kappa_2^2}\right), \tag{3.76}$$

but the description of the left shoulder of the Δ-resonance was not satisfactory. We introduce a more involved structure of the form factor, which leads to a better description of the low-energy data without spoiling the already reasonable agreement with data at the right shoulder of the Δ-resonance. The form factor

$$v(k) = \frac{1}{1+\lambda}\left[1 + \lambda \exp\left(-\frac{k^2}{\kappa_1^2}\right)\right]\ \exp\left(-\frac{k^2}{\kappa_2^2}\right) \tag{3.77}$$

is chosen in such a way that the limit for small k is euqal to one and for large k it behaves like a common form factor. Therefore, we introduce the separable form:

$$v(k) = v_l(k) \ \exp\left(-\frac{k^2}{\kappa_2^2}\right) \tag{3.78}$$

$$v_l(k) = \frac{1}{1+\lambda}\left[1 + \lambda \exp\left(-\frac{k^2}{\kappa_1^2}\right)\right] \tag{3.79}$$

The form factor $v(k)$ cuts off the tail of the resonance, which dies out rather slowly due to the momentum dependent width:

$$\Gamma/2 = \gamma k^3 \ [v(k)]^2 \tag{3.80}$$

The profile of $v(k)$ is chosen to reproduce the $\pi^+ p$ cross section via the unitarity relation (for more details see eq. 3.186 and eq. 3.187 in section 3.4.1)

$$\sigma(\pi^+ p) = -\frac{4\pi}{k}\mathrm{Im} f(\pi^+ p). \tag{3.81}$$

In this way one obtains $\gamma = 1.2$ fm^{-2} , $E_r = 1232$ MeV, and the form-factor parameters $\kappa_1 = 0.118$ GeV/c and $\kappa_2 = 0.552$ GeV/c. With these definitions, we can describe the shape of Δ in the pion-nucleon cross section satisfactorily at the price of introducing some parameters. The description of the Δ-resonance is especially challenging, because we aim for a good description of both shoulders of the resonance. This we guarantee with a rather involved structure of the form-factor which indicates underlying dynamics that are not resolved in our *ansatz*.

Even though the discussion of the underlying quark content is beyond the scope of our studies, the energy dependence of the pion-nucleon and pion-nucleus scattering comes from the excitation of inner degrees of freedom. To understand these effects, we would like to briefly summarize the findings of [EW88]. We follow [DM81, GW05], where the formation of the $\Lambda(1405)$ is described with a model studying the coupling of the bare quark state to the actual baryon. Due to the p-wave character of the Δ-resonance, we apply the WE-model of [DM81, GW05] to p-wave interaction. In their model, they distinguish between two different interaction potentials, which are of separable form. First, there is the interaction between the channels, which is described with a potential U, and second, the additional interaction of the baryon state with the bare-quark state, which we define as V. The bare-quark state with bare mass $m^{(0)}$ is non interacting and therefore has no transitions. To describe the full process, including both interactions, we need to solve a Lippman-Schwinger equation, where the corresponding propagator carries the information of the interaction. The propagators depend on the invariant Mandelstam variable s and on the actual mass, which varies with the interaction. In the case of a bare quark state it reads $g_0 = (\sqrt{s} - m^{(0)})^{-1}$. When a baryon is formed, however, the channels are coupled via a potential, which we assume to be separable

into the strength of the potential λ and form-factors v, hence $U = v\lambda v$. Accordingly, the propagator is $g = (\sqrt{s} - m^{(0)} - U)^{-1}$. The coupling of the channel state to the bare-quark state is generated by an additional potential V, which leads to the following full propagator,

$$G = g + gVG \tag{3.82}$$

including both interaction potentials U and V. This translates into a K-matrix, which is composed of two main contributions: a non-resonant background part $K^{(B)}$, which smoothly varies in energy, and a resonant part $K^{(R)}$. Under the assumption that the interference between background and resonant part is negligible, the K-matrix is simply a sum

$$K = K^{(B)} + K^{(R)}. \tag{3.83}$$

In an effective-range expansion with an additional form-factor $F(q^2)$ to have control of the high energy behaviour, the background term in general is:

$$K_\alpha^{(B)}(q) = \frac{q^{2\ell}}{-\frac{1}{a_\alpha} + \frac{1}{2}q^2 r_\alpha \cdots} F(q^2) \tag{3.84}$$

characterized by a set of effective low-energy range parameters $a_\alpha, r_\alpha \cdots$. $\ell = j \pm \frac{1}{2}$ is the orbital angular momentum, belonging to the total angular momentum j such that the parity $\pi_\alpha = (-)^\ell$ is conserved. πN resonances are contained globally in

$$K_\alpha^{(R)} = \frac{1}{q} \sum_r \frac{\Gamma_r(s)/2}{\sqrt{s} - m_r(s)}. \tag{3.85}$$

The resonance width $\Gamma_r(s)$ and the mass $m_r(s)$ depend on the centre-of-mass energy s. The mass may be expressed in terms of a bare resonance mass $m_r^{(0)}$ and a dispersive mass shift, which can be calculated by the principal value integral

$$P_{a,b}(E) = P \int \frac{d\mathbf{q}}{(2\pi)^2 E_{red}} \frac{q^2 v_a(q) v_b(q)}{\sqrt{s} - \sqrt{s_0}}, \tag{3.86}$$

where $\sqrt{s}_0 = m_\pi + m_N$ denotes the physical energy threshold. The mass shift is generated by $v_{o,c} g_c v_{c,o}$. While the discussions of the structure of the K-matrix are of general kind and valid for the full spectra of πN scattering, we focus on the p-wave Δ-resonance with the final expression

$$K_\Delta = \mathbf{k}\ \mathbf{k}' \left[K^{pot}(k, k') + \frac{v_{c,o}(k) v_{c,o}(k')}{\sqrt{s} - m_r} \right]. \tag{3.87}$$

In figure 3.4 the WE-model is compared to the bare Δ, showing an effect on the Δ-width mostly prominent at low energies..

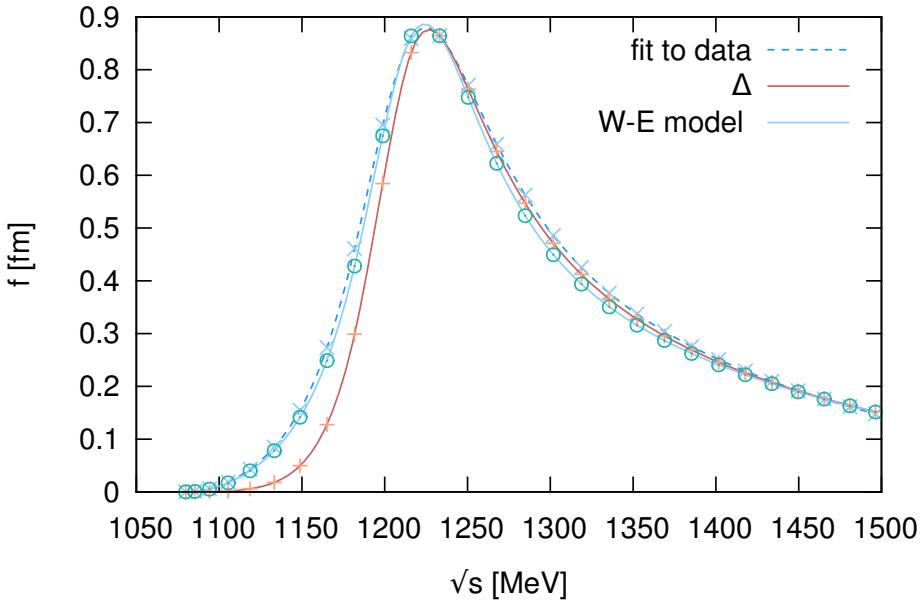

Figure 3.4: Comparison of the Δ-resonance amplitude. The dashed line (blue) is derived by a fit to the experimental pion-nucleon cross section, the solid line (red) represents the bare Δ and the solid line (light blue) is calculated within the WE-model, including a non-resonant term, coming from effects of the bare quark state interacting with the actual baryon. [B+12]

3.2.3 Higher Energies Beyond the Δ-Resonance

In our approach, we are interested in pion-nuclear interactions as possible final states in antiprotonic annihilation reactions. Therefore, we need to have a description for an energy range from about 100 MeV up to 1.5 GeV, without aiming for a detailed spectroscopic description. The higher the energy becomes, the more high partial waves are accessible.

We describe the formation of resonance states in a simple approach by using a Breit-Wigner function. The Breit-Wigner form is a simple way to describe the underlying propagator structure. In the energy range of interest, a long list of resonances is given in the literature [B+12]. Unfortunately, the agreement of different analyses is very poor, which makes the situation still unclear. In tables 3.1 and 3.2 we show the resonances listed in the PDG [B+12]. In their notation, the uncertainty is expressed with the lack of stars, while four stars indicated that this resonance is seen by different experiments and also in other corresponding reactions. Even though the existence of those resonances is confirmed, the width, position and branching ratio might still differ strongly from one analysis to another. Many of the referred analyses have been done, without including the η meson. Because the neighbouring resonances have a

large overlap, there are no clear structures seen in the cross section. Due to these arguments, we decided to proceed in the following way: The PDG listing is used as a guideline, but we combine the (anyhow indistinguishable) neighbouring resonances and introduce an effective multiplicity, which is fitted to the data of the total cross section.

There have been several analyses of the partial-wave decomposition of pion-nuclear

Name (E_r)	Γ [MeV]	R	I J^P	k_r [$1/fm$]
$N(1440)$ P_1	300	0.60	1/2 $1/2^+$	2.013
$N(1520)$ D_3	150	0.35	1/2 $3/2^-$	2.278
$N(1535)$ S_1	150	0.35	1/2 $1/2^-$	2.278
$N(1650)$ S_1	165	0.60	1/2 $1/2^-$	2.362
$N(1675)$ D_5	150	0.40	1/2 $5/2^-$	2.856
$N(1680)$ F_5	130	0.68	1/2 $5/2^+$	2.873
$N(1700)$ D_3	100	0.15	1/2 $3/2^-$	2.940
$N(1710)$ P_1	100	0.15	1/2 $1/2^+$	2.974
$N(1720)$ P_3	100	0.15	1/2 $3/2^+$	3.008

Table 3.1: Higher $I = 1/2$ resonance parameters, (PDG data). The last column is the CM momentum for π N decay. L_{2J} notation.

Name (E_r)	Γ [MeV]	R	I J^P	rank
$\Delta(1600)P_3$	350	$0.10 - 0.20$	3/2 $3/2^+$	$***$
$\Delta(1620)S_1$	118	$0.20 - 0.30$	3/2 $1/2^-$	$****$
$\Delta(1700)D_3$	300	$0.10 - 0.20$	3/2 $3/2^-$	$****$
$\Delta(1750)P_1$	300	$0.10 - 0.20$	3/2 $1/2^+$	$*$
$\Delta(1900)S_1$	200	$0.10 - 0.30$	3/2 $1/2^-$	$**$
$\Delta(1905)F_5$	330	$0.09 - 0.15$	3/2 $5/2^+$	$****$
$\Delta(1910)P_1$	250	$0.15 - 0.30$	3/2 $1/2^+$	$****$
$\Delta(1920)P_3$	200	$0.05 - 0.20$	3/2 $3/2^+$	$***$
$\Delta(1930)D_5$	270	$0.05 - 0.15$	3/2 $5/2^-$	$***$
$\Delta(1940)D_3$	~ 200	$0.05 - 0.15$	3/2 $3/2^-$	$*$
$\Delta(1950)F_7$	285	$0.35 - 0.45$	3/2 $7/2^+$	$****$
$\Delta(2000)F_5$	~ 200	$0.00 - 0.07$	3/2 $5/2^+$	$**$

Table 3.2: Higher $I = 3/2$ resonance parameters, (PDG data). The widths are very uncertain, those recommended by PDG are given in the second column. R are branching factors for the πN channel.

cross sections, but unfortunately, the agreement between different analyses is unclear. Beside the resonances which might be excited in the pion-nucleon interaction, there are also thresholds of pion production, which open at higher energies. To finally describe

the elementary cross section, we make an *ansatz*, indicated by the subscript a, of higher-lying resonances which are put together in a schematic way:

$$Im\ f_a^{1/2} = -Im\ \Sigma_h\ \ \frac{1}{k_h}\frac{\lambda\Gamma/2}{E_h - E - i\Gamma/2}, \tag{3.88}$$

$$Re\ f_a^{1/2} = -Re\ \Sigma_h\ \ \frac{R}{k_h}\frac{\lambda\Gamma/2}{E_h - E - i\Gamma/2} \tag{3.89}$$

with branching ratio R, width Γ and position of the Resonance E_h. The same definition is used for isospin 3/2 amplitudes

$$Im\ f_a^{3/2} = -Im\ \Sigma_h\ \ \frac{1}{k_h}\frac{\lambda\Gamma/2}{E_h - E - i\Gamma/2}, \tag{3.90}$$

$$Re\ f_a^{3/2} = -Re\ \Sigma_h\ \ \frac{R}{k_h}\frac{\lambda\Gamma/2}{E_h - E - i\Gamma/2} \tag{3.91}$$

The sum extends over four "ansatz" states $f^{1/2}_{(1440)}, f^{1/2}_{(1520)}, f^{3/2}_{(1635)}, f^{3/2}_{(1700)}$ specified in Table 3.3.

I	E_h	Γ [MeV]	R	λ	k_h $[1/fm]$
1/2	1440	300	0.60	0.2	2.010
1/2	1520	120	0.50	3	2.311
1/2	1635	165	0.60	1	2.772
1/2	1700	100	0.20	5	2.940
3/2	$\Delta(1232)$		1	2	1.151
3/2	1650	120	0.15	1.8	2.770
3/2	1800	100	0.10	4	3.278
3/2	1950	285	0.40	4	3.789

Table 3.3: *Ansatz* resonances used to describe the local optical potential. The gradient potential due to $\Delta(1232)$ is discussed in the text.

3.2.4 True Absorption – Two-Nucleon Term

Even though the πN interaction builds the basis of πA interactions, there are also reactions which do not have a counter part in the free scattering case. In free space, the absorption is an actual rearrangement, which can be seen by cutting the corresponding Feynman diagrams at different times, finding always the pion line. In the nucleus, however, the surrounding nucleons can absorb flux too, so that a true absorption becomes possible, where the pion vanishes completely in between.

So far, the discussion of pions was focused on the interaction with only one nucleon. In the nuclear medium however, more nucleons are available as interaction partners,

and the higher order of nuclear densities becomes important. In this section, the interaction of one pion with two nucleons will be discussed.
In the literature one finds different approaches to the two-nucleon term. Especially, the inclusion of the real-part is treated differently. [JS96] use a real-part in their calculation, while [GAK98, NLG98, GG82] neglect it. In the following, an *ansatz* is estimated with a simple form factor in order to derive a power series in the momentum and justify the omission of the real part in our calculation. After fixing the structure of the two-nucleon amplitude C, the density dependence is developed on basis of contributing Feynman-diagrams. Finally, a potential and its application to the two-nucleon absorption cross section are presented.

The reaction of the pion with two nucleons is also known as 'true absorption' due to the fact that the pion line in a corresponding Feynman diagram truly vanishes rather than forming a Δ. Hence, the reaction of interest reads

$$V_{\pi NN\to NN}\ G_{NN}\ V_{NN\to\pi NN}. \tag{3.92}$$

Here V are the interaction potentials of absorption and emission of the pion and G_{NN} is the NN propagator. Contributions from two-nucleon interactions are known to be of importance and are taken into account in a phenomenological *ansatz* by assuming the interaction is separable into nuclear density and an amplitude [JS96]:

$$\alpha_2(\mathbf{r}) = 4\pi\ \left[C_0\ 4\varrho_n(\mathbf{r})\varrho_p(\mathbf{r}) - q_\pi C_1\ \varrho_1(\mathbf{r})\varrho_0(\mathbf{r})\right] 2/(1+\gamma_\pi) \tag{3.93}$$

The amplitudes C_i $(i = 0, 1)$ carry the energy dependence and strength of the interaction, while the nuclear densities describe nuclear properties. To the strength of C_i contribute exchange potentials, but in the nuclear medium, NN correlations have an effect. Altogether, the isoscalar, the isovector and the NN correlation amplitudes are three different contributions and should be considered separately, but to simplify the model, we assume $C_i \equiv C$, which is defined by dispersion relation

$$C = f^2_{\Delta N\pi}\frac{(\Gamma/2)^2}{(T_r - T)^2 + (\Gamma/2)^2}\int \frac{d\mathbf{k}}{(2\pi)^2\mu_{NN}}\frac{v(k)^2 P_{NN}(k)}{E_{NN\pi} - E_{NN}(k)}, \tag{3.94}$$

where $f_{\Delta N}\pi$ is a coupling strength, $E_{NN\pi}$ is the initial energy, $E_{NN}(k)$ is the energy of the intermediate NN pair and $P_{NN}(k)$ is the Pauli exclusion operator. An analytic expression can be derived with $P_{NN} = 1$ and a form factor of the form

$$v(k) = k\left[1 + \frac{k^2}{\kappa^2}\right]^{-3/2}, \tag{3.95}$$

leading to a power series

$$C = f^2_{\Delta N}\frac{(\Gamma/2)^2}{(T_r - T)^2 + (\Gamma/2)^2}\ v(k_0)^2[ik_0^3 + \frac{\kappa^3}{8}(1 + k_0^2/\kappa^2)^2 + \frac{\kappa k_0^2}{2}(1 - k_0^2/\kappa^2)], \tag{3.96}$$

where k_0 is the on-shell NN relative momentum determined by the pion energy and binding energies of the nucleons and

$$k_0 = \sqrt{M(E_\pi - 2E_B)} \sim 2 - 3[fm^{-1}]. \tag{3.97}$$

The result 3.96 has both a real and an imaginary part, but analysing it we find that the real part is an order of magnitude smaller than the imaginary part. Nevertheless, in high order Δ, N collisions, the real part becomes important. On the other hand, within the nuclear matter, an averaging over nuclear binding energies has to be carried out, leading to an even smaller real part of C. The corresponding imaginary part gives

$$\text{Im } C = \frac{f^2_{\Delta N\pi}\Gamma/2)^2}{(T_r - T)^2 + (\Gamma/2)^2} < k_0^3 \; v(k_0)^2 >, \tag{3.98}$$

where $< k_0^3 \; v(k_0)^2 >$ is an average over nucleon binding energies which involves a momentum cut-of for k_0 smaller than the Fermi momentum k_f. The energy and density dependence of $\text{Im}(C)$ can be calculated in the local density approximation:

$$< k_0^3 v(k_0)^2 >= \int \frac{d\mathbf{k}_1}{N_1} \int \frac{d\mathbf{k}_2}{N_2} \;\; k_0^3 \; v(k_0)^2 \Theta(k_0 > k_{f1}) \Theta(k_0 > k_{f2}) \tag{3.99}$$

where $N = 4\pi k_f^3$. Form-factor 3.95 was used to derive an analytical expression C, it is now changed to a more realistic p-wave one of the form

$$k(1 + k^2/\beta^2)^2. \tag{3.100}$$

$$v = \frac{1}{1+\lambda}\left(1 + \lambda \mathrm{e}^{-\frac{k^2}{\kappa_1^2}}\right) \mathrm{e}^{-\frac{k^2}{\kappa^2}} \tag{3.101}$$

The imaginary part of C turns fairly stable against the density changes thanks to the exclusion principle. At pion energies larger than 400 MeV the energy dependence may be stronger, but the quadratic resonant factor in equation 3.98 suppresses this capture mode at higher meson energies. Constant C is a fair first-order approximation. Hence, we follow the *ansatz* of [GAK98, AB90]:

$$W_{NN}(r) = -iW_o \frac{(\Gamma/2)^2}{(T_r - T)^2 + (\Gamma/2)^2} \; 4\rho(r)_n \; \rho(r)_p \tag{3.102}$$

and use a purely imaginary amplitude. Because our model of the pion interaction is also applied to final-state interactions of antinucleonic reactions in nuclear matter, deep penetration into the nucleus is expected, and an improved density dependence is demanded. In our model, we assume a two-step process, where the pion gets captured by a nucleon to form a Δ first, and after propagating, it decays into a nucleon, emitting a pion, giving

$$V_{\pi NN\to N} = V_{\pi N,(N)\to\Delta,(N)} \; G_{\Delta N} \; V_{\Delta N\to NN}. \tag{3.103}$$

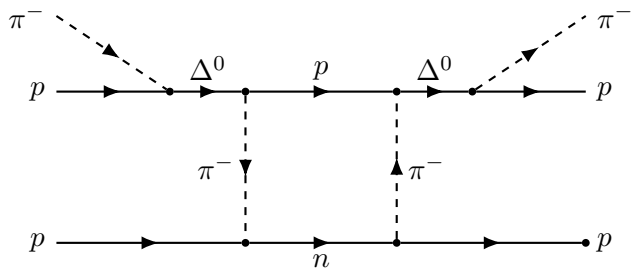

Figure 3.5: Feynman diagram

Vice versa, after the propagation of G_{NN}

$$V_{NN\to NN\pi} = V_{NN\to\Delta N}\ G_{\Delta N}\ V_{(N),\Delta\to\pi N,(N)} \tag{3.104}$$

As an example the Feynman diagram of the interaction of a π^- with two protons is shown in fig. 3.5. In appendix A all considered diagrams are shown. After calculating the Clebsh-Gordan coefficients in the example

$$\sqrt{\frac{2}{3}}\sqrt{\frac{2}{3}}\cdot\sqrt{\frac{2}{3}}\sqrt{\frac{2}{3}}\cdot\rho_n\rho_p = \frac{4}{9}\rho_n\rho_p \tag{3.105}$$

Summarizing over all contributions taken into account gives the density dependence

$$\pi^-: \quad 5\ \rho_p\rho_n + \rho_p^2 \tag{3.106}$$

$$\pi^0: \quad 4\ \rho_p\rho_n + \rho_p^2 + \rho_n^2 \tag{3.107}$$

$$\pi^+: \quad 5\ \rho_p\rho_n \quad + \rho_n^2 \tag{3.108}$$

In terms of isoscalar and isovector densities one gets:

$$\pi^-: \quad \frac{1}{2}[3\rho^2 - 2\delta\rho^2 - 1\rho\delta\rho] \tag{3.109}$$

$$\pi^0: \quad \frac{1}{2}[3\rho^2 - 1\delta\rho^2 \quad\quad] \tag{3.110}$$

$$\pi^+: \quad \frac{1}{2}[3\rho^2 - 2\delta\rho^2 + 1\rho\delta\rho] \tag{3.111}$$

To implement it to the interaction potentials, the density dependence is given with a function ϱ in terms of the charge of the scattered pion:

$$\varrho = \frac{1}{2}[3\rho^2 - (1+q_\pi^2)\delta\rho^2 + q_\pi\rho\delta\rho] \tag{3.112}$$

In addition, the corresponding derivatives are displayed, which are used in the Kisslinger-type potential:

$$\varrho' = \frac{1}{2}[6\rho\rho' - 2(1+q_\pi^2)\delta\rho\delta\rho' + q_\pi(\rho'\delta\rho + \rho\delta\rho')] \tag{3.113}$$

$$\varrho'' = \frac{1}{2}[6(\rho'^2\rho\rho'') - 2(1+q_\pi^2)(\delta\rho'^2 + \delta\rho\delta\rho'') + q_\pi(\rho''\delta\rho + 2\rho'\delta\rho' + \rho\delta\rho'')] \tag{3.114}$$

leading to the Laplacian:

$$\Delta\varrho = 3\rho\Delta\rho - \delta\rho(1+q_\pi^2)\Delta\delta\rho + \frac{1}{2}q_\pi\delta\rho\Delta\rho + \frac{1}{2}q_\pi\rho\Delta\delta\rho + 3\rho'^2 - (1+q_\pi^2)\delta\rho'^2 + \frac{1}{2}q_\pi 2\rho'\delta\rho' \tag{3.115}$$

Finally we obtain the contribution to the interaction potential:

$$\overrightarrow{\partial}\ \alpha_2\ \overrightarrow{\partial} \Rightarrow W_{NN}(r) = -iW_o\frac{(\Gamma/2)^2}{(T_r-T)^2+(\Gamma/2)^2}\ \varrho(r) \tag{3.116}$$

The cross section for the absorption is calculated with the Eikonal wave function ψ, which contains the full interaction potential U_L and the imaginary part of the derived potential W_{NN} given in eq. 3.116:

$$\sigma_{\text{abs}} = \frac{2\omega}{k}\int |\psi|^2 \text{Im}W_{NN}\text{d}^3r. \tag{3.117}$$

3.3 Consequences of Momentum Dependent Potentials

The derivatives in the Kisslinger-potential eq. 3.56 have several effects which need special treatment. In the following the considered consequences are presented, starting with the effect on the nuclear density, followed by the challenges meeting within the eikonal approach.

3.3.1 Nuclear Density: Regularized Fermi-Function

Within this work, the nuclear density is described in form of the commonly used Fermi-function

$$F(x) = \frac{1}{1 + \mathrm{e}^{x}}. \tag{3.118}$$

A good approximation to proton ($q = p$) and neutron ($q = n$) ground-state densities is

$$\rho_q(\vec{r}) \propto \rho_0 F((r - R_q)/a_q) \tag{3.119}$$

where a_q is the diffuseness parameter and R_q the half density radius and the form factor ρ_0, which is about 1.2 fm and has the form

$$\rho_0 = \frac{3N_q}{4\pi R_q^3} \frac{1}{1 + \left(\frac{\pi a_q}{R_q}\right)^2} + \mathcal{O}(\mathrm{e}^{-R_q/a_q}) \tag{3.120}$$

with the normalization

$$N_q = \int \mathrm{d}^3 r \rho_q(\vec{r}) \tag{3.121}$$

giving either the number of protons or the number of neutrons. While ρ_0 in eq. 3.120 leads to a good description of the nuclear density itself, it fails when it comes to derivatives of ρ. The Laplace-operator in the wave equationcontains a term of the first derivative multiplied with the inverse of radius

$$\Delta_r \propto 1/r \partial\rho/\partial r \tag{3.122}$$

leading to a divergence at the origin. This is due to the constant behaviour of the first derivative, which can not compensate the $1/r$ behaviour. However, this is not what one would expect, because close to the origin mainly s-waves contribute to the wave-function

$$\varphi_l(r) \approx a_0 r^l + a_2 r^{l+2} + \ldots \tag{3.123}$$

$$\lim_{r \to 0} \varphi_l \approx a_0 + a_2 r^2 + \mathcal{O}(r^4) \tag{3.124}$$

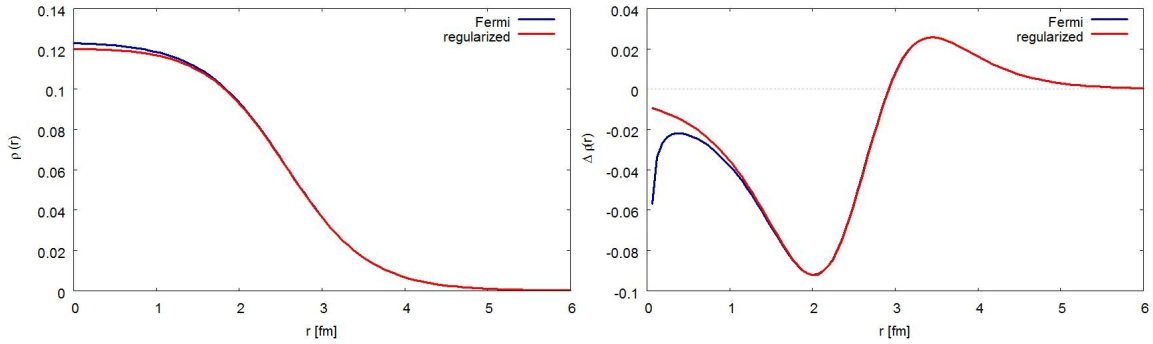

Figure 3.6: Comparison of the Fermi function and the regularized Fermi function for the nuclear density of ^{12}C (left) and its Laplacian (right).

where the nuclear density is calculated by the square of the wave function, giving

$$\rho \propto a_0^2 + 2a_0a_2r^2 + a_2^2r^4 \tag{3.125}$$

$$\lim_{r\to 0}\rho \approx a_0^2 + 2a_0a_2r^2, \tag{3.126}$$

neglecting contributions of the order of r^4. The Laplacian finally gives

$$\rho \approx 12a_0a_2 \tag{3.127}$$

which is constant, as would be expected intuitively.

To derive such a behaviour also within a description in terms of the Fermi function, the divergent $1/r$ term needs to be suppressed for small r. This is achieved by the introduction of an ultraviolet form factor applied to the first derivative, where the divergence arises. The regularized derivative of the Fermi function gives

$$f' = \left(1 - \exp\left(\frac{r}{b}\right)\right) \cdot F'. \tag{3.128}$$

The actual density is derived by integrating *ansatz* 3.128. The general form of the integral of 3.128 gives a hyper-geometric function, but an analytic expression can also be derived when the parameter b of the form factor is chosen to be equal to the diffuseness parameter a_q finally giving

$$f(r) = (1 - \exp(-r/a_q))\, F(r) - \exp(-R_q/a_q)\, [\ln(1 + \exp(-(r_r)/a_q))] \tag{3.129}$$

This regularized Fermi function still has the behaviour of a common Fermi distribution for large and intermediate values of r, but succeeds also in the derivatives of the density at the origin. In figure 3.3.1 the comparison between the Fermi function and the regularized Fermi function is shown for ^{12}C. The nuclear density in this work is hence

$$\rho = \rho_0 f(r), \tag{3.130}$$

where the diffuseness parameter and the half-density radius are described via a parametrization in terms of proton number Z and mass number A derived by fits to Skyrme calculations[1], (similar to [HL98])

$$a_p = 0.4899 - 0.1236\frac{A-2Z}{A} \tag{3.131}$$

$$R_p = 1.2490A^{1/3} - 0.5401 - 0.9582\frac{A-2Z}{A} \tag{3.132}$$

$$a_n = 0.4686 + 0.0741\frac{A-2Z}{A} \tag{3.133}$$

$$R_n = 1.2131A^{1/3} - 0.4415 + 0.8931\frac{A-2Z}{A} \tag{3.134}$$

3.3.2 Krell-Ericson Transformation

In this section, the derivation of the solution of the wave equation is presented. To introduce the procedure in use, it is not necessary to look into the explicit form of the involved potential. The crucial point is that terms enter into the potential which contain a derivative of first order.

$$U_{\pi A} = U_s + \nabla U_p \nabla, \tag{3.135}$$

where U_s is dominated by s-waves and U_p by p-waves, accordingly. The inner structure of U_s and U_p was given in previous chapters. In this section, it is only mentioned that U_s and U_p depend on r and on the nuclear density ρ. In the following, the so called Krell-Ericson transformation is introduced, which leads to an effective potential within a new wave equation.

As has been discussed previously, the scattering of pions with a nucleus can be described by the Klein-Gordon equation, with the momentum dependent potential as in eq. 3.135:

$$\left[\Delta + k^2 - U_s - \nabla U_p \nabla\right] \phi_\pi = 0. \tag{3.136}$$

ϕ_π is the pion wave function, where the Coulomb interaction is neglected for the moment. The aim is to transform 3.136 in such a way that the first derivative term is eliminated. To that end, the wave function is separated into an amplitude a and a transformed pion wave function ψ_π:

$$\phi_\pi = a(r)\psi_\pi. \tag{3.137}$$

To express the Klein-Gordon equation in terms of the *ansatz* wave function, the corresponding derivatives give:

$$\nabla\phi_\pi = (\nabla a)\,\psi_\pi + a\nabla\psi_\pi, \tag{3.138}$$

$$\Delta\phi_\pi = (\Delta a)\,\psi_\pi + a\nabla\psi_\pi + 2\nabla a \cdot \nabla\psi_\pi. \tag{3.139}$$

[1] private communication with Prof. Dr. Lenske, unpublished

These terms appear in the derivative term of the Klein-Gordon equation, which gives explicitly:

$$\nabla U_p \nabla \phi_\pi = (\nabla U_p) \cdot \nabla \phi_\pi + U_p (\Delta \phi_\pi) \tag{3.140}$$
$$= (\nabla U_p) \cdot [(\nabla a) \psi_\pi + a \nabla \psi_\pi] \tag{3.141}$$
$$+ U_p [(\Delta a) \psi_\pi + a \Delta \psi_\pi + 2 \nabla a \cdot \nabla \psi_\pi] . \tag{3.142}$$

After reordering the terms of the Klein-Gordon equation regarding the order of differentiation, we derive:

$$\begin{aligned} &\{[(1 - U_p) a] \Delta \\ &+ [2 (1 - U_p) \nabla a - a \nabla U_p] \cdot \nabla \\ &- U_s - (\nabla U_p) \cdot (\nabla a) + (1 - U_p) \Delta a + k^2 \} \psi_\pi = 0. \end{aligned} \tag{3.143}$$

In order to let the first derivative vanish, the amplitude a must fulfil the equation:

$$2(1 - U_p) \nabla a - a \nabla U_p \stackrel{!}{=} 0 \tag{3.144}$$

and, separated by variables,:

$$\frac{1}{2(1 - U_p)} \nabla U_p = \frac{1}{a} \nabla a. \tag{3.145}$$

giving, with the help of Lebesgue's dominated convergence theorem,

$$\nabla \ln \left(\frac{a}{a_0} \right) = -\frac{1}{2} \ln \left(\frac{1 - U_p}{1 - U_{p0}} \right) \tag{3.146}$$

and finally comparing the arguments:

$$a = a_0 \left(\frac{1 - U_p}{1 - U_{p0}} \right)^{-1/2} = a_0 \sqrt{\frac{1 - U_{p0}}{1 - U_p}} \tag{3.147}$$

For large distances of r, the amplitude must be equal to one

$$\lim_{r \to \infty} a = 1 \tag{3.148}$$

giving $a_0 \sqrt{1 - U_{p0}} = 1$ and therefore:

$$a (\vec{r}) = \frac{1}{\sqrt{1 - U_p(\vec{r})}}. \tag{3.149}$$

The implementation of the amplitude into equation 3.143 gives:

$$\left\{ \sqrt{1 - U_p} \Delta + \nabla - U_s - (\nabla U_p) \cdot (\nabla a) + (1 - U_p) \Delta a + k^2 \right\} \psi_\pi = 0 \tag{3.150}$$

and finally eq. 3.55:

$$\left[-\hbar^2 / (2\mu) \boldsymbol{\nabla}^2 + U_L + V_C \right] \varphi = E_{\mathrm{cm}} \varphi \tag{3.151}$$

with

$$U_L = \frac{U_s}{1 - U_p} - \frac{k^2 U_p}{1 - U_p} - \left[\frac{\frac{1}{2} \boldsymbol{\nabla}^2 U_p}{1 - U_p} + \left(\frac{\frac{1}{2} \boldsymbol{\nabla} U_p}{1 - U_p} \right)^2 \right] \tag{3.152}$$

3.3.3 Higher-Order Corrections to the Eikonal Approach

It is difficult to predict the effect of neglecting higher-order derivatives, as has been presented in the derivation of the Eikonal, especially when the involved potential has such a complex structure. Nevertheless, in the following, two procedures are introduced which have been studied within this work, but happen to be numerically unstable and therefore have not been taken into consideration in the final calculations.

Iterative procedure As a first idea, an iterative procedure is taken into account, where the second derivative is non-zero in the second step of the iteration. In the derivation of the solution of

$$[-\mathrm{i}\Delta S + (\nabla S)^2 - k^2 + U]\phi = 0 \tag{3.153}$$

the derivative of second order, namely the $-\mathrm{i}\nabla^2 S$ term, has been neglected in the previous discussions. Indeed, the second derivative is expected to be small, but to get a better understanding, it is considered in a second step within an iteration process. First it is neglected ($\Delta S_0 = 0$), but in the following step, the second derivative can be calculated from the first result and taken into account

$$K = \sqrt{k^2 - U + \mathrm{i}\Delta S}. \tag{3.154}$$

To derive a formula for the second derivative, an oriented gradient $\partial = \widehat{k}\vec{\partial}$ is applied to K, giving

$$\vec{\partial}\hat{k}K = \Delta S = \frac{\partial(k^2 - U)}{2\sqrt{k^2 - U + \mathrm{i}\Delta S}} + \frac{\mathrm{i}\partial\Delta S}{2\sqrt{k^2 - U + \mathrm{i}\Delta S}}. \tag{3.155}$$

leading to iterative formula

$$\Delta S_{n+1} = \frac{\partial(k^2 - U)}{2\sqrt{k^2 - U + \mathrm{i}\Delta S_n}} + \frac{\mathrm{i}\partial\Delta S_n}{2\sqrt{k^2 - U + \mathrm{i}\Delta S_n}} \tag{3.156}$$

with the initial condition $\Delta S_0 = 0$, and therefore

$$\Delta S_1 = \frac{\partial(k^2 - U)}{2\sqrt{k^2 - U}} = \partial\sqrt{k^2 - U} \tag{3.157}$$

$$\Delta S_2 = \frac{\partial(k^2 - U)}{2\sqrt{k^2 - U + \mathrm{i}\Delta S_1}} + \frac{\mathrm{i}\partial\Delta S_1}{2\sqrt{k^2 - U + \mathrm{i}\Delta S_1}} \tag{3.158}$$

$$= \frac{\partial(k^2 - U)}{2\sqrt{k^2 - U + \mathrm{i}\partial\sqrt{k^2 - U}}} + \frac{\mathrm{i}\partial^2\sqrt{k^2 - U}}{2\sqrt{k^2 - U + \mathrm{i}\partial\sqrt{k^2 - U}}}. \tag{3.159}$$

Unfortunately, the application of these correction terms lead to numerical instabilities. Therefore, another approach was studied, which will be presented in the following.

Alternative procedure Before the next approach to derive higher order corrections is presented, the relevance in terms of the dependence of k is estimated. Reusing the notation from the above, the local momentum is defined

$$K^2 = k^2 - U \tag{3.160}$$

leading to the Eikonal equation

$$\left[-\mathrm{i}\Delta S + \left(\vec{\nabla}S + \vec{k}\right)^2\right] = K^2. \tag{3.161}$$

Using cylindrical coordinates and $\vec{k} = k\hat{e}_z$, the differential equation gives explicitly:

$$\left(\vec{\nabla}S + \vec{k}\right)^2 = \left(k + \frac{\partial S}{\partial z}\right)^2 + \left(\frac{\partial S}{\partial b}\right)^2 \tag{3.162}$$

hence

$$\left(k + \frac{\partial S}{\partial z}\right)^2 = K^2 - \left(\frac{\partial S}{\partial b}\right)^2 + \mathrm{i}\Delta S. \tag{3.163}$$

Analogous to the derivation of the iteration formula, the second order derivatives and derivatives in b are neglected as a first step, giving the known result

$$S_1(b,z) = \int_{-\infty}^{z} \mathrm{d}z' \left(K(b,z') - k\right). \tag{3.164}$$

To estimate the contribution of the derivative of b, it is performed to the first-step solution above, giving

$$\frac{\partial S}{\partial b} \approx \frac{\partial S_1}{\partial b} = \int_{-\infty}^{z} \mathrm{d}z' \frac{\partial K}{\partial b} = \int_{-\infty}^{z} \mathrm{d}z' \left(-\frac{1}{2}\frac{1}{K(b,z')}\frac{\partial U}{\partial b}\right) \sim \mathcal{O}\left(\frac{\partial U/\partial b}{k}\right) \tag{3.165}$$

and correspondingly

$$\frac{\partial^2}{\partial b^2} S \approx \frac{\partial^2 S_1}{\partial b^2} \sim \mathcal{O}\left(\frac{\partial^2 U/\partial b^2}{k}\right) \tag{3.166}$$

while the leading order term is

$$k + \frac{\partial S}{\partial z} = K \sim \mathcal{O}(k) \tag{3.167}$$

hence,

$$\left(\vec{\nabla}(kz + S)\right)^2 = \left(k + \frac{\partial S}{\partial z}\right)^2 + \mathrm{i}\Delta S \left(+ \mathcal{O}\left(\frac{1}{k^2}\right)\right). \tag{3.168}$$

The second derivative in z gives

$$\frac{\partial^2}{\partial z^2}S = \frac{\partial^2}{\partial z^2}(kz+S) = \frac{\partial}{\partial z}K = \frac{-\partial U/\partial z}{2k\sqrt{1-U/k^2}} \sim \mathcal{O}\left(\frac{\partial U/\partial z}{k}\right) \tag{3.169}$$

Summarizing these findings: The derivations in b are of order $\mathcal{O}(U'/k^2)$ and $\mathcal{O}(U''/k)$. For the latter, the additional suppression due to the second derivative in U comes into play, which is usually small. Both terms are considered to be negligible. The second derivative in z, however, is taken into account in the following calculations. Therefore,

$$\left(k+\frac{\partial S}{\partial z}\right)^2 - \mathrm{i}\frac{\partial^2}{\partial z^2}S = K^2 \tag{3.170}$$

To solve this equation we define a new variable

$$\Omega = kz + S \tag{3.171}$$

so that

$$\frac{\partial}{\partial z}\Omega - \mathrm{i}\frac{\partial^2}{\partial z^2}\Omega = K^2 \tag{3.172}$$

Defining $v = \partial\Omega/\partial z$ leads to the differential equation

$$v^2 - \mathrm{i}v' = K^2, \tag{3.173}$$

where the prime indicates the derivative in z. Like in the earlier considerations, v' is neglected in the first attempt, getting

$$v_0 = K. \tag{3.174}$$

v' is expected to be a small correction to v_0, hence

$$v = v_0 + \epsilon, \qquad v^2 \sim v_0^2 + 2\epsilon v_0 \qquad \text{and} \tag{3.175}$$

$$v_0^2 + 2\epsilon v_0 - \mathrm{i}(v_0' + \epsilon') = K^2. \tag{3.176}$$

Substituting $v_0 = K$ gives

$$K^2 + 2\epsilon K - \mathrm{i}(K' + \epsilon') = K^2, \tag{3.177}$$

leading to

$$\epsilon' + 2\mathrm{i}K\epsilon = -K', \tag{3.178}$$

an inhomogeneous differential equation of first order. The solution of the homogeneous equation is

$$\epsilon_0 = A\exp(-2\mathrm{i}S_0) \tag{3.179}$$

where

$$S_0 = \int_{-\infty}^{z} \mathrm{d}z' K \tag{3.180}$$

and, by variation of the constant,

$$A' = -K' \exp(2\mathrm{i}S_0) \tag{3.181}$$

$$A(b,z) = -\int_{-\infty}^{z} \mathrm{d}z' K'(b,z') \exp(2\mathrm{i}S_0(b,z')). \tag{3.182}$$

Finally, the solution of eq. 3.178 is

$$\epsilon = A(b,z) \exp(-2\mathrm{i}S_0(b,z)). \tag{3.183}$$

Getting back to the original variables

$$v = \Omega' = K(b,z) + \epsilon(b,z) \tag{3.184}$$

finally gives

$$S = \Omega - kz = \int_{-\infty}^{z} \mathrm{d}z'(K(b,z') - k) + \int_{-\infty}^{z} \mathrm{d}z' \epsilon(b,z'). \tag{3.185}$$

Unfortunately, the exponential function in ϵ rises too rapidly for small incident energies, giving enormously large cross sections (infinite). This effect dies out so slowly that also regions of interest are spoiled in our calculation. Therefore, these correction terms were not included in our calculations in order to prevent numerical instabilities.

3.4 Results

In this section, the results for pion-nucleon cross sections, as well as the scattering of pions with several nuclei are presented. The parameter set has been fixed to the pion nucleon data. For the calculation of the pion nucleus potential, these parameters have not been changed.

3.4.1 Comparison to Pion-Nucleon Scattering Data

We derive the cross sections of pion scattering with a proton in the following way:

$$\sigma(\pi^+ p) = \frac{4\pi}{k}\left[\mathrm{Im}f^{3/2} + \mathrm{Im}f^{\Delta}\right] \tag{3.186}$$

$$\sigma(\pi^- p) = \frac{4\pi}{k}\left[\frac{1}{3}\left(\mathrm{Im}f^{3/2} + \mathrm{Im}f^{\Delta}\right) + \frac{2}{3}f^{1/2}\right] \tag{3.187}$$

The resulting fit, with experimental data for comparison, is shown in figure 3.7 for $\sigma(\pi^+ p)$ and in figure 3.8 for $\sigma(\pi^- p)$

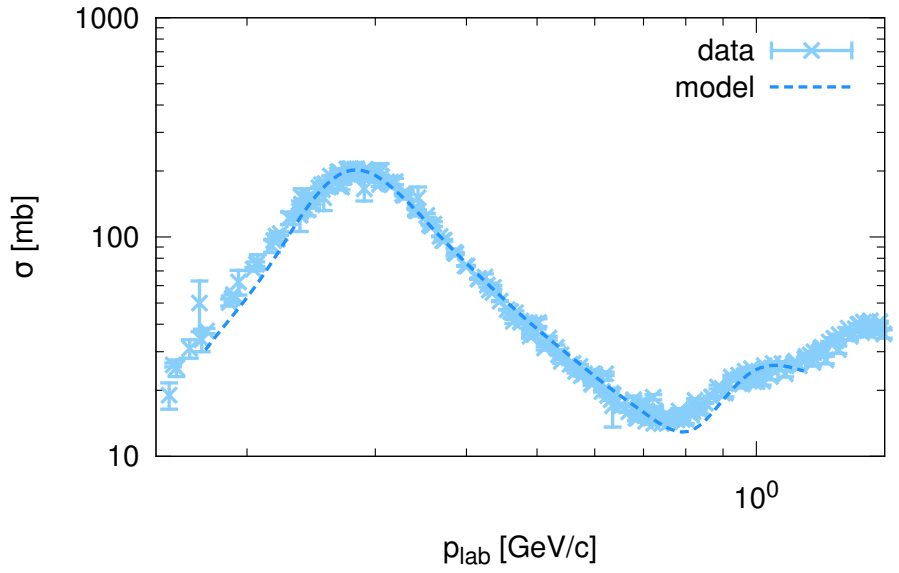

Figure 3.7: π^+ scattering in comparison with data from [B+12]

The derivation of the pion-nucleon cross sections is based on our schematic *ansatz*-amplitudes (see section 3.2.3) due to the uncertain situation of resonances listed in the PDG. We have chosen a special amplitude for the Δ-resonance (eq. 3.75), which dominates the region of interest from 100 MeV up to 1.5 GeV incident pion energy. The

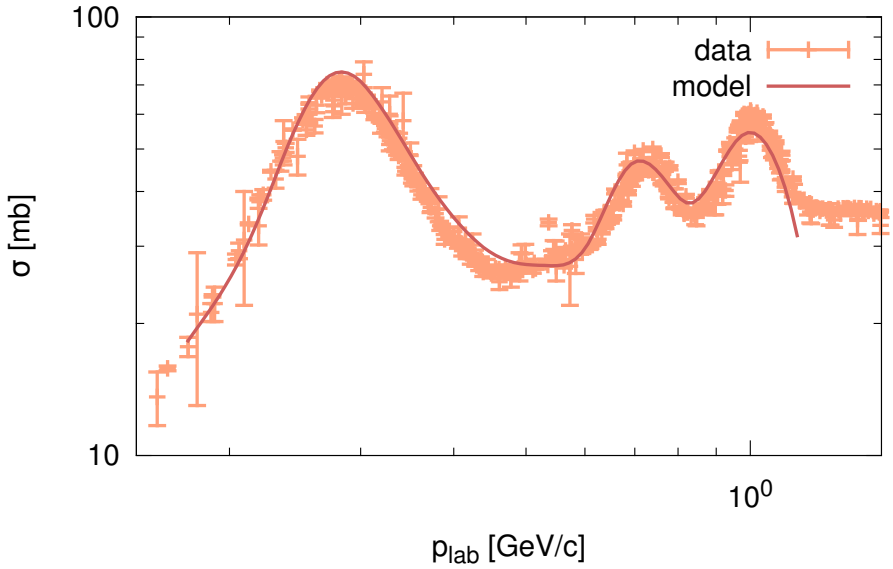

Figure 3.8: π^- scattering in comparison with data from [B+12]

amplitude for Δ has been chosen in such a way that it reproduces the purely isospin 3/2 cross section of $\pi^+ p$ scattering. This was achieved by use of an energy-dependent width and form factors. For all other *ansatz* amplitudes, simple Breit-Wigner functions were used.

3.4.2 Collection of Terms Contributing to the Pion-Nucleus Potential

The final pion-nucleus potential has been developed within the previous sections. The approach of [JS96] has been used as basis, but several changes to the potential have been applied. Nevertheless, the main structure of the used Kisslinger-type potential 3.56 has stayed intact:

$$U_K = U_s + \boldsymbol{\nabla} U_p \boldsymbol{\nabla} \tag{3.188}$$

Using the Krell-Ericson transformation, a local potential 3.152

$$U_L = \frac{U_s}{1 - U_p} - \frac{k^2 U_p}{1 - U_p} - \left[\frac{\frac{1}{2}\boldsymbol{\nabla}^2 U_p}{1 - U_p} + \left(\frac{\frac{1}{2}\boldsymbol{\nabla} U_p}{1 - U_p} \right)^2 \right] \tag{3.189}$$

is derived. The s-wave potential U_s is composed of s-wave contributions. We use the amplitudes $b_{0,1}$ from [JS96] at 291 MeV with an additional higher energy resonance

potential:

$$U_{1/2} = 4\pi\gamma_1 \cdot f^{1/2} \frac{1}{3} (\rho + q_\pi \ \delta\rho) \tag{3.190}$$

$$U_{3/2} = 4\pi\gamma_1 \cdot f^{3/2} \frac{2}{3} \left(\rho - \frac{1}{2} q_\pi \ \delta\rho\right) \tag{3.191}$$

with scattering amplitudes $f^{1/2}$ (eq. (3.88 and 3.89) and $f^{3/2}$ (eq. (3.90 and 3.91). The corresponding s-wave potential reads:

$$U_s(r) = U_s(r)\Big|_{B_{0,1}=0} + U_s(r)\Big|_{b_{0,1}(297 \text{ MeV})} + U_{1/2} + U_{3/2} \tag{3.192}$$

The p-wave potential from [JS96] has been changed in such a way that the amplitudes are not taken from [JS96], but our *ansatz* has been developed where f_Δ (eq. 3.75) is used, leading to:

$$c_0 = \frac{2}{3} \frac{1}{k^2} f_\Delta \tag{3.193}$$

$$c_1 = \frac{c_0}{2} \tag{3.194}$$

implemented into α_1 (eq. 3.61):

$$\alpha_1(r) = 4\pi \ [c_0 \ \varrho_0(r) - q_\pi c_1 \varrho_1(r)]/\gamma_1 \tag{3.195}$$

The two-nucleon contribution did not only introduce a differeynt description of the amplitudes, but also a different density dependence (eq. 3.116)

$$\alpha_2 = 4\pi \left[-iW_o \frac{(\Gamma/2)^2}{(T_r - T)^2 + (\Gamma/2)^2} \ \varrho(r)\right] /\gamma_2 \tag{3.196}$$

with the density (eq. 3.112):

$$\varrho = \frac{1}{2}[3\rho^2 - (1 + q_\pi^2)\delta\rho^2 + q_\pi \rho \delta\rho] \tag{3.197}$$

and therefore the p-wave dominated potential (eq. 3.60):

$$U_p(r) = \frac{\alpha_1}{1 + \xi/3\alpha_1} + \alpha_2. \tag{3.198}$$

Finally, the Coulomb potential is added:

$$U(r) = U_L + V_C \tag{3.199}$$

The Krell-Ericson transformation (see section 3.3.2) leads to a Schrödinger-like equation. It is solved in Eikonal approximation, where the cross sections are defined in the

following. The absorption cross section and the absorption cross section for two-nucleon reactions read:

$$\begin{aligned}\sigma_{\text{abs}} =& \frac{2\mu}{k}\int \mathrm{d}b b 2\pi \mathrm{d}z\,|\psi|^2\,\mathrm{Im}V^{\text{opt}}\\ \sigma_{\text{abs}}^{2N} =& \frac{2\omega}{k}\int \mathrm{d}b b 2\pi \mathrm{d}z\,|\psi|^2\,\mathrm{Im}W_{0NN}\end{aligned} \tag{3.200}$$

The other cross sections depend on χ (eq. 2.71):

$$\chi = -\frac{1}{2k}\int_{-\infty}^{+\infty} U(\vec{b},z)\mathrm{d}z \tag{3.201}$$

giving

$$\begin{aligned}\sigma_{\text{tot}} =& \frac{4\pi}{k}\mathrm{Im}f\,(\vartheta=0) = 4\pi\int_0^\infty \mathrm{d}b\,[1-\exp\left(-\mathrm{Im}\chi\right)\cos\left(\mathrm{Re}\chi\right)]\\ \sigma_{\text{tot}}^{\text{el}} =& \int \mathrm{d}\Omega\,(f_E)^2\\ =& 4\pi\int_0^\infty \mathrm{d}b\,[1-\exp\left(-\mathrm{Im}\chi\right)\cos\left(\mathrm{Re}\chi\right)] - 2\pi\int_0^\infty \mathrm{d}b\,[1-\exp\left(-2\mathrm{Im}\chi\right)]\\ \sigma_{\text{tot}}^{\text{r}} =& \sigma_{\text{tot}} - \sigma_{\text{tot}}^{\text{el}} = 2\pi\int_0^\infty \mathrm{d}b\,[1-\exp\left(-2\mathrm{Im}\chi\right)]\,.\end{aligned} \tag{3.202}$$

3.4.3 Comparison to Pion-Nucleus Scattering Data

The nuclei presented in the following have been chosen due to the availability of data mainly. The data [ANA$^+$81,CTA$^+$74] provides both informations: scattering of π^- and of π^+, giving the opportunity to study also isospin structures. The following results are used for exploratory studies from very light nuclei such as Lithium up to very heavy nuclei like Bismuth. For all calculations we use the same paramter-set. As we have discussed within this work, the highly complicated structure of the amplitudes can quite successfully be described with phenomenological amplitudes. To conserve most information from the microscopic models, we keep the number of free parameters as low as possible. The price we pay are small discrepancies with the data. This is expected from the rather simple *ansatz* we use, which fails to describe the very maximum of the Δ-resonance for almost every nucleus. This could be improved by taking into consideration the separation energy, which is characteristic for valence nucleons of each nucleus. The nuclei which are discussed in this work vary from few MeV in the case of ^{209}Bi to almost 20 MeV in the case of ^{12}C. If a nucleon is bound strongly, more energy is needed to produce a resonance, which in our description leads to a shift of the position of the resonance. The effect of the resonance shift is shown in fig. 3.9.

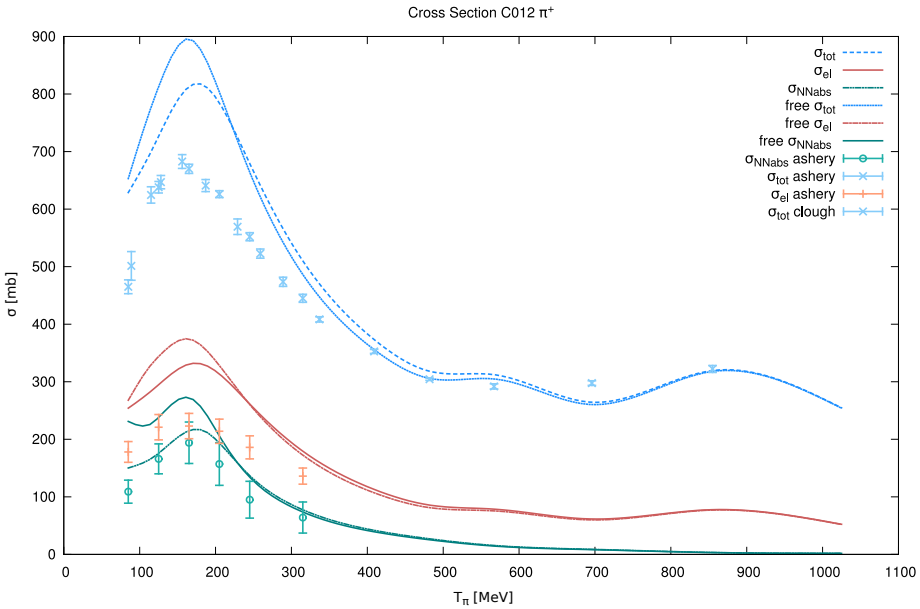

Figure 3.9: Comparison of calculation with (dashed line) and without (solid line) separation energy. Shown are total (blue), elastic (red) and 2 N absorption cross sections for π^+ scattering on ^{12}C

In addition to the resonance shift due to the separation energy, we introduce an additional collision-broadening width, which we assume to be equal for all nuclei and which has the value of 20 MeV. With the introduction of these parameters, our calculation has been improved, but still shows descripancies, where for ^{12}C we do worst.

In the following, these calculations are presented for several nuclei. The lightest nucleus we use is Li, while the heaviest is Bi. The experimental data is mainly taken from [ANA+81, CTA+74].

Lithium

^{7}Li is a stable nucleus and constitutes 95% of Lithium in nature. It is composed of three protons and four neutrons. Because it is very small, it is mainly dominated by surface effects. This leads to a sensitivity to the derivative of the nuclear density and therefore of its shape. For differential cross sections, we compare to data from ^{6}Li, where we find a good description for 100 MeV, but with increasing energy, we cannot describe the second maximum and fail to describe the first minimum for all cases, see fig. 3.10. Due to the neutron excess of ^{7}Li we describe the π^- (fig. 3.11) cross sections better than π^+ (3.12). Unfortunately, there are only two data-points available.

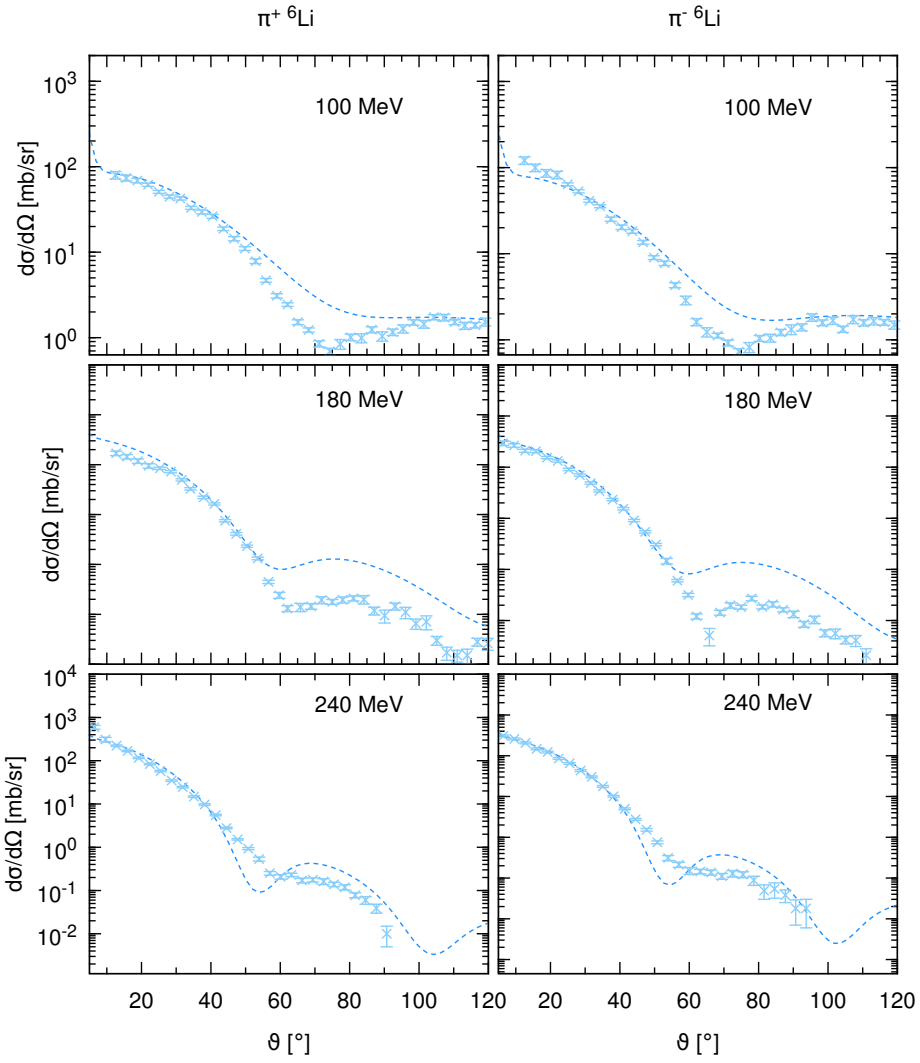

Figure 3.10: Differential cross section for π^+ (left) and π^- (right) scattering on ^{6}Li for the energies 100 MeV, 180 MeV and 240 MeV.

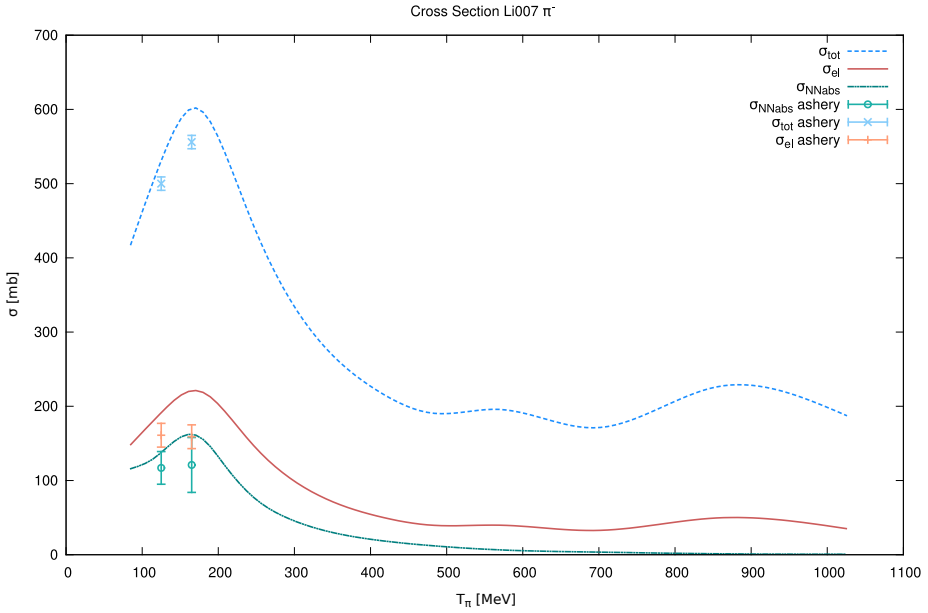

Figure 3.11: Shown are total (blue), elastic (red) and 2 N absorption cross section for π^- scattering on ^{7}Li

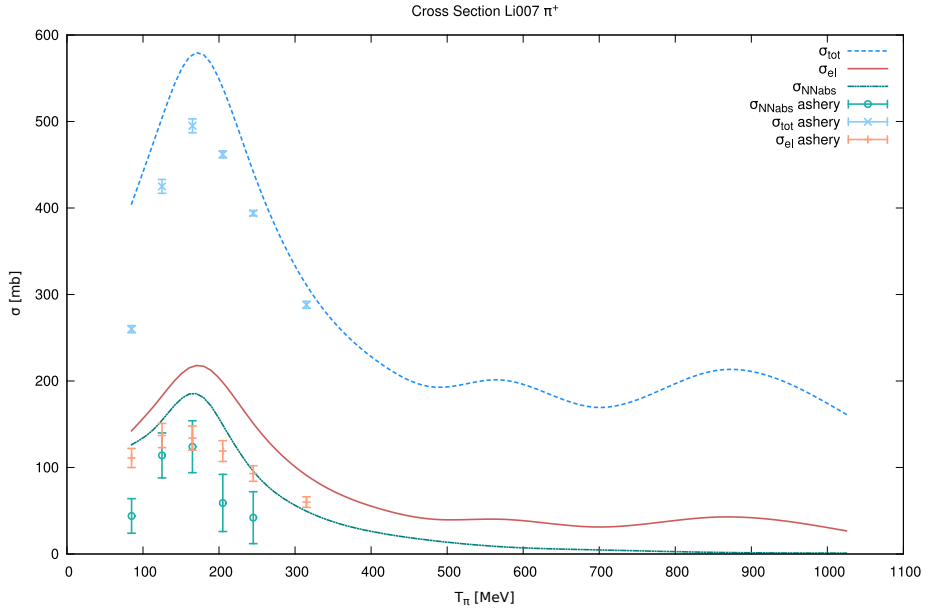

Figure 3.12: Shown are total (blue), elastic (red) and 2 N absorption cross section for π^+ scattering on ^{7}Li

Carbon

Carbon in nature consists to about 98% of the stable ^{12}C, which is built of six protons and six neutrons. Even thogh it is a symmetric nucleus, it is rather complicated, and our model shows the largest discrepancies to the data as can be seen in fig. 3.9. The figure shows also that ^{12}C has the largest effect in our selection of nuclei by shifting the Δ-resonance by the amount of the separation energy, which is almost 20 MeV. This large separation energy can, to some extent, be explained by the nuclear shell model. The valence nucleons (both valence-proton and -neutron) fill the $1p^{3/2}$ shell exactly half.
Half filled shells are known to give a comparable large binding and therefore make this state more stable, but it is unlikely that only these shell effects lead to such high separation energies. In addition to the nuclear shell structure of ^{12}C, there is a contribution to the binding due to the involved structure of ^{12}C. The high separation energy might also be caused by the intrinsic formation of three α-particles, which themselves are known to be strongly bound. However, we aim for a more general description, covering wide ranges of the nuclear chart, without taking into account individual properties of each nucleus. Our simple model is therefore not suited to perform a detailed spectroscopy of each nucleus.

In fig. 3.13 several calculations are displayed. The solid curve (red) represents the

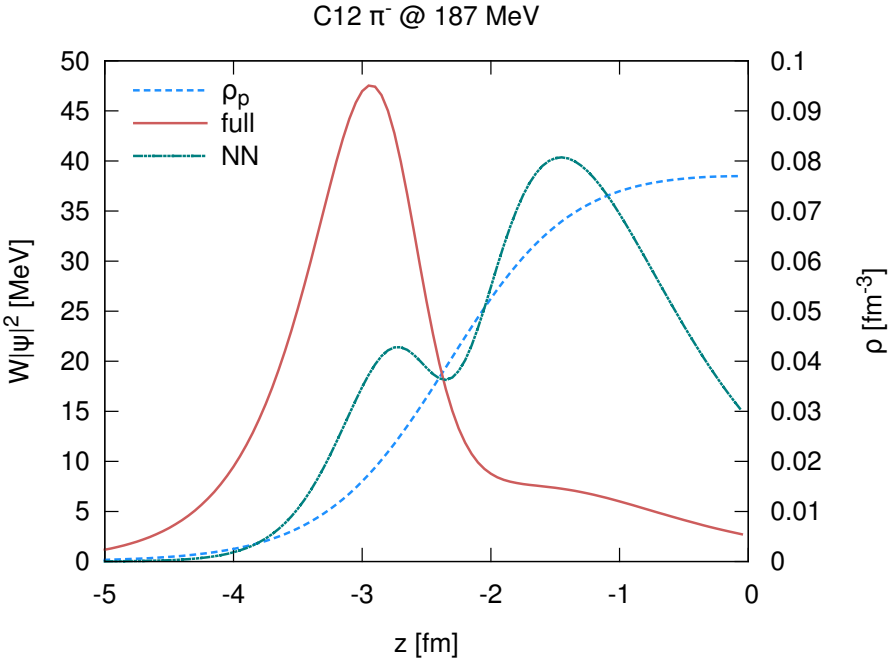

Figure 3.13: Interaction density and nuclear density in the C nucleus, along the meson trajectory ($b = 0$) . Impact momentum $k = 187$ MeV/c.

interaction density of the full potential, the dottet curve (blue) only the two-nucleon contribution, defined as integrand of eq. 3.200, respectively. the dashdotted line (green) is the nulear density. The figure shows, that the interaction with the ^{12}C is surface dominted., having not much overlab with the nuclear density. The contribution of the two-nucleon absorption term is very high and can be understood by the estimated effective number of participating nucleons N_{eff} from [ANA$^+$81] at about $\Gamma_\Delta/2$ from the maximum, which gives 1.39.

Oxygen

^{16}O is one of the double-magic nuclei, which are known to be especially stable due to their closed shell. ^{16}O has 8 protons and 8 neutrons filling up the 1p shell. For oxygen, experimental data exists for differential cross sections well beyond the Δ-resonance to check our approach. The comparison is shown in fig. 3.14, where the differential cross

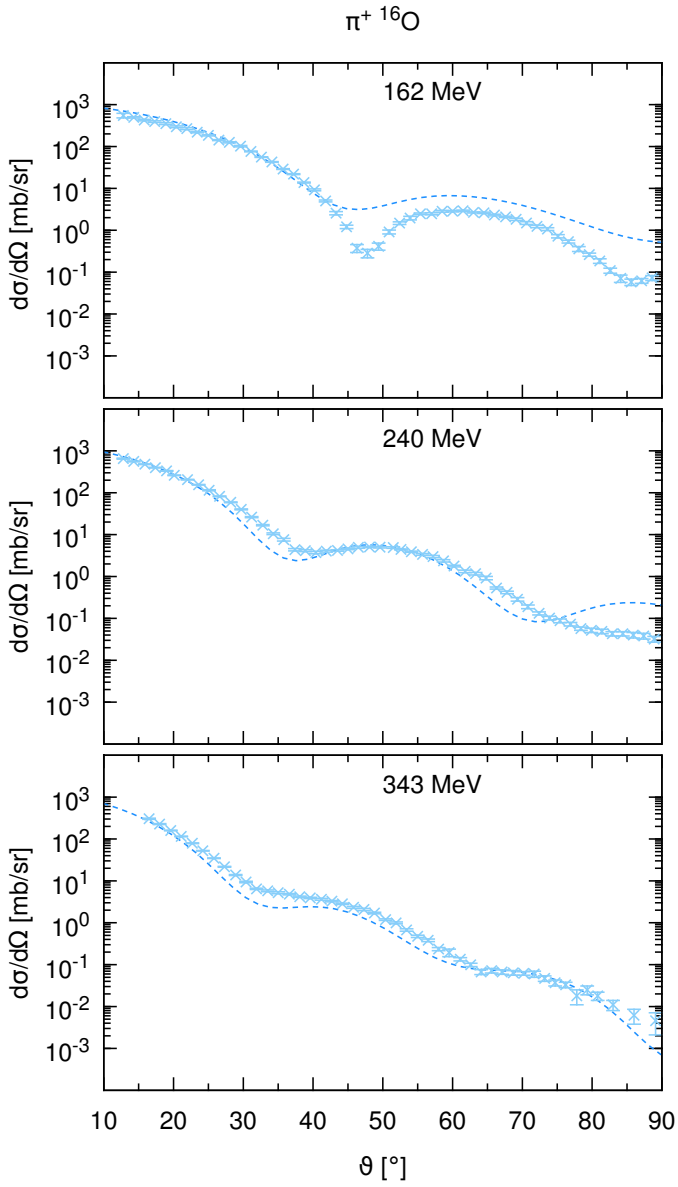

Figure 3.14: Differential cross section for π^+ scattering on ^{16}O for the energies 162 MeV, 240 MeV and 343 MeV.

section is shown for π^+ scattering on ^{16}O for 162 MeV, 240 MeV and 343 MeV incident

energy of the pion. The description improves with increasing incident energy. The calculation of the highest energy in fig. 3.14 agrees satisfactorily well over five orders of magnitude and is surprisingly good at large angles. The Eikonal approximation is expected to work well for high energies, but is conceived actually for small angles. One argument might be that the ^{16}O nucleus is rather round and may be easier described within our model, which does not take into account advanced nuclear structure effects or vibrational excitation modes. Nevertheless, despite the round shape, ^{16}O can even form a linear chain structure by clustering into four α-particles like ^{12}C, as discussed in [IMIO11].

Bismuth

^{209}Bi is a heavy nucleus with a closed neutron shell $3p$ with 126 neutrons. The number of protons is 83, which is one additional proton to the closed $3s$ shell of 82 protons, leading to a high nuclear spin of 9/2 and a corresponding magnetic moment of 4.1106 μ/μ_N. ^{209}Bi can be treated as a stable nucleus because its estimated half-life is about 100 billion times larger than the age of the universe. In figures 3.15 and 3.16 the cross sections are plotted for π^+ and π^-scattering, respectively. The description of all three cross sections, namely total, elastic and absorption, is satisfactorily well for π^+, but surprisingly weak for π^-. The π^- mainly reacts with the valence proton. The valance proton may be covered by the neutron skin, which is not taken into account in our approach, and might cause the discrepancies. Nevertheless, the data for π^- scattering is scarce and accompanied with large error-bars. Comparing ^{209}Bi with ^{12}C, we find that the pion penetrates more deeply into the nucleus. This can be seen in fig. 3.17, where the full and the two-nucleon absorption terms are plotted together with the neutron density. In comparison to ^{12}C (fig. 3.13), the two-nucleon absorption term is drawn more into the nucleus and has approximately only half the magnitude. This can be understood from the estimated effective number of participating nucleons N_{eff} from [ANA+81] at about $\Gamma_\Delta/2$. It indicates that on average there are more than 2 nucleons involved (4.32), which are therefore not contributing to the two-nucleon term and explain the big difference.

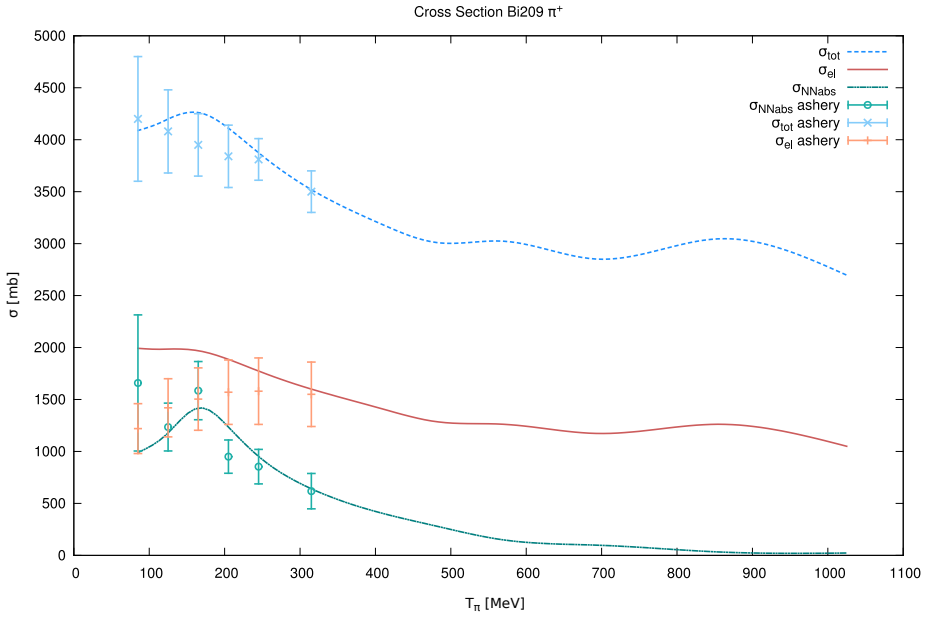

Figure 3.15: Shown are total (blue), elastic (red) and 2 N absorption cross section for π^+ scattering on ^{209}Bi

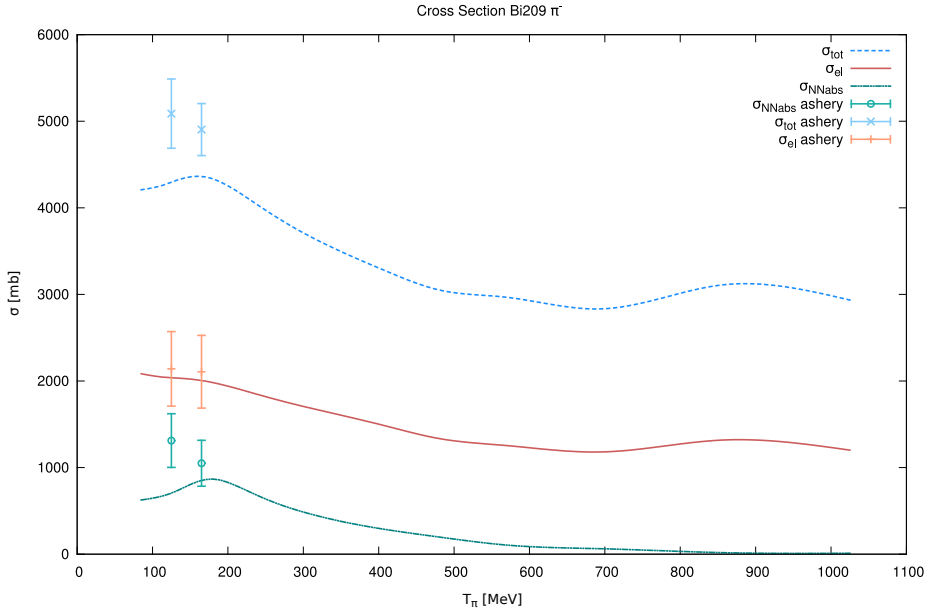

Figure 3.16: Shown are total (blue), elastic (red) and 2 N absorption cross section for π^- scattering on ^{209}Bi

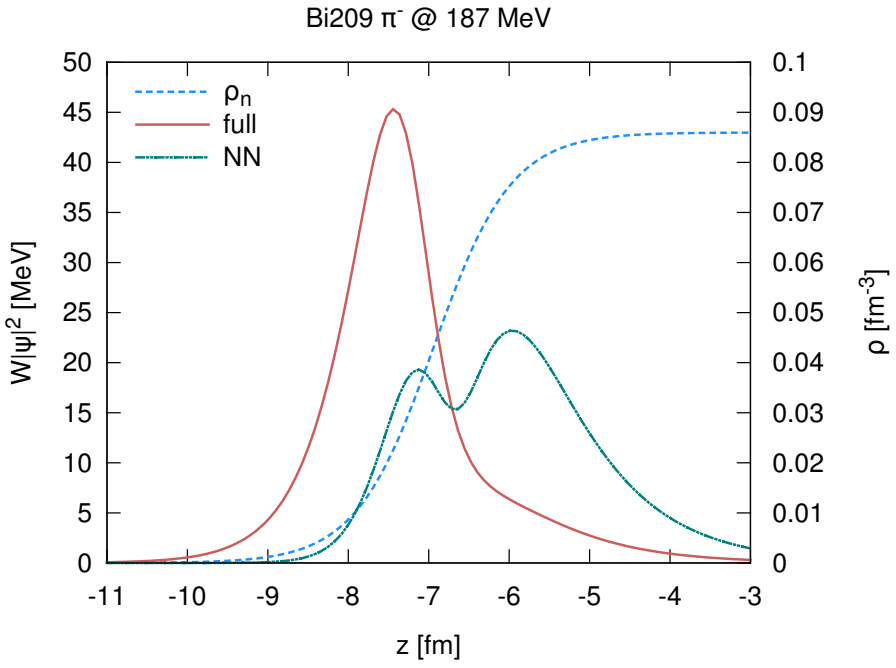

Figure 3.17: The interaction density (integrand of absorption cross section) in the Bi nucleus, along the meson trajectory ($b = 0$). Impact momentum $k = 187$ MeV/c.

4 Antiproton-Nucleus Interactions

4.1 Antinucleon-Nucleus Potential

Following the strategy introduced for pions in chapter 3, we will first discuss aspects of the two-body antinucleon-nucleon interaction and second apply our ansatz to the nuclear medium by using a folding approach, where the nuclear density contributes.

4.1.1 Antinucleon-Nucleon Interaction

Investigating interactions involving antinucleons is challenging, but provides unique possibilities. First, the interaction of antinucleons with matter is interesting itself. The annihilation is known to play a dominant role in the interaction process, but is still not fully understood. Especially in the quark picture, the description is very complex and unclear. The fundamental understanding of antimatter-matter interactions is of renewed interest these days due to many upcoming experimental set-ups. Due to the manifold reactions and the ensuing large background, however, the experimental situation is quite challenging too.

Second, the antinucleon, in particular the antiproton, is well suited for use as a probe for nuclear matter investigations. It allows to study nuclear properties along isotopic chains as proposed in AIC. The antiproton is also sensitive to the nuclear radii [LK07, Len09] and yields a possibility of the estimation of the radius of both proton and neutron in the same experiment, which has never been done.

In this work, we investigate the meson production in a reaction of antinucleons with different nuclei. Therefore, we are interested in a wide energy range which will be, for example, covered by the PANDA experiment at GSI in the near future. We would like to pave the way towards the full description of meson production in antinucleon-annihilation reactions on nuclei on a quantum mechanical level.

To derive the description of antinulceon-nucleus interactions, we follow the procedure which has been introduced for the pions. Similar to the pion, the antinucleon cannot penetrate deeply into the nuclear medium, and the interaction therefore takes place mainly at the peripheral surface region of the nucleus, at very low densities.

The interaction of antinucleons with nucleons is strongly related to the interaction of pions with nucleons. The involved Feynman diagrams can be transformed from one interaction into another by simple rotation. A detailed description of the underlying

symmetries which link those two reactions is discussed in [RHKS96]. Because the antiprotons are absorbed in nuclear matter even more strongly, we use a folding approach, where the elastic free-space antinucleon-nucleon T-matrix is folded with the nuclear densities, taken from self consistent Hartree-Fock-Bogoliubov calculations.

The Eikonal approximation, which will yield us the information about the incoming and outgoing wave function, works even better for antinucleons than pions, due to the higher mass.

Over the last decades microscopic models have been quite successful to describe antinucleon-nucleon interaction. The advantage of a description on a hadronic level is, that cross references to other reactions, such as pion-nucleon interactions, is possible. The corresponding Feynman diagrams share the same vertices and can be obtained from rotation in Mandelstam-space as discussed in [RHKS96]. Those microscopic models, however, face a big problem, because the exchanged particles, which are used as mediators of the interaction, are themselves composite objects. The corresponding theories are therefore not fundamental, and renormalization is a challenge. With increasing energy, more and more complicated interaction-graphs can be constructed. We present two possible ways to tackle this problem.

First, we focus on specific channels, which are treated explicitly, while all other contributions are taken into account by an ansatz optical potential. This is done by the Jülich/Bonn group, the Paris group and the Nijmegen group. The work of the first two will be briefly introduced in the following.

Second, the existing data can be used to find a description for the full energy range, starting from 100 MeV and going up to a few GeV by making an phenomenological ansatz, inspired by observables. This will be discussed after introducing the microscopic models mentioned above.

4.1.2 Microscopic Models

The microscopic models, such as Bonn/Jülich, take advantage of the Feshbach-projectors, which allow to give a full solution even though they are generated only inside a chosen model-space. In other words: In these models, specific channels are treated explicitly, depending on the selection of quantities and observables. This has been very successful in the energy-range up to 300 MeV. Depending on the energy, many channels open, and the number of possible intermediate states increases. Because there are no limits to the complexity of the interaction, there are infinitely many Feynman diagrams which can be included into the description of antinucleon-nucleon interaction. For general understanding, however, the number of diagrams can be truncated to only three classes of diagrams. These build the basis of the description and can be put together or iterated to derive more complicated structures. The three basic Feynman diagrams for elastic antinucleon-nucleon interaction are:

1. the purely elastic part expressed in one-meson exchange

2. the dispersive part, which has no counterpart in NN interaction
3. the resonance part.

Those digrams are shown in fig.4.1.

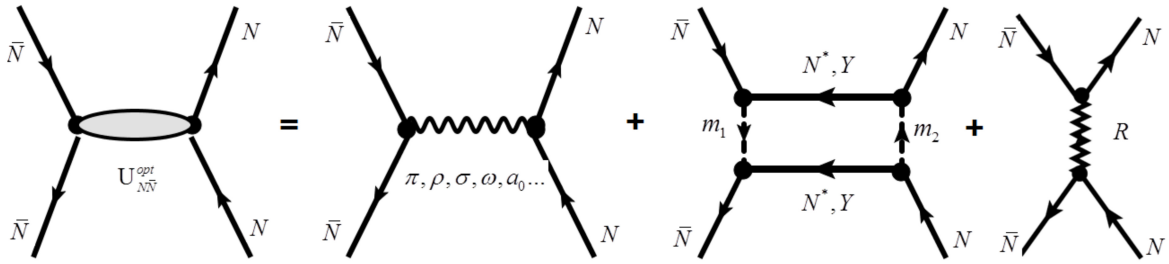

Figure 4.1: Classes of diagrams for $\overline{N}N$ interaction. Left: purely elastic part (from G-parity transformation), middle: dispersive parts, right: resonance contribution.

Purely elastic part The elastic part is built from models describing NN interaction. To derive the $\overline{N}N$ amplitudes, the G-parity transformation of the NN potentials is performed, which includes a charge conjugation plus 180° rotation around the y axis in isospin space. The G-parity transformation can be understood as a more generalized form of the charge conjugation, which transforms, for example, the electron into its antiparticle, the positron. Accordingly, for fermion-antifermionic systems the selection rules are

$$(-1)^{L+S+I} \,. \tag{4.1}$$

In a meson-exchange picture, this leads to a simple change of sign for G-parity-transformation of the NN (Paris [EBLLW09], Bonn [MH95]) interaction for some mesons, while others stay the same:

odd G-Parity vertices

$$V_{NN}(\pi, \omega, \delta) = -V_{\bar{N}N}(\pi, \omega, \delta)$$

even G-parity vertices

$$V_{NN}(\sigma, \rho, \eta) = V_{\bar{N}N}(\sigma, \rho, \eta)$$

This procedure has been criticized, because the early microscopic models calculated very large potential depths of about a few GeV with the G-parity transformation. The G-parity transformation is used for both microscopic models [BP68,KW86], which will be briefly introduced in the following.

Paris [EBLLW09] The Paris $\overline{N}N$ model is based on NN interactions, namely the NN Paris potential, which is then transformed with G-parity transformation. The Paris model is built in such a way that it is globally defined. This is achieved by using a linear energy dependent optical potential, which has both real and imaginary parts. The potential is optimized by a fit to the data.

Bonn [MH95] The $\overline{N}N$ potential of the Bonn/Jülich group is derived from the Bonn NN potential, accordingly. The Bonn/Jülich group treats two-meson intermediate states explicitly, while all other contributions are taken into account by a purely imaginary potential with no additional energy dependence. No fitting procedure is used to optimize parameters.

Nevertheless, both models use boson-exchange diagrams as the fundamental model and therefore work with hadronic degrees of freedom. Because hadrons are composed objects and therefore have to be understood as mediators of an effective interaction, they do no obey a fundamental theory. This is no disadvantage, as long as one is restricted to a rather small energy range or the treatment of specific channels only. With increasing energy, the complexity of the system increases accordingly, and the number of terms contributing to Feynman diagrams have to be added, which is at some point no longer manageable. The Paris and Bonn models provide good descriptions of the existing scattering data up to an incident energy of the antiproton of about 300 MeV. At about 1232 MeV the threshold of the $\Delta(1232)$-resonance opens along with many more Δ and N-resonances, which makes the description difficult.

4.1.3 Phenomenology

Rather than treating specific chennels explicitly and therefore being restricted to small energy-ranges, we aim for a description for wide energy ranges. In the following, a phenomenological approach for $N\overline{N}$ interactions is introduced [LLW14], leading to a satisfacory description of the $\overline{p}p$ total and elastic cross section. Like the microscopic model introduced above, we use a complex potential as a starting point for our calculations:

$$V = U - \mathrm{i}W \tag{4.2}$$

The Energy Dependence Because the cross section changes its behavior drastically from a rapid decrease at low laboratory momentum to a smooth slope at the high momentum range, we introduce two parameter-sets:

$$V_j = U_j - \mathrm{i}W_j \qquad j = 1, 2 \tag{4.3}$$

Both the real and imaginary part are parametrized in terms of Gaussian radial form factors with energy dependent strength and width parameters:

$$U(r,k) = U(k)\mathrm{e}^{-\frac{r^2}{a^2(k)}}; W(r,k) = W(k)\mathrm{e}^{-\frac{r^2}{b^2(k)}} \tag{4.4}$$

with the momentum dependent amplitude

$$U(k) = U_1 \; f(k) + U_2 \; (1 - f(k)) \tag{4.5}$$

and the same form used for the range parameters $\alpha(k) = a(k), b(k)$:

$$\alpha = \alpha_1 \; f(k) + \alpha_2 \; (1 - f(k)), \tag{4.6}$$

where

$$f(k) = \frac{1}{1 + \mathrm{e}^{(k-Q)/q}} \tag{4.7}$$

This separation into two sections can be interpreted as a visualization of the modification of scales. In the high-energy range the hadrons are no longer the degree of freedom, but quark and gluon induced reactions become important. Later, the fit to the antiproton-proton and antiproton-nucleon data will reveal that this separation of scales happens at a larger laboratory momentum p_{lab}, as one might expect from a look at the cross sections. This might indicate an influence of the underlying quark dynamics up to higher momenta.

The Strength of the Potential Microscopic approaches, as e.g. in [HHP89, MH95, TRdS94,ZT12,CLL$^+$82,EBLLW09], use G-parity transformed NN potentials which are usually accompanied by an absorptive potential that is anomalously deep at very short distances. The analysis of our approach shows a different behaviour. The imaginary bare potential is rather long-ranged and comparatively shallow. The overall strength, however, as expressed by the volume integral shown in fig. 4.2, agrees well with the

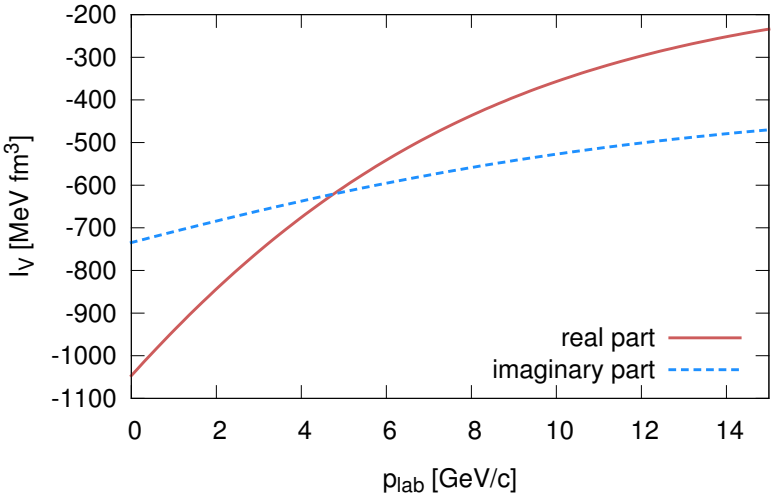

Figure 4.2: Volume integral I_V of the potential as a function of p_{lab}.

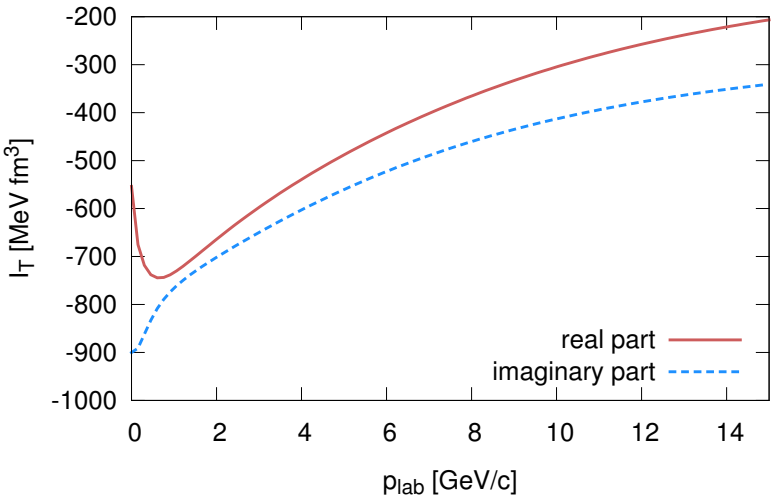

Figure 4.3: Volume integral I_T of the T-matrix as a function of p_{lab}.

strength used in other approaches. We derive the strength of the real and imaginary parts of our potential by simultaneously fitting the total and elastic cross sections. This allows us to have control of the challenging real part. To get a better understanding of the quite strong real part and the long range characteristic of the potential, we study the T-matrix, assuming a local operator:

$$\hat{T}\left(k^{'},k\right)=\int d^{3}rT\left(\vec{r}|k\right)e^{i\left(\vec{k}-\vec{k}^{'}\right)\cdot\vec{r}}=T\left(k-k^{'}\middle|\,k\right). \tag{4.8}$$

In Eikonal theory the Fourier-transformed T-matrix is given by

$$T\left(\rho,z|k\right)=V(\rho,z|k)e^{iS(\rho,z|k)} \tag{4.9}$$

where the complex Eikonal $S=\phi+i\kappa$ is devided into a plane wave contribution κ and a residual Eikonal depending on ϕ. The cross section is calculated in Eikonal approach using formulas 3.202. This complex Eikonal leads to a mixing of the real and imaginary parts of the potential in the T-matrix:

$$\text{Re}(T)=\left(U\cos(\phi)+W\sin(\phi)\right)e^{-\kappa}$$

$$\text{Im}(T)=\left(U\sin(\phi)-W\cos(\phi)\right)e^{-\kappa}$$

Due to the mixing of the real and imaginary parts, there is a strong cancellation, which reduces the unexpected long range of the potential to a typical short-range interaction.

The volume integral of the T-matrix

$$I_V = \int \mathrm{d}^3 r V \tag{4.10}$$

$$I_T = \int \mathrm{d}^3 r T \tag{4.11}$$

is shown in fig. 4.3. The resulting elastic and total cross sections in comparison to the data [B+12] are shown in fig. 4.4.

In this section, a phenomenological approach to antinucleon-nucleon scattering has been presented. Due to the visible modification of scales in the antiproton-proton cross section, a two-parameter set was introduced. The ansatz was fitted to the available data of total and elastic cross section simultaneously, giving control over the challenging real part. The surprisingly long range potential has a comparable strength as other approaches due to strong cancelations

4.2 Step Towards Pion Production in Antinuleon Annihilation in Nuclear Reactions

As has been discussed in this work, the interactions of pions and antiprotons with nuclear matter is very interesting and challenging at the same time. Both types of particles are strongly absorbed in nuclear matter. To overcome the difficulties which

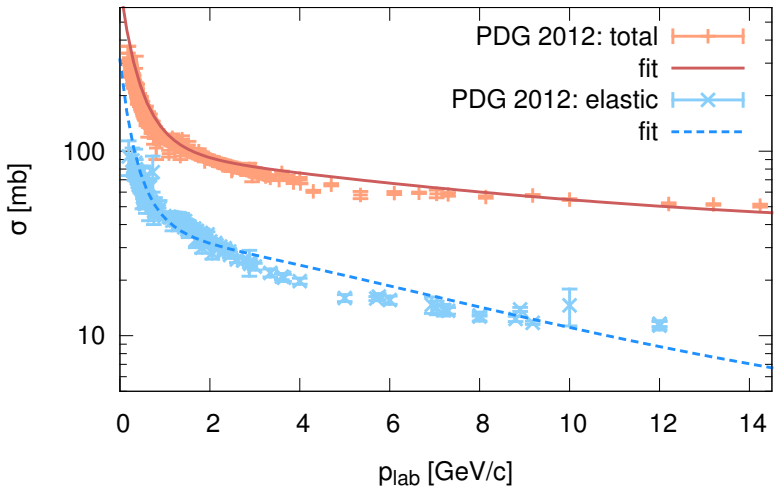

Figure 4.4: Phenomenological model total and elastic $\overline{p}p$ cross sections compared to data [B+12].

are introduced by the use of microscopic models, phenomenological models are used as described in sections 3.4.2 and 4.1.3. The interactions have been developed in an Eikonal theory framework, which gives also access to the involved wave functions. The knowledge of both the wave functions and the potential available gives the opportunity to reuse them in a more complex reaction: the pion production in antiproton-nucleus annihilation reactions. Similar to the antiproton- and pion-nucleus interactions, the corresponding Feynman diagrams can be divided into different classes of diagrams, depending on the available energy. In Fig. 4.5, the Feynman diagrams are shown for

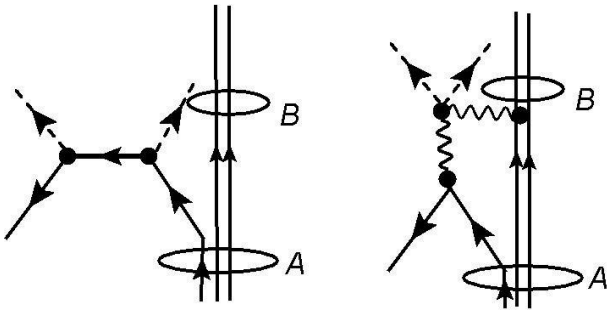

Figure 4.5: Feynman diagrams for the production of two pions within antinucleon-nuleon annihilation in nuclear matter

t- and s-channel interactions for the reaction

$$\overline{N} + A \rightarrow B + m_1 + m_2. \tag{4.12}$$

The solid line indicates nucleons (traveling forward in time) and antinucleons (going backward in time). First, the nucleons are bound within a nucleus A indicated by a circle, where in the final state the residual nucleus is B. The dashed lines represent the pions and the wavy line a ρ-meson. The antinucleon, indicated by the arrow going backwards in time, annihilates with a nucleon from the initial nucleus $A = A(N, Z)$, creating an intermediate state, which then decays into two mesons m_1 and m_2. The residual nucleus B can either be formed after an annihilation with a neutron, hence $B = B(N-1, Z)$ or after an annihilation with a proton, giving $B = B(N, Z-1)$, accordingly. Even if the produced mesons are reabsorbed and do not escape the nucleus, we consider the nucleus to be in a well-defined quantum state, also neglecting higher-order core polarization.

To derive a description of the process shown in fig. 4.5, it is divided into three main steps: The initial-state antinucleon-nucleus interaction, the production mechanism and the final-state pion-nucleus interaction. The description of the full reaction gives the opportunity to gain information about the annihilation reaction or the nuclear properties of the involved nucleus. These are especially of interest for several new upcoming experiments at the FAIR facility at GSI, such as the PANDA experiment [Lan09], but

also suitable for nuclear structure studies of short living isotopes at the AIC experiment [Kru05]. Both initial- and final-state interactions are important and need to be implemented in the calculation to achieve a full description of the pion production. Only then it is possible to investigate nuclear properties and information about annihilation processes by measuring the produced pions.

Despite the challenges which are met in calculations, there are also a lot of difficulties to perform the actual experiment. The higher the incident energy of the antiproton is, the deeper it can penetrate the nucleus and collect data of its inner structure. In our investigation, however, we are limited to non-excited residual nuclei, which stay intact after the reaction. This becomes less likely with increasing energy. In addition, there is a lot of background to this reaction, especially coming from multi-pion production. As has been discussed in [Ghe74, Ams98], the average pion multiplicity peaks at around five and reaches up to fifteen pions. The challenge will be to distinguish reactions where multiple pions were produced, but only two or even fewer escaped the nucleus, from reactions were only two pions were produced. Furthermore, a 4π detector would be needed to cover the whole reaction space, because also backward scattering is possible. Under these circumstances, it is worthwhile to identify the concrete reaction mechanisms, which will be discussed in the following.

The derivation of the interaction of antinulceons with a nucleus and the interactions of pions with a nucleus are used as initial- and final-state interactions, respectively. As shown before, we have a reasonable understanding of both the initial- and final-state interaction. The corresponding studies contribute to the calculation of the cross section for the whole reaction mechanism:

$$d^9\sigma_{\alpha\beta} = N_{\alpha\beta}\left(\frac{\hbar c}{2\pi}\right)^9 \frac{d^3k_1}{E_1}\frac{d^3k_2}{E_2}\frac{d^3k_B}{E_B}\left|M_{\alpha\beta}\left(\vec{k_1},\vec{k_2},\vec{k_B};\vec{k_\alpha}\right)\right|^2 \times \delta\left(\vec{k_1}+\vec{k_2}+\vec{k_B}\right)\delta\left(E_1+E_2+E_B-\sqrt{s}\right) \tag{4.13}$$

where $N_{\alpha\beta}$ is a normalization constant and the subscripts 1 und 2 stand for each pion, while B denotes the residual nucleus and s is the total centre-of-mass energy. While the delta accounts for energy and momentum conservation, the underlying physics is described by the matrix element:

$$M_{\alpha\beta} \approx t_{\overline{N}N\to 2\pi}(s)\langle\chi^{(-)}_{1\beta}\chi^{(-)}_{2\beta}\left|\varphi_B\right|\chi^{(+)}_{\overline{N}A}\rangle. \tag{4.14}$$

In eq. (4.14), the nuclear amplitude and the production amplitude are factorized. This is a good approximation, because the nuclear contribution proceeds on the scale of the Fermi-momentum (≈ 250 MeV/c), while the production involves baryon exchange (≈ 1 GeV/c), and therefore a separation of scales is introduced. The description of the cross section and the matrix element has been chosen to be rather general, but in fact the interpretation of φ_B, $t_{\overline{N}N\to 2\pi}$ and $\chi^{(-)}_{1\beta}\chi^{(-)}_{2\beta}$ strongly depends on the reaction scenarios which will be indicated below.

4.2.1 Peripheral In-Flight Reactions

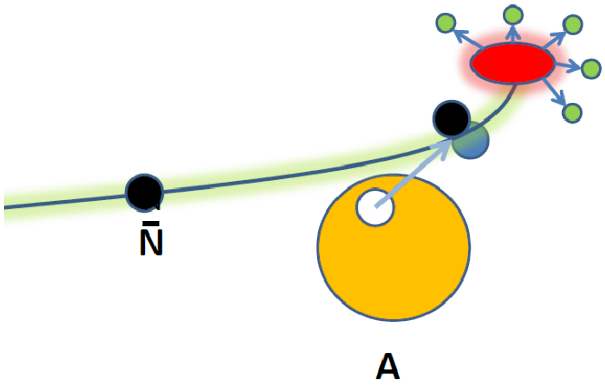

Figure 4.6: Demonstration of peripheral in-flight reactions. The nucleon is picked up and annihilates with the incoming antinucleon outside of the nulceus. The produced pions, however, might scatter back, penetrating the nucleus.

In this mechanism, the antinucleon picks up a target nucleon and forms an intermediate $\overline{N}N$ correlated state, subsequently decaying into mesons in free space, shown pictographically in fig. 4.6. The produced mesons then interact with the residual nucleus in the final state. Their self-interactions, however, are not considered here. Therefore, the outgoing wave functions $\chi^{(-)}_{1\beta}\chi^{(-)}_{2\beta}$ of eq. (4.14) are of baryonic character, as they describe the propagation of $\overline{N}N$. The intermediate $\overline{N}N$ state is expressed in terms of the centre-of-mass and relative motion. Approximating the short-ranged $\overline{N}N$ interaction by a contact interaction, the relative-motion wave function is integrated out analytically. The amplitude $t_{\overline{N}N\to 2\pi}$ then describes the decay of $\overline{N}N$ and the production of the mesons.

As a first step we calculated the production of a hadron cloud. Fig 4.7 shows the pick-up of valence neutrons of ^{48}Ni, stable ^{58}Ni and neutron-rich ^{78}Ni target nuclei. The low-momentum transfer in this reaction leads to clearly visible nuclear structure effects indicated by the diffraction pattern of the angular distributions shown in in Fig. 4.7. Such differences between the different annihilation partner visualizes the idea of studying nuclear structer effects from reactions of antiprotons with nuclei, like proposed for the AIC experiment [Kru05]. The calculation is presented in [LLW14] using the folding approach to derive the optical potential:

$$U_{\mathrm{opt}}(\boldsymbol{r}) = \sum_{N=p,n} \int \frac{\mathrm{d}^3 r}{(2i)^3} \rho_N(q) t_{\overline{p}N}(T_{\mathrm{lab}}, q^2) \mathrm{e}^{\mathrm{i}qr} \tag{4.15}$$

The corrsponding matrix element $M_{\alpha\beta}$ reads

$$M_{\alpha\beta} = G \int \mathrm{d}^3 r_\beta \mathrm{d}^3 r_\alpha \xi^{(-)*}_\beta(\boldsymbol{r}_\beta, \boldsymbol{k}_\beta) \varphi(\boldsymbol{r}_n) \xi^{(+)}_\alpha(\boldsymbol{r}_\alpha, \boldsymbol{k}_\alpha) \tag{4.16}$$

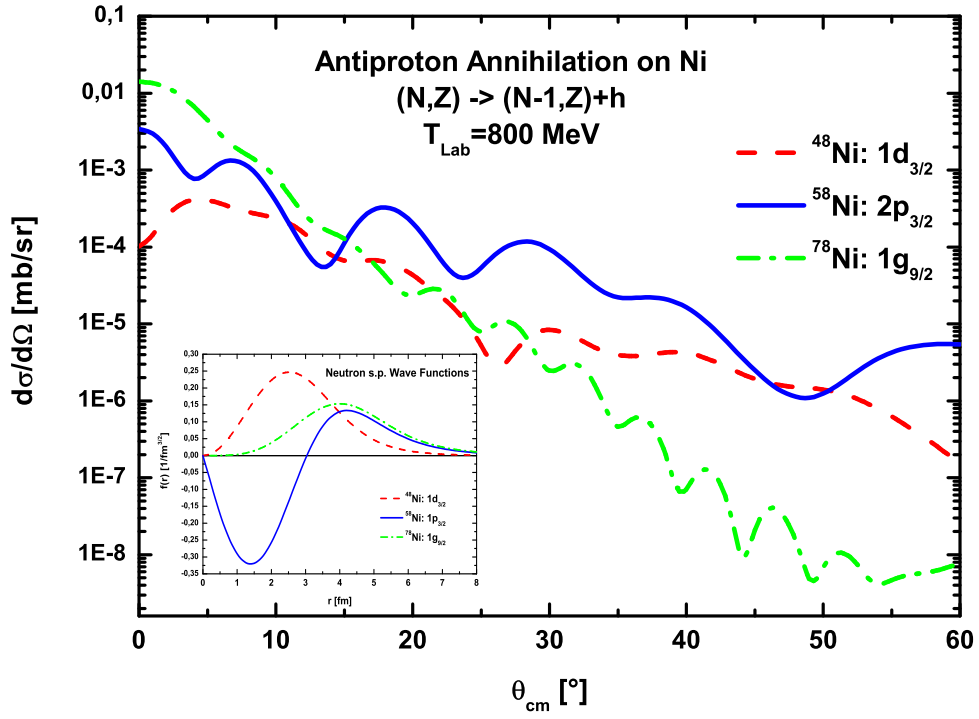

Figure 4.7: As a first step, we calculate the cross section of the production of a hadron cloud with a mass of a pion, not resolving its inner structure. The differential cross sections are shown for valence neutrons of ^{48}Ni, stable ^{58}Ni and neutron-rich ^{78}Ni and $T_{lab} = 800$ MeV.

where G is the coupling constant and ξ indicate distorted waves. The nucleon wave function $\varphi(\boldsymbol{r}_n)$ corresponds to the nucleon, which annihilated with the antiproton. The matrix element 4.16 reveals the direct connection between the cross section and the underlying nuclear structure, making nuclear spectoscropy possible

4.2.2 In-Situ Reactions

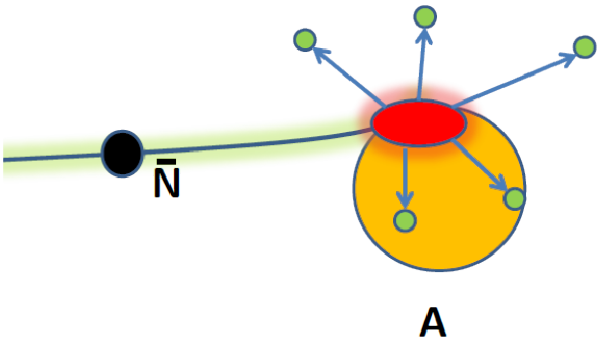

Figure 4.8: In-situ reaction. The antinucleon gets stopped inside the nucleus and produces the pions inside. Here, also higher density regions are of interest, which are usually not reached in pion-nucleus scattering due to the strong absorption at the nuclear surface already.

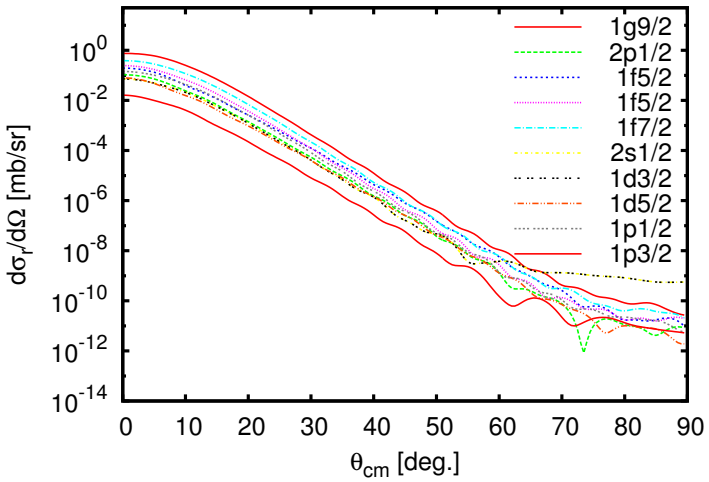

Figure 4.9: As a first step, we calculate the cross section of one meson production, namely ρ^-, which then decays into two pions. The relative motion of the two pions has been integrated out. The differential cross sections are shown for meson production on a ^{78}Ni target and $T_{lab} = 800$ MeV.

This reaction mechanism is quite similar to former experiments at LEAR [A$^+$91]. The antinucleon is stopped in the nucleus, annihilates and produces mesons in the nuclear medium, displayed in fig. 4.8. φ_B is the corresponding initial and final nuclear overlap function, while the mesonic $\chi_{1\beta}^{(-)}\chi_{2\beta}^{(-)}$ are the outgoing distorted waves for each pion.

As a first step, we consider ρ-meson production, which then decays into two pions. The relative motion of those pions has been integrated out. In Fig 4.9, the cross section is shown for the valence neutrons of a ^{78}Ni target, taken from [LLW14].

Strangeness production, either by $K\overline{K}$ pairs or hyperon-antihyperon pairs, will be favourable at high energies, proceeding mainly through the s-channel annihilation.

In this section the most basic facts of the antinucleon-nucleon microscopis models were recovered. An alternative phenomenological approach was presented, overcoming the difficulty to extend the models beyond 300 MeV incident energy. The antinucleon-nucleus and pion-nucleus description developed within this thesis have been applied to formulas describing more complex processes. Two different reaction mechanisms were presented.
Interactions with antiprotons and interaction with pions have been calculated within the same approach. This gives the oportunity to replace parts of the interaction easily. This is suitable for improved potentials, but also other calculations could easily be performed such as kaon production.

5 Conclusion and Outlook

This work paved the way for the description of pion production in antinucleon-nucleus reactions. To describe pion production from annihilation of protons with nucleons in nuclear matter, the calculation of initial state and final state interactions are mandatory. Both have been tackled within this work and have been calculated on the basis of two body interactions.

Within the next years the FAIR facility will be built, and many experiments concerning antiprotons will be active. Because the pion is the lightest meson, it will be produced in many reactions and also appear as background in more rare events. Therefore, the interaction of pions with nucleons and also with nuclei was studied in this work. Even though, there have already been investigations for the interaction of pions with nuclei, they were restricted to a quite limited energy range or used an extra parameter-set for each nucleus. In this work pion nucleus differential and total cross sections have been presented for elastic and inelastic reactions. The so called true absorption cross section of pions reacting with two nucleons was studied in detail. The results presented cover very light nuclei, such as Lithium, passing Carbon and also heavy nuclei such as Bismuth have been shown. The nuclear densities were taken from parametrizations of self-consistent Hartree-Fock-Bogoliubov calculations and have been considered up to quadratic order in the pion-nucleus optical potential. The description of the differential and also total cross sections could be improved by taking more nuclear structure effects into account. Overall a satisfactory agreement with the available data could be achieved.

To calculate the cross sections the Eikonal model was used and the implementation of momentum dependent potentials was presented in this work. The calculation has been structered in such a way that quantum-mechanical amplitudes derived from fundamental optical potentials were used and can also be used as input. This general structure gives the opportunity to extend the model to describe additional reactions. The strangeness production (in nuclear matter) is of high interest and kaon production can easily been applied to the ansatz used in this work.

The description of antinucleon-nucleon interactions has been developed by several groups (Paris, Juelich Nijmegen) using a G-parity transformation from their corresponding NN potentials. Within their models, various channels are selected to be treated explicitly, while all other contributions are taken into account via an optical potential. This procedure is sucsessful up to an incident energy of the antinulceon of

about 300 MeV. Beyond this threshold, too many channels open and the microscopic models come to their limit. To overcome this difficulty, a phenomenological ansatz has been presented within this work. Despite the simple structure a very good description of the actual available antiproton-proton cross section data could be achieved. This ansatz indicates that the antiproton seems to pass two "phases", depending on the energy. It seems that the change of behaviour is due to the change of relevant degrees of freedom. If so, the influence of the quark degrees of freedom is more extended than initially expected.

After the derivation of pion-nucleus and also antinucleon-nucleus interaction, possible reaction scenarios have been briefly introduced. Within this work, the in flight and the in situ reaction mechanisms are taken into account. The first describes the scenario where the nucleon gets caught by the antinucleon in flight. On average 5 pions are emitted, mainly outside of the nucleus. The in situ reaction is similar to the former LEAR experiment where the antinucleon gets stopped inside the nucleus. The formulation of the cross section to describe the pion production in an annihilation reaction with antiprotons in nuclear matter have been shown. The separation of scales gives the opportunity to study nuclear properties separated from the reaction process itself.

So far, the calculation of pion production in antinucleon-nucleon annihilation within nuclear matter is covered by the presented ansatz. The important steps, to finally calculate the corresponding cross sections have been presented. To improve the description of nuclear structure effects, a more advanced description of nuclear densities could be used. The calculations are organized in such a way that alternative descriptions of e.g. pion-nucleon or antinucleon-nucleon amplitudes could be used easily. Especially, the use for strangeness production in form of kaons would be very interesting.

Acknowledgements

Das Anfertigen einer Doktorarbeit ist niemals nur die Arbeit eines Einzigen, sondern immer ein Ergebins vieler helfender Hände und vor allem vieler denkender Köpfe. An dieser Stelle möchte ich die Gelegenheit ergreifen und ein paar Menschen danken, die mich bei meiner Doktorarbeit unterstützt haben.

Zuerst möchte ich Herrn Prof. Dr. Horst Lenske danken, der nicht nur das Thema meiner Arbeit gestellt und mit mir viele Diskussionen geführt hat, sondern auch einen Traum für mich erfüllt hat. Denn mit den nötigen Reisemitteln war es mir möglich mit Herrn Lenske meine erste Reise nach Japan anzutreten, auf die noch viele folgten. Hiermit möchte ich Ihnen ganz besonders danken, dass sie nicht nur mein Traumziel Japan sondern auch viele weitere Konferenzbesuche für mich ermöglicht haben! Außerdem möchte ich Herrn Prof. Dr. Slawomir Wycech danken, der mit seinen Aufenthalten in Gießen viel Licht ins Dunkle bringen konnte und Kontakte nach Paris zu Herrn Loiseau herstellte, dem ich auch danken möchte für das Zuverfügungstellen von Amplituden.

Herrn Dr. Johann Haidenbauer möchte ich danken für die Unterstützung zum Verständis des Jülich-Codes und meine nette Aufnahme am Forschungszentrum Jülich. Weiterhin möchte ich Herrn Prof. Dr. Christian Fischer danken für die Unterstützung vor allem in der Endphase meiner Arbeit und die konstruktive Kritik an meiner Thesis. Besonderer Dank gilt auch Elke Jung, die sich unermüdlich für die Interessen Ihrer Schützlinge einsetzt, und ohne die vermutlich so einiges nicht so glatt laufen würde. Vielen Dank! Weiterer Dank gilt auch den anderen Institutssekretärinnen Ilka Sproates, Monika Weingärtner und Lara Seehawer. Und schließlich möchte ich noch allen Institutsangehörigen danken, die das Institut natürlich ausmachen und neben konstruktiven Gesprächen zu wissenschaftlichen Themen auch allerlei lustige Ablenkung zum manchmal trüben Uni-Alltag schenken.¸

Zu guter Letzt möchte ich meinen Freunden und meiner Familie danken und besonders meinem Mann Thomas, die mir Halt gegeben haben während der Zeit meiner Doktorarbeit.

A Feynman Diagrams

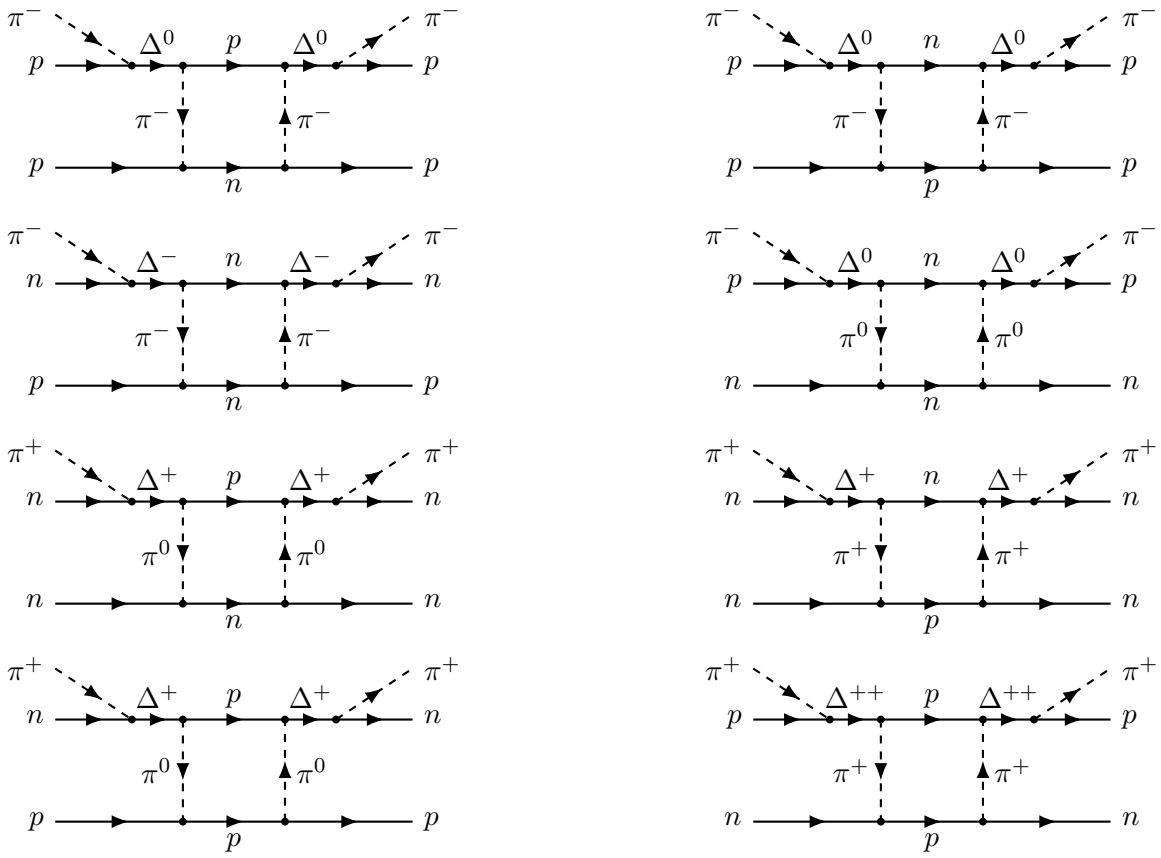

Figure A.1: Feynman diagrams contributing to true absorption ($\pi^{\pm}$)

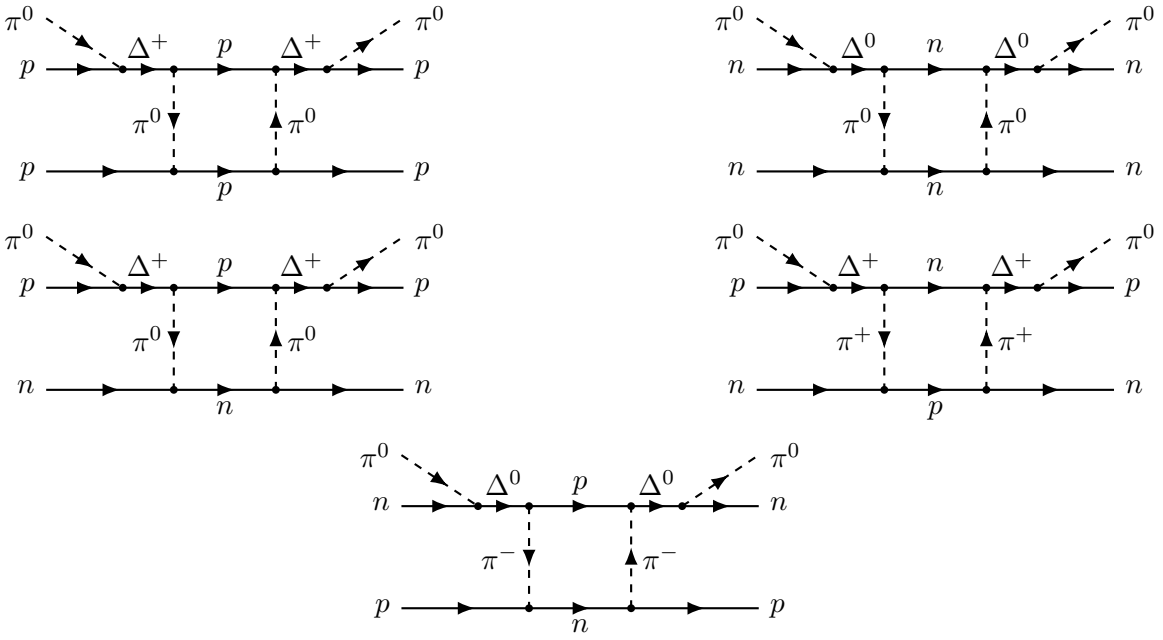

Figure A.2: Feynman diagrams contributing to true absorption (π^0)

Bibliography

[A+91] R. Adler et al. Status of the cp lear experiment and first results. *Nuclear Physics B - Proceedings Supplements*, 24(1):45 – 54, 1991.

[AB90] C. Alexandrou and B. Blankleider. Effects of short range Δ N interaction on observables of the π NN system. *Phys. Rev. C*, 42:517–529, Aug 1990.

[Ams98] Claude Amsler. Proton-antiproton annihilation and meson spectroscopy with the crystal barrel. *Rev. Mod. Phys.*, 70:1293–1339, Oct 1998.

[ANA+81] D. Ashery, I. Navon, G. Azuelos, H. K. Walter, H. J. Pfeiffer, and F. W. Schlepütz. True absorption and scattering of pions on nuclei. *Phys. Rev. C*, 23:2173–2185, May 1981.

[B+12] Beringer et al. Review of particle physics*. *Phys. Rev. D*, 86:010001, Jul 2012.

[BP68] R.A. Bryan and R.J.N. Phillips. Nucleon-antinucleon potential from single-meson exchanges. *Nuclear Physics B*, 5(2):201 – 219, 1968.

[Bru95] H. Bruns. *Das Eikonal*, volume 21. Leipziger Sitzgsber., 1895.

[CLL+82] J. Côté, M. Lacombe, B. Loiseau, B. Moussallam, and R. Vinh Mau. Nucleon-antinucleon optical potential. *Phys. Rev. Lett.*, 48:1319–1322, May 1982.

[CTA+74] A.S. Clough, G.K. Turner, B.W. Allardyce, C.J. Batty, D.J. Baugh, W.J. McDonald, R.A.J. Riddle, L.H. Watson, M.E. Cage, G.J. Pyle, and G.T.A. Squier. Pion-nucleus total cross sections from 88 to 860 mev. *Nuclear Physics B*, 76(1):15 – 28, 1974.

[DM81] R. H. Dalitz and J. G. McGinley. *Remarks Bearing on the Interpretation of the $\Lambda(1405)$ Resonance*, pages 381–409. Springer Netherlands, Dordrecht, 1981.

[DO08] M. Döring and E. Oset. s-wave pion-nucleus optical potential. *Phys. Rev. C*, 77:024602, Feb 2008.

[dWS86] B. de Wit and J. Smith. *Field Theory in Particle Physics, Volume 1 (North-Holland Personal Library)*. North Holland, August 1986.

[EBLLW09] B. El-Bennich, M. Lacombe, B. Loiseau, and S. Wycech. Paris nn potential constrained by recent antiprotonic-atom data and np total cross sections. *Phys. Rev. C*, 79(5):054001, May 2009.

[EE66] M Ericson and T.E.O Ericson. Optical properties of low-energy pions in nuclei. *Annals of Physics*, 36(3):323 – 362, 1966.

[EM12] Evgeny Epelbaum and Ulf-G. Meissner. Chiral dynamics of few- and many-nucleon systems. *Ann. Rev. Nucl. Part. Sci.*, 62:159–185, 2012.

[EW88] T.E.O. Ericson and W. Weise. *Pions and nuclei*. Oxford Science Publications. Clarendon Press, 1988.

[GAK98] W. R. Gibbs, Li Ai, and W. B. Kaufmann. Low-energy pion-nucleon scattering. *Phys. Rev. C*, 57:784–797, Feb 1998.

[GBD67] RJ Glauber, WE Brittin, and LG Dunham. Lectures in theoretical physics, vol. 1 (interscience, new york, 1959). *WE Brittin edn*, page 315, 1967.

[GG82] Humberto Garcilazo and W.R. Gibbs. The contribution of pion absorption with two-nucleon emission to the pion-nucleus optical potential. *Nuclear Physics A*, 381(3):487 – 506, 1982.

[Ghe74] Claude Ghesquière. An inclusive view on $\overline{p}p \to n\pi$ at rest. 1974.

[GJ80] Joseph N. Ginocchio and Mikkel B. Johnson. Effect of the pion and Δ optical potential on deep inelastic pion-nuclear reactions. *Phys. Rev. C*, 21:1056–1064, Mar 1980.

[GM70] R. J. Glauber and G. Matthiae. High-energy scattering of protons by nuclei. *Nucl. Phys.*, B21:135–157, 1970.

[GROS88] C. García-Recio, E. Oset, and L. L. Salcedo. S -wave optical potential in pionic atoms. *Phys. Rev. C*, 37:194–214, Jan 1988.

[GW05] A. M. Green and S. Wycech. η-nucleon scattering length and effective range uncertainties. *Phys. Rev. C*, 71:014001, Jan 2005.

[HHP89] T. Hippchen, K. Holinde, and W. Plessas. Bonn meson-exchange potential in the N-N system. *Phys. Rev. C*, 39:761–765, Mar 1989.

[HL98] F. Hofmann and H. Lenske. Hartree-fock calculations in the density matrix expansion approach. *Phys. Rev. C*, 57:2281–2293, May 1998.

[Hü75] Jörg Hüfner. Pions interact with nuclei. *Physics Reports*, 21(1):1 – 79, 1975.

[IMIO11] T. Ichikawa, J. A. Maruhn, N. Itagaki, and S. Ohkubo. Linear chain structure of four-α clusters in ^{16}O. *Phys. Rev. Lett.*, 107:112501, Sep 2011.

[IYSNH] Natsumi Ikeno, Junko Yamagata-Sekihara, Hideko Nagahiro, and Satoru Hirenzaki. *Formation of Deeply Bound Pionic Atoms and Pion Properties in Nuclei.*

[Joa75] C.J. Joachain. *Quantum collision theory.* North-Holland, 1975.

[JS83a] Mikkel B. Johnson and E. R. Siciliano. Isospin dependence of second-order pion-nucleus optical potential. *Phys. Rev. C*, 27(2):730–750, Feb 1983.

[JS83b] Mikkel B. Johnson and E. R. Siciliano. Pion single and double charge exchange in the resonance region: Dynamical corrections. *Phys. Rev. C*, 27(4):1647–1668, Apr 1983.

[JS96] Mikkel B. Johnson and G.R. Satchler. Characteristics of local pion–nucleus potentials that are equivalent to kisslinger-type potentials. *Annals of Physics*, 248(1):134 – 169, 1996.

[KE69] M. Krell and T.E.O. Ericson. Energy levels and wave functions of pionic atoms. *Nuclear Physics B*, 11(3):521 – 550, 1969.

[KFW02] N. Kaiser, S. Fritsch, and W. Weise. Nuclear mean field from chiral pion–nucleon dynamics. *Nuclear Physics A*, 700(1–2):343 – 358, 2002.

[Kis55] L. S. Kisslinger. Scattering of mesons by light nuclei. *Phys. Rev.*, 98:761–765, May 1955.

[Klu91] W Kluge. Pion-nuclear scattering. *Reports on Progress in Physics*, 54(10):1251, 1991.

[KR66] D. S. Koltun and A. Reitan. Production and absorption of s-wave pions at low energy by two nucleons. *Phys. Rev.*, 141:1413–1418, Jan 1966.

[Kru05] R. Krucken. Technical proposal for the design, construction, commissioning and operation of the aic project. 2005.

[KW86] M. Kohno and W. Weise. Proton-antiproton scattering and annihilation into two mesons. *Nuclear Physics A*, 454(3–4):429 – 452, 1986.

[KW01] N. Kaiser and W. Weise. Systematic calculation of s-wave pion and kaon self-energies in asymmetric nuclear matter. *Physics Letters B*, 512(3–4):283 – 289, 2001.

[Lan09] Jens Sören Lange. The panda experiment—hadron physics with antiprotons at fair. *International Journal of Modern Physics A*, 24(02n03):369–376, 2009.

[Len09] H. Lenske. Antiprotons for nuclear structure research. *Hyperfine Interactions*, 194(1-3):277–282, 2009.

[LK07] Horst Lenske and Paul Kienle. Probing matter radii of neutron-rich nuclei by antiproton scattering. *Physics Letters B*, 647(2–3):82 – 87, 2007.

[LLW12a] Stefanie Lourenço, Horst Lenske, and Slawomir Wycech. Pion production on exotic nuclei by antiproton annihilation. *Hyperfine Interactions*, 209(1-3):117–120, 2012.

[LLW12b] Lourenço, S., Lenske, H., and Wycech, S. Meson production in antinucleon annihilation on nuclei. *EPJ Web of Conferences*, 37:06009, 2012.

[LLW13] S Lourenço, H Lenske, and S Wycech. Meson production in coherent antiproton-nucleus annihilation. *Journal of Physics: Conference Series*, 426(1):012005, 2013.

[LLW14] S. Lourenço, H. Lenske, and S. Wycech. Coherent meson production in antinucleon annihilation on nuclei. *Hyperfine Interactions*, 229(1):53–58, 2014.

[LR02] T.-S. H. Lee and R. P. Redwine. Pion-nucleus interactions*. *Annual Review of Nuclear and Particle Science*, 52(1):23–63, 2002.

[MFJ+89] O. Meirav, E. Friedman, R. R. Johnson, R. Olszewski, and P. Weber. Low energy pion-nucleus potentials from differential and integral data. *Phys. Rev. C*, 40:843–849, Aug 1989.

[MH95] V. Mull and K. Holinde. Combined description of N N scattering and annihilation with a hadronic model. *Phys. Rev. C*, 51:2360–2371, May 1995.

[MP00] H Müther and A Polls. Two-body correlations in nuclear systems. *Progress in Particle and Nuclear Physics*, 45(1):243 – 334, 2000.

[NLG98] Mutazz Nuseirat, M. A. K. Lodhi, and W. R. Gibbs. Pion-nucleus scattering. *Phys. Rev. C*, 58:314–319, Jul 1998.

[NV86] John W. Negele and E. Vogt, editors. *Advances in nuclear physics. Vol. 16*. 1986.

[OGRN95] E. Oset, C. García-Recio, and J. Nieves. Pion cloud contribution to the s-wave repulsion in pionic atoms. *Nuclear Physics A*, 584(4):653 – 664, 1995.

[OTW82] E. Oset, H. Toki, and W. Weise. Pionic modes of excitation in nuclei. *Physics Reports*, 83(4):281 – 380, 1982.

[RHKS96] A. Reuber, K. Holinde, H.-C. Kim, and J. Speth. Correlated $\pi\pi$ and kk exchange in the baryon-baryon interaction. *Nuclear Physics A*, 608(3):243 – 304, 1996.

[Sat92] GR Satchler. Local potential model for pion-nucleus scattering and $\pi+$ π- excitation ratios. *Nuclear Physics A*, 540(3-4):533–576, 1992.

[Sch72] C. Schmit. Pion- 12c elastic scattering in the (32,32) resonance region. *Nuclear Physics A*, 197(2):449 – 484, 1972.

[SHS+95] C Schütz, K Holinde, J Speth, BC Pearce, and JW Durso. Dynamical model for correlated two-pion exchange in the pion-nucleon interaction. *Physical Review C*, 51(3):1374, 1995.

[SS74] M M Sternheim and R R Silbar. Meson-nucleus scattering at medium energies. *Annual Review of Nuclear Science*, 24(1):249–278, 1974.

[TRdS94] R. Timmermans, Th. A. Rijken, and J. J. de Swart. Antiproton-proton partial-wave analysis below 925 mev/ *c. Phys. Rev. C*, 50:48–73, Jul 1994.

[ZT12] Daren Zhou and Rob G. E. Timmermans. Energy-dependent partial-wave analysis of all antiproton-proton scattering data below 925 mev/c. *Phys. Rev. C*, 86:044003, Oct 2012.

Eigenständigkeitserklärung

Ich erkläre:

Ich habe die vorgelegte Dissertation selbstständig und ohne unerlaubte fremde Hilfe und nur mit den Hilfen angefertigt, die ich in der Dissertation angegeben habe. Alle Textstellen, die wörtlich oder sinngemäß aus veröffentlichten Schriften entnommen sind, und alle Angaben, die auf mündlichen Auskünften beruhen, sind als solche kenntlich gemacht. Bei den von mir durchgeführten und in der Dissertation erwähnten Untersuchungen habe ich die Grundsätze guter wissenschaftlicher Praxis, wie sie in der "Satzung der Justus-Liebig-Universität Gießen zur Sicherung guter wissenschaftlicher Praxis" niedergelegt sind, eingehalten.

Stefanie Geßler,
geb. Lourenço